ASD-TDR-63-154

DESIGN CONSIDERATIONS AND METHODS FOR LOW-DENSITY WIND TUNNELS OPERATING WITH HIGH STAGNATION TEMPERATURES

TECHNICAL DOCUMENTARY REPORT NO. ASD-TDR-63-154

April 1963

Directorate of Engineering Test
Aeronautical Systems Division
Air Force Systems Command
Wright-Patterson Air Force Base, Ohio

Project No. 1426, Task No. 142603

(Prepared under Contract No. AF 33(616)-6582
by the Engineering Projects Laboratory, Department of Mechanical Engineering, Massachusetts Institute of Technology, Cambridge, Mass.;
G. A. Brown and A. E. Bergles, authors.)

NOTICES

When Government drawings, specifications, or other data are used for any purpose other than in connection with a definitely related Government procurement operation, the United States Government thereby incurs no responsibility nor any obligation whatsoever; and the fact that the Government may have formulated, furnished, or in any way supplied the said drawings, specifications, or other data, is not to be regarded by implication or otherwise as in any manner licensing the holder or any other person or corporation, or conveying any rights or permission to manufacture, use, or sell any patented invention that may in any way be related thereto.

Qualified requesters may obtain copies of this report from the Armed Services Technical Information Agency, (ASTIA), Arlington Hall Station, Arlington 12, Virginia.

This report has been released to the Office of Technical Services, U.S. Department of Commerce, Washington 25, D.C., in stock quantities for sale to the general public.

Copies of this report should not be returned to the Aeronautical Systems Division unless return is required by security considerations, contractual obligations, or notice on a specific document.

28-679T, 400, 5-21-63

FOREWORD

This report was prepared by the Engineering Projects Laboratory, Department of Mechanical Engineering, Massachusetts Institute of Technology, Cambridge, Massachusetts, on Air Force Contract AF 33(616)-6582, Project 1426 under Task No. 142603, "Experimental Simulation of Flight Mechanics." The work was administered under the direction of the Aerodynamics Division, Aeronautical Systems Division, with supervision by Dr. Wilhelm F. Knackstedt and Mr. Paul A. Czysz.

The study was started in and concluded in August 1962. The authors, Mr. G. A. Brown and Mr. A. E. Bergles, were the principal investigators; however, a portion of the study was conducted by Mr. G. Zeiders.

Many of the references were provided by the Institute of Engineering Research, University of California (Berkeley) and the Institute of Aerophysics, University of Toronto. In addition, discussions of rarefied gas dynamics were held with Professors L. Talbot and F. C. Hurlbut of the University of California and with Drs. G. N. Patterson and I. I. Glass of The University of Toronto.

This report concludes the work on Contract AF 33(616)-6582.

ABSTRACT

A study was made of design techniques for low-density wind tunnels operating with high stagnation temperatures and hypersonic flow.

An approximate boundary layer analysis was developed to predict feasible ranges of operating conditions for low-density wind tunnels.

Detailed calculations were made for three nozzles including boundary layer corrections for isentropic contours.

It became obvious that the use of a high stagnation temperature wind tunnel for investigations of rarefied gas dynamics could produce situations in which it would not always be clear whether the experimental results were associated with rarefied gas flow phenomena or related to high temperature physical phenomena.

It appears that unless an enormous amount of money is devoted to the construction of an extremely large low-density wind tunnel, it will never be feasible to test large models

such that Knudsen numbers in the free-molecular-flow range are produced.

This Technical Documentary Report has been reviewed and is approved.

Robert L. Colligan Jr

ROBERT L. COLLIGAN, JR.
Colonel, USAF
Deputy for Test and Support

REVIEW AND APPROVAL OF ASD TECHNICAL DOCUMENTARY REPORT ASD-TDR-63-154

PROJECT ENGINEER:

PAUL A. CZYSZ
Chief, High Temperature Section
Aerodynamics Division

CONCURRED IN:

for WILLIAM J. DuBOIS
Lt Colonel, USAF
Acting Director Engineering Test
Deputy for Test and Support

CONCURRED IN:

HUGH S. LIPPMAN
Technical Director
Deputy for Test and Support

APPROVED BY:

ROBERT L. COLLIGAN, JR
Colonel, USAF
Deputy for Test and Support

TABLE OF CONTENTS

LIST OF ILLUSTRATIONS

NOMENCLATURE

a	velocity of sound
a	radius of throat section of nozzle in centimeters, Ref. (20)
A	cross-sectional area of nozzle
A	constant in boundary layer correction method, Eq. (50)
A	concentration of atoms, Eq. (37)
A_2	concentration of molecules, Eq. (37)
B	constant in boundary layer correction method, Eq. (51)
$\overline{C}$	boundary layer thickness constant based on $\rho_e V_e L_t/\mu_o$, Eq. (18)
C	boundary layer thickness constant for flat-plate flow, Eq. (19)
C	boundary layer thickness constant for predicting boundary layer growth in nozzle, Fig. 26
C'	constant in boundary layer correction method, Eq. (52)
D	cylinder diameter
D	diameter of nozzle cross-sectional area
D^*	diameter at nozzle throat
D_{se}	diameter at exit section of isentropic nozzle contour
D'_{se}	diameter of isentropic core at exit section of actual nozzle contour
D_e	diameter at exit section of actual nozzle contour
g_o	acceleration given to unit mass by unit force
h	enthalpy
k	Boltzman's constant
K_1, K_2	constants in boundary layer correction method, Eqs. (43) and (44)

K_n	Knudsen number
l	frozen flow parameter, Ref. (20)
L	any characteristic dimension
L	distance along flat plate surface
L_t	axial distance between nozzle throat and exit sections
m	mass of molecule
M	Mach number
p	pressure
q	minimum heater power
r	radius of nozzle cross-sectional area
r'_{se}	radius of isentropic core at exit section of actual nozzle
r_s^+	dimensionless nozzle radius, Eq. (45)
R	individual gas constant
$\bar{R}$	universal gas constant
Re	Reynolds number based on some L and a $\rho u/\mu$ product for a single state
Re_{L_t}	Reynolds number, Eq. (48), $\rho_e u_e L_t/\mu_o$
Re/ℓ	Reynolds number per unit length, $\rho u/\mu$
S	molecular speed ratio
S_p	volume flow rate at nozzle exit density, Eq. (59)
T	absolute temperature
u	velocity
u_s^+	dimensionless velocity, Eq. (47)
V	velocity
$\bar{V}$	mean velocity for Maxwellian velocity distribution
w	mass flow rate
W	molecular weight of dissociated gas

W_o	molecular weight of undissociated gas
x	dimensionless distance along nozzle axis, Eq. (49)
y	distance normal to a surface
y_m	number of molecules per initial molecule of air
y_a	number of atoms per initial molecule of air
Z	compressibility factor, Eq. (7)

Greek:

α	mass fraction of gas dissociated, Eq. (37)
γ	isentropic exponent
δ	boundary layer thickness (99% velocity)
δ^*	boundary layer displacement thickness
δ^+	dimensionless boundary layer thickness, Eq. (41)
θ	total angle for divergent section of a conical nozzle
λ	mean-free-path
μ	viscosity
ρ	density
ρ_s^+	dimensionless density, Eq. (46)
τ	dimensionless speed of sound parameter, Eq. (6)

Subscripts:

a	atmospheric conditions
A	nozzle section at which actual expansion process deviates from equilibrium-flow process
B	nozzle section at which actual expansion process becomes a frozen-flow process
C	nozzle section at which a frozen-flow process is started on equilibrium flow curve
e	exit section or conditions for actual nozzle contour
n,n + 1	successive sections along nozzle

o	nozzle stagnation state
r	a reference condition
s	isentropic process
s	boundary layer seam
se	exit section or conditions for isentropic nozzle contour
∞	free-stream conditions for a flat-plate flow

Superscript:

*	throat section of nozzle

INTRODUCTION

Objectives of Study

This report summarizes some analytical results of a study of low-density wind tunnels. Specific operating conditions for these wind tunnels are selected so that experimental data can be obtained for flows about models corresponding to the various regimes of rarefied gas dynamics. The general considerations for the design of such wind tunnels are presented along with specific designs for several wind tunnels. The study was supported by the Aeronautical Systems Division of the United States Air Force Systems Command at Wright Patterson Air Force Base, Ohio and is part of ASD's continuing policy to improve and to obtain experimental facilities which will support a high-level "in house" research program. Since the future plans of the group interested in hypersonic flow involves an experimental program in rarefied gas dynamics, this study was initiated to determine the limitations on the use of low density wind tunnels in the rarefied-gas-dynamics region. For those operating conditions such that the use of the wind tunnel is feasible, specific design information is desired for planning new facilities at ASD.

The objectives of this study as set forth in the contract were:

1. To determine the state of the art on the design of low density wind tunnels which could produce flow conditions such that models of reasonable size could be tested in the transition flow and free-molecular-flow regimes.

Manuscript released by the authors February 1963 for publication as an ASD Technical Documentary Report.

2. To determine those ranges of operating conditions where a low density wind tunnel could be utilized.

3. To determine which phases of the nozzle design procedure must be modified so as to account for the conditions encountered in low-density hypervelocity wind tunnels and to generate these new techniques insofar as time permitted.

4. To design several nozzles for use with available and proposed high temperature heaters at ASD. A range of stagnation temperatures between 7000° and 12000° R was selected for the study. The nozzle designs were to be based upon the use of air or other non toxic gases and the nozzle exit velocities were to be as high as possible consistent with the stagnation temperature range. The nozzle designs were to include contour specifications and the pressures, temperatures, flow rates, etc., associated with these contours.

5. To survey the available literature relative to rarefied gas dynamics with a special emphasis on free-molecular-flow testing techniques.

The results of the literature survey were published in Reference (1)*. Some 700 references were presented on rarefied gas dynamics and topics associated with low-density wind tunnel design. The references were cross indexed on a subject basis. The literature survey and this report constitute the final report of this study.

* Numbers in parentheses refer to items in the Bibliography.

Rarefied Gas Dynamics

In order to discuss intelligently the design considerations for low-density wind tunnels it is desirable to review briefly the basic factors which control rarefied gas dynamics. This is best accomplished by reference to Fig. 1 which shows some recent experimental data on the drag coefficient for a cylinder. These data were obtained by Maslach and Schaaf (2) at the University of California. The drag coefficient is plotted versus the Knudsen number (based on cylinder diameter) and the results were obtained at a Mach number of about 6. According to its usual definition, the Knudsen number, Kn, is:

$$Kn_D = \frac{\lambda}{D} \tag{1}$$

where λ is the mean-free-path and D is the cylinder diameter. It will be seen that at small values of the Knudsen number, about 0.01, the experimental values of the drag coefficient approach the value corresponding to continuum flow. However, at a Knudsen number of 0.1, deviations from the continuum flow value are already about 10 percent. As the Knudsen number is increased, the drag coefficient deviates more and more from the continuum flow value until at a Knudsen number of about 10, the drag coefficient is 2.8 and has practically achieved a value corresponding to the free-molecular-flow limit.

Normally the first departures from the results of continuum gas dynamics occur at a Knudsen number of 0.01. The flow regime in the Knudsen number range from 0.01 to 0.1 is called the slip flow regime. In this regime the first effects of particle-surface interaction are encountered in that it is no

longer possible to relate in a simple manner flow properties in the fluid near a surface to those properties at the surface. In the case of continuum gas dynamics, values of temperature (or temperature gradient), velocity, mass transfer rates, etc., in a fluid at a surface are equated to values of these quantities at the surface. In the range of Knudsen numbers between 0.1 and 10 the particle-surface interactions become more significant and this flow regime is called the transition flow regime. Finally when the Knudsen number is 10 or greater the free-molecular-flow regime is encountered and the particle-surface interactions are controlling. The two limiting values indicated in Fig. 1 for the free-molecular-flow regime correspond to the cases of diffuse and specular reflection of particles from the surface. Table I summarizes the flow regimes and the corresponding Knudsen number ranges which are involved.

TABLE I

FLOW REGIMES OF RAREFIED GAS DYNAMICS

Regime	Knudsen Number Range
Slip Flow	0.01 - 0.1
Transition Flow	0.1 - 10
Free-Molecular-Flow	10 - ∞

The results shown in Fig. 1 also depend upon the value of the Mach number, M, defined as:

$$M = \frac{V}{a} \tag{2}$$

or equivalently the molecular speed ratio, S, defined as:

$$S = \frac{V}{\sqrt{2 g_o RT}} \tag{3}$$

The relationship between the Mach number and the molecular speed ratio is:

$$S = \sqrt{\frac{\gamma}{2}}\, M \tag{4}$$

where γ is the ratio of specific heats.

Based on the above discussion it is apparent that in the design of low-density wind tunnels it is necessary to select tunnel operating conditions such that correct values are produced for those independent variables which control the heat, mass and momentum transfer processes of the three flow regimes in rarefied gas dynamics. In addition to the obvious need for certain values of the Knudsen number and the molecular speed ratio, it is necessary to control all factors which enter into the particle-surface interaction especially in the transition and the free-molecular-flow regimes. It is easier to state that those independent variables for the particle-surface interaction be controlled than to identify them. These independent variables include the surface condition of the model, the temperature of the surface and the temperature of the incoming stream. However, even use of the term temperature for the incoming stream is a substitute for an exact specification, since we are more properly concerned with the distribution function of the incoming stream and with the equilibrium or non-equilibrium state of this stream. In the results that follow some of these variables will be related directly to the tunnel design; some of the variables will be introduced in a somewhat vague manner and some of them will be no more than commented upon.

Present Status and Problems

At the present time most of the experimental work on external aerodynamic problems in rarefied gas dynamics has been obtained with either of two types of experimental equipment. The first piece of equipment is the low-density wind tunnel. The second piece of equipment is the molecular beam apparatus for studying particle-surface interaction phenomena. Most of the existing experimental data from low-density wind tunnels have been obtained with relatively low tunnel stagnation temperatures, the order of a few hundred degrees Fahrenheit, and in the Mach number range from 0 to approximately 7. It is only within the last two years that some experimental drag data for spheres were obtained in a hypersonic wind tunnel (3) and to the authors' knowledge these are the only experimental data taken at a high stagnation temperature. Therefore, there is a need for additional test facilities for obtaining aerodynamic data on models of various shapes under high stagnation temperature and high Mach number flow conditions in the rarefied-gas-dynamic regions. However, a word of caution is required on the use of such high temperature hypersonic facilities. In general, a high temperature plasma tunnel tends to be a difficult piece of apparatus in which to measure a large number of individual quantities. Although the plasma tunnel serves an important function in producing experimental data which can be subsequently scaled for use in the solution of design problems for re-entry vehicles, etc., it is not the best piece of equipment from which to get accurate and sufficient data to confirm or deny proposed theoretical results. For this reason it is well to keep in mind that there will be a continuing need for a variety of low-density wind tunnels

capable of operation over a wide range of stagnation temperatures and Mach numbers, and using gases which are not necessarily related to any practical problem, present or future. This requirement exists because it is necessary to identify those factors which are related to rarefied gas dynamics and those factors which are related to high-temperature physical phenomena.

The available analytical and experimental information on the surface-particle interaction problem of rarefied gas dynamics is poor. A recent survey of accommodation coefficients by Harnett (4) lends independent support to this conclusion. Analytical treatments of the interaction phenomena are practically nonexistent, and those which exist are so superficial as to be almost useless. Although much of the available experimental data on the interaction phenomena are excellent, in many cases data have obtained under what amounts to unspecified conditions. The basic problem would seem to be quite simple: there aren't enough experimental data. Although this lack of information has been specifically referenced for the free-molecular-flow regime, it is apparent that similar information is needed as a basis for analytical treatments of the slip and transition regimes.

There are few analytical treatments of the slip and transition flow regimes. Attempts to analyze these regimes probably suffer as much from a lack of a solid theoretical basis as they do from a lack of highly accurate data against which to test new theoretical treatments. The analytical solutions to problems in the free-molecular-flow regime are excellent if the appropriate interaction data are available. Additional work

is required on problems of non-equilibrium flows with non-Maxwellian velocity distributions.

Conclusions

At the present time there is a need for additional experimental data on the slip, transition and free-molecular-flow regimes of rarefied gas dynamics. The need is especially great for conditions corresponding to hypervelocity conditions. In order to run controlled experiments in these regions, it will be necessary to produce certain ranges of Knudsen numbers and molecular speed ratios, and to control the surface conditions of any models used in the experimental test facility. An accurate knowledge of the state of the flow approaching the model will also be required, and this may be one of the major stumbling blocks in obtaining controlled experimental data for use as design information and as a basis for the confirmation or denial of new theoretical considerations of rarefied gas dynamics.

THE LOW DENSITY WIND TUNNEL

Configuration

Figure 2 shows schematically the low-density wind tunnel being considered. Gas obtained from either storage tanks or a compressor is supplied to a flow meter and then passes through a heating section, a settling chamber, and to the nozzle section of the wind tunnel. The heater will probably be of the arc type. It is felt that a settling chamber of some kind is required for low-density wind tunnels in order to insure that equilibrium has been achieved prior to the nozzle expansion process, and consequently, that a known set of stagnation conditions exist for the wind tunnel. The requirement for a state of equilibrium prior to entry into the nozzle is particularly important for low-density wind tunnels, since the ranges of stagnation pressures and stagnation temperatures which are encountered inevitably lead to a combination of equilibrium, non-equilibrium and frozen flow in the nozzle. The particular combination of these types of flow exerts a very strong influence on the final test section conditions. The use of a nozzle supplied immediately from an arc-type of heater will probably lead to unknown test-section conditions, since the flow in this case certainly does not achieve an equilibrium condition prior to entry into the nozzle, and therefore the expansion process in the nozzle is unknown. The specific model to be tested is suspended in the jet at the exit plane of the nozzle. Upon leaving the nozzle, the jet expands into an additional chamber and then in turn passes through a precooler section and finally into

the cryogenic pumping unit. It is felt that a cryogenic pumping unit will be required, since in order to achieve flow conditions in the free-molecular-flow region, test section pressures of the order of one micron will be required. Conventional mechanical pumping units are not suited for the volume flow rates which will be encountered at these pressures. The capacity of a cryogenic pumping unit is low, of the order of a few thousand watts, and the precooler is a critical component in the system since it must remove a sufficient amount of heat from the gas stream so that the cryogenic unit is not overloaded. Adequate radiation shielding must also be supplied around the cryogenic unit to keep the heat load at a minimum. Pressure drop through the precooler section obviously must not be excessive.

Static Pressure Requirements

The requirements for low-density wind tunnels are identical with the requirements which have always been imposed on wind tunnels; namely, that a uniform region of flow at known conditions must be produced. As has been mentioned before, an exact knowledge of known conditions may be difficult to obtain due to the instrumentation difficulties. Some of the quantitative requirements for such wind tunnels can be calculated as follows.

There exists a relatively simple relationship between the Knudsen number, Mach number, and Reynolds number, which will

permit the calculation of required test-section pressures. The relationship is derived in Appendix A and is presented below:

$$Kn = \frac{8}{5}\sqrt{\frac{2}{\pi}\tau}\quad\frac{M}{Re} \tag{5}$$

The quantity τ in Eq. (5) is a speed-of-sound parameter defined by the following equation:

$$\tau = \frac{a^2\rho}{p} \tag{6}$$

For flow of a gas under conditions such that the composition is frozen, the speed of sound parameter, τ, corresponds to the isentropic exponent or the ratio of specific heats, γ. For flow conditions under which the composition is controlled by chemical equilibrium considerations, τ and γ are not identical. Figure 6 of Ref. (5) shows the speed-of-sound parameter for air under equilibrium conditions for a wide range of pressures and temperatures. The compressibility factor, Z, is defined as:

$$Z = \frac{p}{\rho T}\cdot\frac{W_o}{\overline{R}} \tag{7}$$

Values of Z for air under equilibrium conditions are shown in Fig. 1 of Ref. (5). For conditions such that τ and γ are equal, Eq. (5) reduces to the following form:

$$Kn = \frac{8}{5}\sqrt{\frac{2\gamma}{\pi}}\quad\frac{M}{Re} \tag{8}$$

As γ varies between 1.0 and 1.667, the coefficient of Eq. (8) varies between 1.277 and 1.648. The important significance of the above equations is that selected values of Knudsen number and Mach number determine a value for the Reynolds number if a value of either τ or γ is known for the particular flow conditions.

It is interesting to rearrange Eq. (8) into the following form:

$$Re_{\lambda} = \frac{8}{5}\sqrt{\frac{2\gamma}{\pi}}\ M \qquad (9)$$

where Re_{λ} represents a mean-free-path Reynolds number defined as:

$$Re_{\lambda} = \frac{\rho V \lambda}{\mu} = Kn \cdot Re \qquad (10)$$

Equation (10) indicates that for a desired value of Mach number there is a single value of the mean-free-path Reynolds number which is required. Figure 3 shows Eq. (10) for the limiting values of γ. In the range of Mach numbers from 0 to 20, the mean-free-path Reynolds number varies between 0 and a maximum of approximately 35. Since Eq. (10) shows that the mean-free-path Reynolds number is equal to the product of the Knudsen number and the usual Reynolds number, it is easy to appreciate that in order to obtain Knudsen numbers of the order of 10 to 100, Reynolds numbers of unity or less will be encountered.

The Reynolds number is related to test-section pressure by the following equation:

$$\frac{Re}{L} = \frac{M}{\mu}\ p\sqrt{\frac{W_o}{\overline{R}T}\cdot\frac{\tau}{Z}} \qquad (11)$$

This equation is derived in Appendix A. For prescribed values of the Reynolds number per unit length, Mach number, and test-section static temperature, it is possible to calculate the required test-section static pressure from the above equation. Two additional assumptions were made in the calculation of the static pressure. First, the viscosity of the gas mixture was

calculated from the Sutherland equation corresponding to undissociated air (or diatomic molecules)

$$\mu = 0.073225 \times 10^{-5} \frac{T}{1 + \frac{201.6}{T}} \qquad (12)$$

where μ has the units of lbm/ft-sec and T is in Rankine temperature units. This approximation has been shown to be valid by Hansen (5). Second, it has been assumed that the expansion between the stagnation section ahead of the nozzle and the test section could be approximated by an isentropic expansion with a constant value of γ. Values of γ of 1.2, 1.4 and 1.67 were used and represent reasonable values for the equilibrium flow or frozen-compositional flows which might occur in the nozzle. In Eq. (11) values of T were calculated using the values of T_o, M and γ. The ratio τ/Z (or γ/Z) was taken as unity. This means that at low temperatures (or high M) where $Z \sim 1$ and $\gamma \neq 1$ the values of p shown in Figs. 4 and 5 will be somewhat too high. Further comments will be made on this point later in the report. Minimum and maximum stagnation temperatures of 7000 R and 12000R were used. Figures 4 and 5 show the results of these calculations in terms of test-section static pressure versus Reynolds number per unit length. Lines of constant test-section Mach number are also indicated, as are lines corresponding to constant values of the Knudsen number - characteristic length product, or equivalently, the mean-free-path, λ. The values of Mach number and Reynolds number per unit length corresponding to a constant Kn · L product were calculated from Eq. (8). The values of mean-free-path were selected so that, based on a one-inch model characteristic dimension, the three regimes of rarefied gas dynamics are covered. For a stagnation temperature

of 7000 R (Fig. 4), the static pressure range for mean-free-paths between 0.01 and 100 inches (considering all Mach numbers) ranges from approximately 1000 microns (1 mm Hg) down to approximately 0.01 micron. The main grid on Fig. 4 corresponds to a value of γ of 1.4. In addition, two lines for a value of γ of 1.2 are shown for Mach numbers of 1 and 10. The effect on static pressure of a change in the value of γ near a Mach number of unity is extremely small, while at a Mach number of 10 there is an increase by almost a factor of 2 in the required static pressure as γ is decreased from 1.4 to 1.2. These effects are to be expected in view of the fact that from Eqs. (11) and (12) the static pressure dependency on temperature is as follows:

$$p \sim T \tag{13}$$

For Mach numbers near unity, the ratio of stagnation to static temperature can be written as follows:

$$\frac{T_o}{T} \sim 1 \tag{14}$$

Thus, for a constant value of the stagnation temperature, changes in γ should not affect values of the static pressure. On the other hand, for Mach numbers which are large compared to unity, the ratio of the stagnation to static temperature can be written as follows:

$$\frac{T_o}{T} \sim \frac{\gamma - 1}{2} M^2 \tag{15}$$

Thus, the static temperature dependency on γ involves a (γ - 1) relationship. For the values of 1.2 and 1.4, the static temperature ratio for a given stagnation temperature should be in the ratio of about 2:1. This checks the variation of static pressure shown in Fig. 4. Figure 5 shows the static pressure at a stagnation temperature of 12000 R. It will be seen that the values of static pressure are about 70 percent larger than those shown for 7000 R. This effect is also expected as a result of Eq. (13), since the static pressure for a given Mach number and γ should vary directly as the stagnation temperature.

In order to put these values of static pressure in proper perspective it can be mentioned that present-day low-density wind tunnels using much lower stagnation temperatures, namely, 100-200 F, have been operated in a range of test section pressures extending down to about 10 microns. From Fig. 4 it will be seen that if a one inch model is placed in a low density wind tunnel and a Knudsen number of 100 is desired, test section pressures between 1 micron and 0.01 micron will be required. Such an operating point will put a severe load on existing cryogenic pumping units. Figures 4 and 5 also indicate the necessity for using extremely small models in cases where large values of the Knudsen number are required. For example, if a pumping system were available which could operate in the range from about 5 microns to 50 microns and it was desired to get a Knudsen number of 100, Fig. 4 indicates that due to the pumping restriction, a mean-free-path of about 1 inch would be possible. The combination of a Knudsen number

of 100 and a mean-free-path of 1 inch would require a characteristic length for the model of 0.01 inches. This is in fact the method by which large values of the Knudsen number have been obtained experimentally to date. Curves for a value of γ of 1.67 have also been included on Figs. 4 and 5. Again only the limiting Mach numbers of 1 and 10 have been used.

Two additional comments should be made about Figs. 4 and 5. First, values of the static pressure corresponding to a new stagnation temperature can be estimated from Eq. (13) using either Figs. 4 or 5. The grid on these figures is displaced vertically to a new position such that the ratio from Eq. (13) is produced. Results for the limiting values of stagnation temperature for this study have been shown independently for illustration purposes. Second, the information given in Figs. 4 and 5 can be shown on a single graph. The static pressure is plotted versus Mach number for a particular value of the Reynolds number per unit length. At any new value of the Reynolds number per unit length the static pressure can be obtained by a multiplication of the ratios of the Reynolds number per unit length involved. If the subscript r is used to indicate the values shown on this reference plot and the unidentified symbols are used to indicate new conditions then the new static pressure can be obtained as follows:

$$p = p_r \cdot \frac{(Re/L)}{(Re/L)_r} \tag{16}$$

Similarly the effect of a change in stagnation temperature may be calculated from the following equation:

$$p = p_r \cdot \frac{(T_o)}{(T_o)_r} \tag{17}$$

The last equation is restricted to high stagnation temperatures due to the approximation upon which Eq. (13) is based. This method of plotting has been used to present the results of the approximate boundary layer analysis for the nozzle in Figs. 13 and 14.

Stagnation Pressure Requirements

It has already been mentioned that non-equilibrium flow effects will be encountered due to the stagnation pressures and temperatures which are involved. Since a range of stagnation temperature has already been selected it is appropriate that the possible range of stagnation pressure also be estimated. Based on the results shown in Figs. 4 and 5, it appears that a reasonable "average" test-section pressure for the wind tunnel might be about 10 microns. This value was selected since static pressures less than this value will require large wind tunnels while static pressures above this value will permit the use of reasonably sized wind tunnels but will necessitate the use of small models such as are presently used. Fig. 6 shows values of the nozzle stagnation pressure which will be required for a static pressure of 10 microns and the Mach numbers indicated on the figure. The values of γ which were used previously have been used in Fig. 6. For a Mach number of 10 and a value of γ of 1.2, the required stagnation pressure is approximately 23 atmospheres. As γ is increased to 1.4 the

stagnation pressure decreases to approximately 0.56 atmospheres. Finally, if a monatomic gas is employed the stagnation pressure is approximately 0.09 atmospheres. At this point it is actually not known whether or not a static pressure of 10 microns can be tolerated since no estimate has been made of nozzle size, boundary layer thickness, etc.; however, the results shown in Fig. 6 do indicate that stagnation pressures below approximately 100 atmospheres will be required for the operation of the low-density hypervelocity wind tunnel.

APPROXIMATE BOUNDARY LAYER ANALYSIS

Introduction

In general, the nozzle of any wind tunnel is designed by means of a two-step procedure. The first step involves a selection of the stagnation pressure, the stagnation temperature and a desired exit Mach number for the nozzle. The specification of these quantities permits a study of the thermodynamic states and the isentropic exponent for the nozzle expansion process. If the range of thermodynamic states involved is small, a constant value for γ can be used to design the isentropic contour for the nozzle. Usually some distribution of Mach number along the centerline of the nozzle is used to generate the isentropic contour. It is necessary to keep the angle of divergence of the isentropic contour small enough in order to avoid separation of the flow in the expansion portion of the nozzle. On the other hand, if the range of thermodynamic states is large, the use of a constant value of γ may not be permissible, and it may be necessary to use a variable value of γ to design the isentropic contour. A study by Guentert and Neumann (9) has shown that significant errors may be introduced by the use of a constant value of γ in those cases where large variations in γ exist.

The second step in the design process involves a calculation of the boundary layer thickness along the nozzle. The quantity of interest is the displacement thickness of the boundary layer, δ^*. The boundary layer growth is calculated from an integral solution of the boundary layer equations. The free-stream conditions for the boundary layer

calculation are assumed to be those from the isentropic contour calculation. For the case of high-density wind tunnels the boundary layer thicknesses are usually small and represent a small percentage increase in the coordinates of the isentropic contour. On the other hand, for the low-density wind tunnel, the boundary layer corrections are large and may change the isentropic contour coordinates by large factors. Examples of such calculations for low-density wind tunnels are to be found in References 10, 11, 12. Thus, the designer of nozzles for high-density wind tunnels can, with a great degree of certainty, start a nozzle design with assurance that the boundary layer corrections will be practically negligible compared to the isentropic contour coordinates. However, the designer of low-density wind tunnel nozzles must face the possibility that the boundary layer corrections will be of such a magnitude that, when added to the isentropic contour, there will be no region of uniform isentropic flow in which to place a test model. Unless it is acceptable to utilize such a nozzle design it is necessary to repeat the entire process for a new set of conditions until a suitable operating point is found. In order to eliminate this possibility and in order to determine suitable ranges for the operation of low-density hypervelocity wind tunnels, the following approximate boundary layer analysis has been developed.

Summary of Existing Information

The analysis and experimental data for several nozzles from the low density research groups at the University of Toronto and the University of California are given in References 10, 11, 12, 14-19. The analytical techniques which have been developed for

boundary layer calculations for low-density nozzles have been highly successful as will be seen from an inspection of the experimental results in these references. In particular, the results of Reference (10) have been utilized for boundary layer calculations in this report. In addition, a correlation based on the experimentally determined values of boundary layer thickness will be employed for the approximate analysis given here. One form of this correlation for the boundary layer thickness is:

$$\frac{\delta}{L_t} = \frac{\bar{C}}{\sqrt{\frac{\rho_e V_e L_t}{\mu_o}}} = \frac{\bar{C}}{\sqrt{Re_{L_t}}} \tag{18}$$

In Eq. (18) $\bar{C}$ is a constant which depends on the exit Mach number of the nozzle. The length Reynolds number is based on the stagnation viscosity rather than free-stream viscosity at the exit plane of the nozzle. Equation (18) has the same form as the expression for the laminar boundary layer thickness on a flat plate, namely:

$$\frac{\delta}{L} = \frac{C}{\sqrt{\frac{\rho_\infty V_\infty L}{\mu_\infty}}} \tag{19}$$

In Eq. (19), C is a constant which depends on the free-stream Mach number and on the ratio of the flat plate surface temperature to the free-stream temperature. Actually, all this latter ratio controls is the property variation in the laminar boundary layer for a specific set of conditions. If, in addition, dissociation of the gas in the boundary layer is

important, then the free-stream pressure level would have to be introduced as one of the controlling variables for the constant C. Also, the Reynolds number in Eq. (19) is based on the free-stream viscosity. Manipulation of Eq. (18) yields the following equation:

$$\frac{\delta}{L_t} = \frac{\bar{C}\sqrt{\frac{\mu_o}{\mu_e}}}{\sqrt{\frac{\rho_e V_e L_t}{\mu_e}}} \tag{20}$$

The suggested equivalence between the two constants C and $\bar{C}$ then becomes:

$$C = \bar{C}\sqrt{\frac{\mu_o}{\mu_\infty}} \tag{21}$$

It will be seen in Eq. (18) that the axial distance between the nozzle throat and the nozzle exit plane has been used in the Reynolds number. Normally, one would expect that the distance along the wall of the nozzle would be the controlling length parameter in determining the boundary layer thickness. However, the argument can be made that since the angle of divergence in most wind tunnel nozzles is kept relatively small the difference between the lengths along the wall of the nozzle and the nozzle axis will not be large. Table II summarizes some of the data upon which Eq. (18) is based. A check on the validity of Eq. (19) will be presented later in this section.

The analytical boundary layer correction method which suggested the use of Eq. (18) is presented in Reference (10).

TABLE II

EXPERIMENTAL BOUNDARY LAYER THICKNESSES FOR LOW-DENSITY WIND TUNNEL NOZZLES

Ref.	M_e -	p_e Microns	δ Inch	r_e Inch	L_t Inch	$\bar{C}$ -	C Based on Eq. (21)	C Van Driest Fig. 10
(14)	2	20	2.41	2.911	9.205	4.99	6.36	7.4
(15)	2.6	111-116	1.16	2.761	13.321	5.76	8.31	8.3
(16)	3.94	92	1.58	3.577	24.023	7.43	14.27	10.8
(17)	3.98	90	1.01	2.155	13.399	6.63	12.86	10.8
(18)	4	40.1	1.05	1.351	6.374	6.44	12.55	10.8
(19)	6	84.7[1]	1.13	2.638	17.294	8.86	26.0	16.4

Notes:

1. Calculated from stagnation pressure, M_e and $\gamma = 1.4$
2. Stagnation temperatures assumed to be 85F

This method uses a sine-arch velocity profile in order to solve the integral boundary layer equations. The equation for the sine-arch velocity profile is:

$$\frac{V}{V_\infty} = \sin\left(\frac{\pi}{2}\ \frac{y}{\delta}\right) \tag{22}$$

Based on Eq. (22) it can be shown that the ratio of the boundary layer thickness, δ , to the displacement thickness, δ^*, can be expressed as follows:

$$\delta^* = (1 - B)\delta \tag{23}$$

The parameter B is:

$$B = \frac{2}{\pi}\ \frac{\tan^{-1}\left[M\sqrt{\frac{\gamma - 1}{2}}\right]}{M\sqrt{\frac{\gamma - 1}{2}}} \tag{24}$$

These results will now be used to develop an approximate analysis of the boundary layer growth in a low-density wind tunnel nozzle.

Summary of Approximate Boundary Layer Analysis

The nomenclature for the approximate boundary layer analysis of low-density wind tunnel nozzles is given in Fig. 7. Figure 7a shows the divergent section of the isentropic nozzle contour which will be used. This divergent section has a conical shape with a total included angle, θ. The nozzle throat diameter is D^* and the exit diameter of the isentropic contour is D_{se}. The axial distance between the nozzle throat and the nozzle exit section is L_t. Figure 7b shows the final nozzle contour. The displacement thickness δ^* has been added to the isentropic contour in order to obtain the final nozzle contour. The exit diameter of the final

contour is D_e. Since the boundary layer thickness at the exit of the nozzle is greater than the displacement thickness at this section, not all of the exit diameter is free from viscous boundary layer effects. The diameter of the isentropic core at the exit of the final nozzle, D'_{se}, will be determined by the values of δ and D_e through the following relationship:

$$D_e = D_{se} + 2\delta^* = D'_{se} + 2\delta \tag{25}$$

In Fig. 7b the line which is marked "edge of boundary layer" is not meant to indicate the exact shape of the boundary layer. It will be seen from the following analysis that only the value of the boundary layer thickness at the exit of the nozzle is important.

It can be shown that an expression for δ can be written as follows: (See Appendix B)

$$\frac{\delta}{r_e} = \frac{1}{\dfrac{\sqrt{Re_{Dse}}}{\sqrt{2}\,C\sqrt{\cot\frac{\theta}{2}}\sqrt{1-\dfrac{1}{\sqrt{A/A^*}}}} + (1 - B)} \tag{26}$$

The boundary layer thickness has been given as a fraction of the exit radius of the final contour, r_e. This equation involves five unknown quantities, namely, B, C, θ, A/A*, and Re_{Dse}. The angle θ can be selected at some reasonable value, while a specification of the Mach number and γ will determine values for B and A/A*. The quantity C is determined by M and the heat transfer or temperature boundary condition at the nozzle surface.

Finally, a specification of a value for Re_{Dse} will permit the solution of Eq. (26). There is a more direct approach based on a rearranged form of Eq. (26):

$$Re_{Dse} = 2B^2C^2 \cot\frac{\theta}{2} \cdot \left[\frac{\sqrt{A/A^*-1}}{\sqrt{A/A^*}}\right]\left[\frac{1}{B}\left(\frac{1}{\delta/r_e} - 1\right)+1\right]^2 \qquad (27)$$

Although both equations involve the same variables, the use of Eq. (27) permits a specification of a desired value of δ/r_e. Since the boundary layer becomes thicker as the Reynolds number is decreased, there is a minimum value of the Reynolds number for which the boundary layers just meet and close at the nozzle exit section. For this condition there is no isentropic core left in which to place a model. The value of Re_{Dse} for which this condition exists, or δ/r_e is unity, can be written down directly from Eq. (27).

$$(Re_{Dse})_{min} = 2B^2C^2 \cot\frac{\theta}{2}\left[\frac{\sqrt{A/A^* - 1}}{\sqrt{A/A^*}}\right] \qquad (28)$$

It is also evident from Eq. (27) that values of Re_{Dse} can be calculated for any specified values of δ/r_e. An alternate method is to use the following equation:

$$(Re_{Dse}) = (Re_{Dse})_{min} \cdot \left[\frac{1}{B}\left(\frac{1}{\delta/r_e} - 1\right) + 1\right]^2 \qquad (29)$$

The actual boundary layer thickness can be calculated from the following expression (See Appendix B):

$$\delta = \frac{BC^2 \cdot \cot\frac{\theta}{2} \cdot \left[\frac{\sqrt{A/A^* - 1}}{\sqrt{A/A^*}}\right]}{Re/L} \cdot \left[\frac{1}{B}\left(\frac{1}{\delta/r_e} - 1\right) + 1\right] \qquad (30)$$

It will be noted that it is necessary to specify the value of the Reynolds number per unit length. However, this quantity is directly related to the results shown in Figs. 4 and 5 and therefore can be related to a desired operating point for the wind tunnel. The boundary layer thickness corresponding to a value of δ/r_e of unity follows from Eq. (30):

$$(\delta)_{\frac{\delta}{r_e}=1} = \frac{BC^2 \cdot \cot\frac{\theta}{2} \cdot \left[\frac{\sqrt{A/A^*}-1}{\sqrt{A/A^*}}\right]}{Re/L} \tag{31}$$

Boundary layer thicknesses for values of δ/r_e different from unity can be calculated from the following equation which results from combining Eqs. (30) and (31).

$$\delta = (\delta)_{\frac{\delta}{r_e}=1} \cdot \left[\frac{1}{B}\left(\frac{1}{\delta/r_e} - 1\right) + 1\right] \tag{32}$$

Once a value of δ has been calculated the displacement thickness is immediately known from Eq. (23). The exit diameter of the isentropic contour, the exit diameter of the final contour, and the diameter of the isentropic core region in the final contour, can be calculated from the following three equations:

$$D_{se} = \frac{Re_{Dse}}{Re/L} \tag{33}$$

$$D_e = D_{se} + 2\delta^* \tag{34}$$

$$D'_{se} = D_e - 2\delta \tag{35}$$

Some calculated results based on the above analysis will be presented later in this section of the report.

Discussion of Assumptions of Approximate Analysis

Before using the results of the above analysis it is worthwhile to investigate the validity of the assumptions for the case of high-stagnation temperature flows.

The use of a sine-arch velocity profile to solve the integral boundary layer equations has been successful in the solution of laminar boundary layer problems at relatively low stagnation temperatures. Two results of the sine-arch velocity profile assumption will be considered. First, the correlation equation, Eq. (18), has been used to predict the boundary layer thickness. Although the basis for this equation is entirely experimental, there is an implication that the calculated values of the boundary layer thickness from the sine-arch velocity profile analysis agree with the measured values of the boundary layer thickness. Second, the calculated values of the boundary layer thickness, δ, are converted to values of the displacement thickness, δ^*, by the parameter B which does depend on use of the sine-arch velocity profile assumption.

Figure 8 shows values of the parameter B as a function of Mach number and γ. At values of the Mach number near unity the values of B differ only slightly, whereas at a Mach number of 10 there is a factor of 2 between the values of B corresponding to values of γ of 1.1 and 1.667.

Figure 9 shows a comparison of the ratio of boundary layer thickness to displacement thickness for the sine-arch velocity profile assumption and the theoretical values of Romig and Dore (6). The calculations of Romig and Dore were made for the

case of the laminar boundary layer on the flat plate with zero free-stream pressure gradient. Air was used as the working fluid and it was assumed that thermodynamic equilibrium existed at all points in the boundary layer. The effects of dissociation and property variation were included. For a free-stream pressure of one atmosphere and a free-stream temperature of 800 R the theoretical result is in good agreement with the sine-arch predictions at a Mach number of approximately 3 and falls on a curve for γ of 1.3. As the Mach number is increased the points gradually move over to the curve for γ of 1.2. This variation would be expected for the following reason. At a pressure of 1 atmosphere and a temperature of 800 R air is relatively undissociated and would have a value of γ of about 1.38. As the free-stream Mach number is increased, with free-stream static temperature remaining constant, the variation of temperature through the boundary layer would increase since the results shown in Fig. 9 were obtained for a boundary condition at the plate surface corresponding to an insulated plate. The temperature at the plate surface will correspond approximately to the stagnation temperature. Therefore, at a Mach number of about 3, the plate temperature will be about 2300 R. At this temperature and a pressure of 1 atmosphere the value of γ is about 1.3 (See Fig. 6, Reference 5). The average value of γ in the boundary layer must therefore be somewhere between 1.3 and 1.38. At this same free-stream temperature and a Mach number of 6, the adiabatic-wall temperature is about 5000 R and the corresponding value of γ at a pressure of 1 atmosphere is about 1.15. Thus, the data point of Romig and Dore at a Mach number of 6 should fall on

a curve for γ of approximately 1.2 which it does as can be seen from Fig. 9. The data points for free-stream static temperatures between 1575 R and 7000 R are all above the sine-arch prediction for $\gamma = 1.1$. This shift would also be anticipated based on the calculations of Hansen (5). The general conclusion, based on the results shown in Fig. 9, is that the use of the sine-arch velocity profile to calculate the values of the displacement thickness from the boundary layer thickness should be accurate to about 10%. Additional comments on this comparison will be made at the end of this section.

The use of the boundary layer thickness constant C will now be investigated. Figure 10 shows values of C from three different sources. All values are based on theoretical analyses of compressible flow over a flat plate. Two curves from the work of Van Driest (7) are shown. The upper curve corresponds to an insulated flat plate and the lower curve corresponds to the case where the plate surface is cooled to a temperature equal to the free-stream static temperature. Van Driest's solutions were obtained for air and accounted for variable fluid properties although a constant value of γ of 1.4 was used. No considerations of dissociation were involved. The data of Romig and Dore are also shown. Since Romig and Dore did not present their results in terms of the constant C, the boundary layer thicknesses given in Table I of Reference (6) were converted to a dimensionless form using the viscosity equation given in this report and values of the compressibility estimated from Reference (5). The third set of data given in Fig. 10 correspond to the prediction for C from Howarth (8). His result expresses the boundary layer thickness as a function

of Mach number and γ. His equation is as follows:

$$\frac{\delta}{L} = \frac{5.2\left[1 + 0.1987\ (\gamma - 1)\ M^2\right]}{\sqrt{Re_L}} \qquad (36)$$

Howarth's results have been included since they give an expression for the boundary layer thickness in closed form.

It will be seen that for a value of γ of 1.4, the agreement between Howarth's results and the Van Driest solution for adiabatic-wall conditions is good up to a Mach number of approximately 5. However, at a Mach number of 10, there is about a 40% difference in the values of C. The data of Romig and Dore, for a free-stream static temperature of 800 R are in excellent agreement with the Van Driest solution for adiabatic-wall conditions. The data points fall on the Van Driest curve up to a Mach number of 6 and the only other point at a Mach number of about 11 has fallen below the Van Driest curve. The agreement at low Mach numbers is to be expected since the amount of dissociation in the boundary layer is small and both studies took into account variable fluid properties. The fact that the agreement extends up to a Mach number of 6 is interesting in itself, for as has been seen in Fig. 9, the Romig and Dore data for this free-stream static temperature of 800 R deviated from the sine-arch prediction for $\gamma = 1.4$ at a Mach number of 3 and had come into coincidence with the predictions for $\gamma = 1.2$ at a Mach number of 6. Therefore it appears that the ratio of the boundary layer thickness to the displacement thickness is very sensitive to an average value of γ. The boundary layer thickness constant C, on the other hand, seems

to be dependent both on the actual range of fluid properties involved and on an average value of γ. It is also interesting to note that for the case of a free-stream stagnation temperature of 800 R the first amounts of dissociation are not felt until a Mach number of somewhat greater than 6 has been achieved. This can be seen from the plot of the compressibility factor in Fig. 1 of Reference (5). A close inspection of the Romig and Dore data will show that as the free-stream static temperature is increased the deviations from the Van Driest solution occur at successively lower Mach numbers. This observation is also in agreement with the fact that at a higher free-stream static temperature a lower Mach number is required to produce significantly higher amounts of dissociation in the laminar boundary layer. The curve for the Van Driest solution where the wall temperature of the flat plate is maintained equal to the free-stream static temperature has been included since a difference of about a factor of 2 is obtained between the insulated-plate and the cooled-plate cases. If these theoretical results are valid, this means that a much thinner boundary layer can be maintained in the nozzle of the low-density wind tunnel if nozzle wall cooling is employed. Such an approach has been justified theoretically by Chuan (13) and in the operation of his low-density wind tunnel at the University of Southern California he is attempting to verify experimentally the benefits of nozzle wall cooling.

Equation (21) has been used to convert the values of $\bar{C}$ from the wind tunnel data to values of C. In turn, these values

of C have been compared to the Van Driest values in order to verify the use of Eq. (19) in the approximate boundary layer analysis. The viscosity ratio in Eq. (21) was calculated from Eq. (12) using static temperatures obtained at the Mach numbers in Table II. The stagnation temperature for the data of Table II was taken as 85 F and a value of γ of 1.4 was used. The calculated results are given in the last two columns of Table II. The agreement between the experimental values of C and the Van Driest values is excellent up to a Mach number of 4 although there is scatter in the experimental values at this point. The data point at a Mach number of 6 is about 60 percent higher than the Van Driest value. However based on the agreement shown in Table II, Eq. (19) will be used in the approximate boundary layer analysis. Values of C will be taken from various sources, and these sources will be indicated. Additional comments on the values of C given in Table II will be made in the discussion of Fig. 26.

Although the actual processes which occur in the nozzle of the low density wind tunnel will be discussed in more detail in the next main section of this report, a few comments are in order due to our discussion of laminar boundary layer flows on a flat plate. The Van Driest solution represents a case in which a gas of constant composition and variable fluid properties is used in the solution of the boundary layer equations. The Romig and Dore solution represents a case in which a gas of variable composition and variable fluid properties is used. In the latter case, the composition is determined by the requirement that thermodynamic equilibrium exists throughout the flow field. Intermediate between these two extremes and undoubtedly more complex is the case where a

gas is used whose composition is controlled by finite rates of chemical dissociation and recombination and whose fluid properties are also variable. For the ranges of stagnation temperature and pressure which will be encountered in low-density wind tunnels, the flow process in the nozzle will correspond to some combination of equilibrium flow, non-equilibrium flow, and frozen-compositional flow. It is also to be anticipated that the flow will probably freeze shortly after the throat of the nozzle, and hence most of the boundary layer growth in the nozzle will occur under conditions of constant composition but varying fluid properties. The implication of this situation is that perhaps the solutions of Van Driest or solutions of this type will be more realistic than those of Romig and Dore where thermodynamic equilibrium has been assumed. Presently few solutions for non-equilibrium flow conditions over a flat plate exist. Based on this physical picture, the results of Van Driest have been employed throughout the next section on the results of the approximate boundary layer analysis, although the equation of Howarth has been employed to show at least order or magnitude changes in the results due to variation of γ. This decision was based on the fact that most of the expansions to higher Mach numbers are terminated at sufficiently low free-stream static temperatures so as to be close to that temperature used in the Van Driest solution. The principal factor which might invalidate the use of the Van Driest solution is that the actual composition corresponds to a frozen flow situation at a Mach number of about 1 and a static temperature close to the stagnation temperature used in the wind tunnel. If this composition is not radically different from undissociated air, then the use of the Van Driest or

Howarth solutions should lead to fairly accurate results.

The detailed calculations which were made later in this study indicated that the Van Driest values of C are too low at the higher Mach numbers. The best values for C at the present time are given in Fig. 26.

Results of Approximate Boundary Layer Analysis

Fig. 11 shows the minimum exit diameter Reynolds number, Re_{Dse}, (for the isentropic contour) for which the boundary layers just close at the exit plane of the axial nozzle. These results are based on Eq. (28). The angle on the isentropic contour has been selected at 6° (See Fig. 7). This value was selected after inspecting isentropic contours for a variety of nozzles. The sine-arch velocity profile was used to determine the value of B. The Van Driest values for C based on adiabatic-wall conditions were used for one of the curves shown in Fig. 11, while the Howarth values for C were used in the other three curves. The minimum Reynolds number for the Van Driest results varies between 0 and approximately 1600 as the Mach number is increased from 1 to 10. For the same value of γ, namely, 1.4, the Howarth solution shows an increase of the Reynolds number from 0 to approximately 2900 in the same Mach number range. Thus, at a Mach number of 10 there is a difference of almost 2 between the values of the Reynolds number. This is due to the fact that the minimum Reynolds number depends upon C^2 and there is approximately a 40% difference in the values of C given by these two solutions.

At a given Mach number any value of Re_{Dse} greater than that shown on a particular curve in Fig. 11 will produce some region of isentropic flow at the exit section of the actual nozzle.

Figure 12 shows values of Re_{Dse} which are required to produce a given size isentropic flow area. The results in Fig. 12 have been restricted to a value of γ of 1.4 and a nozzle angle of 6°. The Van Driest results for C have been used and the sine-arch profile approximation for B has also been employed. The strong variation of Re_{Dse} with δ/r_e at a given Mach number shows that a rather severe restriction is placed on the wind tunnel designer according to the amount of isentropic core area which is desired.

Figures 13 and 14 show the calculated results for some specific wind tunnel conditions based on the approximate boundary layer analysis. The method of calculating these results was outlined previously in this section. Each figure shows a group of three quantities which are related in a rational manner. In Fig. 13 the exit diameter of the isentropic contour is shown first, then the displacement thickness which must be added to the isentropic contour and finally the actual exit diameter for the nozzle. This procedure is represented by Eq. (34). In Fig. 14 the three quantities which are shown are the actual exit diameter, the boundary layer thickness, and the diameter of the isentropic core. These three quantities are related by the operation represented by Eq. (35).

The assumptions for these calculations are indicated on each figure. The only new condition which must be mentioned is the selection of a specific value for the Reynolds number per unit length. The value for the figures was taken as 10^3 $inches^{-1}$. The form of presentation in Figs. 13 and 14 was

discussed previously relative to the presentation of the required static pressures for specific test section conditions, namely Figs. 4 and 5. This new form has been used since the number of curves which were to be presented would have presented an unintelligible cross-hatching if done in the manner similar to Figs. 4 and 5. The numerical values given Figs. 13 and 14 can be changed as a function of the value of the Reynolds number per unit length by simple proportional scaling. If the Reynolds number per unit length is <u>increased</u> by a factor of 10, all diameters are <u>reduced</u> by a factor of 10, etc. The fact that a proportional scaling with Reynolds number per unit length is involved indicates why the particular value of 10^3 inches^{-1} was used. This can be seen from the values of the actual exit diameters which are encountered for these conditions. If Reynolds numbers per unit length of either 10 or 100 inches^{-1} had been used the actual exit diameters would have become very large.

The exit diameters for the isentropic contours shown in Fig. 13 vary between approximately 0.1 inch and 1.4 inches for the case where the boundary layers just close at the exit plane of the actual nozzle or a value of δ/r_e of unity. As δ/r_e is reduced from unity to 0.8, at Mach number of 10, the exit diameter for the isentropic contour increases from about 1.4 to approximately 7 inches. This factor of 5 was encountered earlier in Fig. 12 where the minimum Reynolds number for the isentropic contour was presented. The displacement thicknesses which must be added to the isentropic contour dimensions are shown in the middle section of Fig. 13. At a Mach number of 10 and a value of δ/r_e of unity the displacement thickness is about 2.9 inches. This means that a radial dis-

placement thickness of 2.9 inches must be added to the exit radius of the isentropic contour which is approximately 0.7 inches. Thus, the displacement thickness is approximately four times the exit radius of the isentropic contour. For a Mach number of 10 and a value of δ/r_e of 0.8 the exit radius of the isentropic contour is about 3½ inches while the displacement thickness is approximately 6½ inches. The actual exit diameter is about 20 inches. Thus, for these latter conditions, the displacement thickness is about twice the exit radius of the isentropic contour. These figures again illustrate that the boundary layers which are encountered in low-density wind tunnel nozzles are appreciable compared with either the isentropic contour dimensions or the actual nozzle contour dimensions. These actual exit diameters are reasonable and represent nozzle dimensions which could be used without overloading either the heater or pumping capacities of most hypersonic flow installations.

Figure 14 shows the actual exit diameter of the nozzle, the boundary layer thickness and the isentropic core diameter at the exit plane of the actual nozzle. The actual exit diameters are those shown in Fig. 13. The values of the boundary layer thickness follow immediately from the actual exit diameters since the curves shown in the middle section of Fig. 14 correspond to specific values of δ/r_e. However, in the actual calculation of the results shown in Fig. 14 the value of δ was calculated from Eq. (30) and a check was made to see that the assumed value of δ/r_e was satisfied. The isentropic core diameter is shown in the third section of Fig. 14 and the values for δ/r_e of unity are obviously zero. For a value of δ/r_e of

0.9 the isentropic core diameter varys from approximately 0.03 inch to about 1.2 inches as the Mach number is varied between 2 and 10. For a higher value of δ/r_e, namely, 0.8, the isentropic core diameter varys between 0.09 inch and about 4 inches over the same Mach number range. The size of the isentropic core is certainly large enough for models of reasonable size.

Conclusions

The results of the approximate boundary layer analysis shown in Figs. 13 and 14 can now be used to draw some conclusions about possible operating ranges and test section conditions for low density wind tunnels. It is obvious that no where in the boundary layer analysis has specific mention been made of nozzle stagnation pressures or temperatures. These numbers actually enter the analysis only as they effect the values of γ and C which are used in the boundary layer analysis and thirdly, as they effect the value of Reynolds number per unit length. It will be seen in the next main section of this report that due to the combination of equilibrium, non-equilibrium and frozen compositional equilibrium flows which are accounted in nozzles of low density wind tunnels that a value of γ of 1.3 perhaps should have been employed. However, conclusions based on a value of γ of 1.4 will not be significantly different from those for a value of γ of 1.3. Since the results shown in Figs. 13 and 14 have been based on a value of the Reynolds number per unit length of 10^3 inches^{-1} it is possible to determine what the allowable operating range for the low density wind tunnel will be. In other words, the Reynolds number per unit length is the important link between the approximate boundary layer analysis and the operating conditions as given in Figs. 4 and 5 or charts similar to these.

In Fig. 4 for a stagnation temperature of 7000 R and Reynolds number per unit length of 10^3 inches^{-1}, it will be seen that a Mach number of 10 the mean-free-path is about 0.02 inch and the static pressure at the nozzle exit is about 80 microns. Thus a model having a characteristic length of 0.02 inch would have a Knudsen number of 1 under these conditions. If the characteristic length was reduced to 0.002 inch, the Knudsen number would increase to 10. Both of these Knudsen numbers are in the transitional flow regime but the model size cannot be called large. In fact, these model sizes are comparable to currently used sizes in low-density wind tunnels.

From Fig. 14 it will be seen that if the exit diameter of the nozzle is about 12 inches, corresponding to the value of δ/r_e of 0.9, then the isentropic core region will have a diameter of approximately 1.3 inches. Thus, both of the model sizes mentioned could be placed in a region of uniform flow at isentropic flow conditions. Obviously, if an exit diameter for the actual nozzle of 120 inches could be tolerated, then the Reynolds number per unit length could be decreased to about a value of 10^2 inches^{-1}. This would increase the mean-free-path to 0.2 inch and the model size would be increased by a factor of 10 keeping the same value of Knudsen number or the model size could be maintained thus increasing the Knudsen numbers by the same factor of 10. The isentropic core region would have a diameter of some 13 inches. Since the size of the isentropic core region is somewhat large compared to the allowable model sizes it is then possible to consider a reduction in the value of δ/r_e that is required. The practical implication of such a reduction is that the exit diameter of some 120

inches can probably be brought down to a more realistic value without changing either the Reynolds number per unit length from 10^2 inches^{-1} or increasing the mean-free-path from 0.2 inch.

It is also possible to speculate on the effects of uncertainties in the approximate boundary layer analysis or in certain methods of boundary layer reduction. For example, a curve was shown in Fig. 10 for C corresponding to a cooled nozzle wall. This curve was lower by a factor of approximately 2 than the curve for C corresponding to the Van Driest adiabatic-wall conditions. Since C centers the expressions for the minimum value of Re_{Dse} and the boundary layer thickness as a squared term, the values shown for lengths in Figs. 13 and 14 would be reduced by approximately 4. It can be estimated that by proper juggling of model size and wall cooling conditions that the Reynolds number per unit length could be driven down to a value of approximately 10 inches^{-1}. Under such conditions, at a stagnation temperature of 7000 R, a mean-free-path of 1 inch would be possible and the static pressure in the test section would be about one micron. Similarly, for a stagnation temperature of 12000R (Fig. 5) the same estimates will be valid. It does not appear that it will be possible to test a model having a characteristic dimension of 0.1 inch in a low-density wind tunnel at high Mach numbers under conditions such that the Knudsen number based on this length is 100!

REAL-GAS EFFECTS IN LOW-DENSITY WIND TUNNELS

Description of Real-Gas Effects

There are two limiting processes by which the characteristics of a nozzle expansion process can be calculated. For states corresponding to a high pressure and low temperature, the gas composition is constant during the expansion process and it is only necessary to account for variations of various thermodynamic properties with temperature. This approximation to a real expansion process is called the frozen-flow approximation. It should be noted that the reference to a frozen condition refers specifically to the composition of a gas. This condition may be accompanied by either variable or constant thermodynamic properties. For states corresponding to a low pressure and a high temperature the gas composition may no longer remain constant throughout the expansion process. If the expansion process is a "gradual" one, then at each section in the nozzle a condition of thermodynamic equilibrium will exist. This approximation to a real expansion process is called the equilibrium-flow approximation. In addition to variable gas composition throughout the nozzle, the thermodynamic properties will also be variable. Both of these limiting approximations are isentropic, and the nozzle expansion process may be calculated independently of a specific nozzle contour. For the ranges of stagnation pressure and stagnation temperature encountered in low-density wind tunnels, it is found that neither of the limiting approximations gives an accurate picture of the nozzle expansion process. Consideration must be given to the actual rates at

which the molecular and atomic species of the gas are dissociating and recombining.

Figure 15 shows schematically the composition and static temperature variations in a hypersonic nozzle. It is assumed that a pure diatomic gas is used. The quantity α is a local mass fraction of gas dissociated and defined as

$$\alpha = \frac{(A)}{(A) + 2(A_2)} \tag{37}$$

where A is the atomic concentration and A_2 is the molecular concentration. Both α and the static temperature ratio are plotted as a function of area ratio based on the throat area of the nozzle. Negative values of the area ratio are upstream of the throat section and positive areas are in the divergent section of the nozzle. The local mass fraction of gas dissociated at stagnation conditions is α_o. For an expansion process in which the chemical dissociation and recombination rates are zero α remains constant along the length of the nozzle at the stagnation state value. This is shown by the upper curve in Fig. 15a. If the nozzle expansion process occurs under thermodynamic equilibrium conditions, then α follows the lower curve in Fig. 15a labeled "infinite reaction rate". Since under the particular conditions involved for this study neither of these approximations will be valid, one must consider the third curve shown in Fig. 15a As the gas passes through the convergent section of the nozzle, the expansion rate is low and the curve for the actual expansion follows closely the curve for the equilibrium-flow approximation. At some point, A on the equilibrium curve the expansion process becomes sufficiently rapid so that the actual rates of dissociation and recombination become controlling. The balance of these rate processes is such as to produce a value of α at any

section of the nozzle which is intermediate between the frozen-flow and the equilibrium flow values. As the nozzle expansion process proceeds, the Point B is reached such that the composition of the gas becomes frozen. The expansion process beyond Point B may be calculated by a frozen-flow approximation. If the actual nozzle exit conditions for the nozzle are located downstream of Section B, it is necessary to consider three distinct processes in the nozzle. The process from the stagnation state to Point A is an infinite-reaction rate or equilibrium-flow process, the process from Point A to Point B is a finite-reaction rate or non-equilibrium-flow process, and the region from Point B to the nozzle exit plane is a zero-reaction rate or frozen-compositional flow process.

Since the static temperature is the flow parameter most affected by the non-equilibrium-flow conditions, it is shown schematically in the lower half of Fig. 15. The upper curve in Fig. 15b corresponds to the equilibrium-flow process. The lower curve in Fig. 15b corresponds to the frozen-flow process starting at stagnation conditions. Two intermediate curves have been shown in Fig. 15b. The lower curve of this pair corresponds to the actual non-equilibrium-flow process and it deviates from the equilibrium curve at Point A as did the curve for α in the upper half of Fig. 15. The remaining curve in Fig. 15b represents an approximation which is often used to the actual non-equilibrium expansion process. A freezing criterion is selected such that based on the equilibrium expansion curve which may be easily obtained, it is possible to predict when "appreciable" freezing has occurred. This defines a Point C on the equilibrium curve and some value of the fraction dissociated. The expansion process downstream of Point C is

assumed to be a frozen compositional flow (corresponding to α_C) and account is usually taken of variable thermodynamic properties during the remainder of the expansion process from Point C. The fourth curve in Fig. 15b corresponds to this approximation to the actual non-equilibrium-flow process. The closeness of the curve for the approximate process to the curve for the actual non-equilibrium-flow process will obviously depend on the accuracy of the freezing criterion, on the size of the increment between α_A and α_B, and on the area ratios between these two points. The theoretical treatments, calculated results, and experimental data on the non-equilibrium-flow processes have been presented in References 20 through 48.

Typical Results

Figures 16, 17, 18 and 19 show the results of calculations for non-equilibrium expansion processes of oxygen in a 15° hyperbolic nozzle (Reference 35).
The first three figures show distribution of composition along the nozzle. The stagnation temperature for these calculations was 5900 K, or approximately 10600 R. Fig. 16 shows the results for a stagnation pressure of approximately 1 atm. For these conditions the oxygen is almost completely dissociated and α_o is 0.9937. The difference between the results for the finite-reaction-rate calculations and the infinite-reaction-rate calculations are quite large. The flow freezes very shortly downstream of the throat at an area ratio of approximately 1.4. After freezing has occurred, the value of α is approximately 0.985. On the other hand, for the equilibrium expansion the value of α has dropped to 0.86 at an area ratio of approximately 2. In Fig. 17 where the stagnation pressure has been raised to 9.4 atm. about 94 percent of the oxygen has been dissociated at

stagnation conditions. For these conditions freezing occurs at an area ratio of approximately 3, and the value of α at freezing is approximately 0.85. Finally in Fig. 18 where the upstream stagnation pressure has been increased to 82 atm. the fraction dissociated at stagnation conditions is about 69 percent. Freezing does not occur until an area ratio of about 10 is reached and the frozen composition corresponds to a value of α of about 0.45. Thus it can be seen that the position of freezing and the composition at the freezing point are strong function of stagnation pressure at this temperature of 5900 K.

The static temperature distributions shown in Fig. 19 are similar to those presented schematically in Fig. 15b. However, the difference in the final static temperature at a given area ratio is illustrated dramatically in a quantitative manner in Fig. 19. At an area ratio of 1000, for example, the static temperature ratio for the equilibrium or infinite-reaction-rate expansion is about 0.45 while that for the frozen expansion process is only 0.05. If the nozzle expansion process is taken to a sufficiently large area ratio, it will be found that the difference in the velocity for the actual nozzle expansion process and the equilibrium expansion process is not large. However, the strong dependency of static temperature on the particular expansion process will produce a greatly different Mach number at a given area ratio due to the dependency of the speed of sound on temperature. The pressures and densities are less dependent on the particular expansion process than is the temperature.

The preceding results for the non-equilibrium flow of oxygen in a hypersonic nozzle are interesting, since they show in a quantitative manner the nature of the non-equilibrium flow process. However, results are available for the non-equilibrium

flow of air in a hypersonic nozzle (20). Some of these results are presented below. The results for a stagnation temperature of 6000 K and a stagnation pressure of 100 atm. have been selected due to their closeness to the desired stagnation conditions for low-density wind tunnels. The nozzle shape is hyperbolic. Although no curves for the composition of the flow are presented, these results are given in a tabular and graphical manner in Reference (20). Figure 20 shows the static temperature ratio versus area ratio for these conditions. Curves for the equilibrium-flow and frozen-flow approximations are shown. For the frozen-flow curve the flow is assumed to be frozen at the throat composition conditions. Two intermediate curves are shown, corresponding to two calculated points for freezing in the nozzle. The relaxation length criteria of Reference (35) has been used to determine several freezing points along the equilibrium-expansion curve. The quantity l is a length which characterizes the nozzle geometry and is the ratio of the half-height of the nozzle at the throat section (in centimeters) divided by the tangent of the nozzle semi-angle (See Reference (20)). The freezing point is shown for two assumed values for l. The curves in Fig. 20 are similar to those shown in Fig. 15b and Fig. 19. The point of departure for either frozen curve from the equilibrium curve corresponds to Point C in Fig. 15a or 15b. Once more it will be seen that at a particular value of the area ratio the value of the static temperature is greatly affected by the prior history of the flow before it reaches a given section. Since most of our past experience with nozzles expansion processes has been based on the concept of some average value of the isentropic exponent for the overall process, three lines of constant γ have been imposed on Fig. 20. Curves for

values of γ of 1.2, 1.3 and 1.4 are shown. For nozzle sections near the throat it will be seen that the equilibrium expansion curves follow a curve for a value of γ of about 1.2. As the expansion proceeds along the nozzle, the equilibrium curve first deviates toward values of γ less than 1.2, then reverses itself toward the curve for 1.2, passes underneath this curve, and eventually reaches values of temperature corresponding to a value of γ of 1.4. This behavior of the curve for the equilibrium process is to be expected in view of the values of γ given in References (5) and (49). The curve for the frozen flow (composition frozen at throat) falls between the two curves for γ of 1.3 and 1.4. Near the throat section the frozen curve is closer to the 1.3 curve, while during the expansion process throughout the remainder of the nozzle, the frozen-equilibrium curve gradually shifts over to the curve for a value of γ of 1.4.

Figure 21 shows some additional details from Fig. 20. Two curves corresponding to values of γ of 1.3 and 1.4 have been drawn starting at the point of departure of the frozen-flow curves from the equilibrium-flow curve. For both frozen flow curves it will be seen that near the point of departure the initial phase of the frozen-flow expansion process is characterized by a value of γ somewhat less than 1.3, and at later stages in the expansion process there is a gradual shift to a curve having a value of γ equal to 1.4. This means that if one follows the nozzle expansion process from the stagnation region to the point of freezing, a variation in γ is observed which has the following general characteristics. For that phase of the expansion process corresponding to an equilibrium expansion,

the values of γ are liable to be about 1.2 or less. As one passes from the equilibrium curve, through the freezing point and along the frozen-flow curve, a discontinuity in the value of γ occurs, such that there is a jump from a fairly low value of 1.2 or less to a value which is closer to 1.3. Following along the frozen flow curve, γ undergoes a gradual transition from 1.3 to 1.4. Obviously, these remarks depend on the particular set of nozzle stagnation conditions and to a certain extent on nozzle geometry. The values of γ for the equilibrium expansion as has been mentioned, are to be expected based on many calculations for air in thermodynamic equilibrium. The values of γ for the frozen flow process are also to be expected in view of the following expressions for γ given in Reference (48). For the case of frozen composition and frozen molecular vibrations, γ should have a value of:

$$\gamma = \frac{7y_m + 5y_a}{5y_m + 3y_a} \tag{38}$$

where y_m is the number of molecules per initial molecule or air and y_a is the number of atoms per initial molecule of air. Equation (38) predicts values of γ between 1.4 and 1.67. On the other hand, if the composition is frozen but the molecular vibrations are in equilibrium, a value of γ given by the following equation is to be expected:

$$\gamma = \frac{9y_m + 5y_a}{7y_m + 3y_a} \tag{39}$$

Equation (39) predicts values of γ ranging from approximately 1.29 to 1.67. Since the results shown in Figs. 20 and 21 were calculated assuming molecular vibrations were in equilibrium, the results of Eq. (39) should apply, and the observed values of γ check those predicted by Eq. (39).

Figure 22 shows the velocity as a function of area ratio for the same nozzle stagnation conditions. Up to an area ratio of 5, at which point the velocity is approximately 10,500 ft/sec, there is no difference between any of the nozzle flow approximation curves. At area ratios above this value, the curves begin to diverge, but it appears that the maximum difference between any of the curves is only of the order of about 10 or 15 percent. Figure 23 shows the Mach number as a function of area ratio. The velocity of sound for these curves has been calculated from the usual equation, namely:

$$a = \sqrt{\left(\frac{\partial p}{\partial \rho}\right)_s} \tag{40}$$

The equation was solved using either the frozen-flow or the equilibrium-flow derivative. The important implication of Fig. 23 is that for a desired value of Mach number a significantly different area ratio is required, once more depending on whether the flow is in equilibrium or frozen. Based on the preceding requirements for low-density wind tunnels, and the approximate boundary layer analysis, it is obvious that the use of a shorter nozzle will produce thinner boundary layers and therefore a wider range of satisfactory operation for the wind tunnel. Figure 24 shows the static pressure ratio for the hypersonic nozzle. Factors of between 2 and 3 are encountered in the static pressure, depending on the actual flow

process in the nozzle. Finally, Fig. 25 shows the density ratio for the nozzle, and it is found that the density is the flow parameter which is least affected by the actual nozzle expansion process.

Conclusions

In view of the ranges of stagnation pressures and temperatures which are required for low-density wind tunnels, it will be necessary to consider chemical kinetic effects and the non-equilibrium flow processes which are produced. Current calculations of non-equilibrium air flows have not been made at stagnation pressures below 100 atm. Based on the results presented earlier in this report, it now appears that these calculations should be extended into the range of stagnation pressure between 0.1 and 100 atm. The range of stagnation temperature which should be considered extends from 3000 K to 10000 K. The detailed curves for the equilibrium, non-equilibrium and frozen-flow processes show that a wide range of values of γ are encountered; namely, from about 1.1 to 1.4. The upper limit of 1.4 was selected based on the calculations presented in this report. However, at higher stagnation temperatures, where larger amounts of dissociation and ionization to monatomic species will be encountered, the upper limit of γ will rise towards 1.67. This range of γ creates somewhat of a dilemma for the nozzle designer. In order to calculate nozzle exit conditions, a value of γ of perhaps 1.4 may be appropriate when used with the upstream stagnation conditions. However, to the nozzle contour designer a value of γ of 1.3 may be more characteristic for an isentropic contour upon which

to base the actual nozzle design. The real solution to this problem is to design nozzles such that the actual thermodynamic processes are connected directly to the isentropic contour design and to any boundary layer correction method which will be employed.

DETAILED NOZZLE CALCULATIONS

Introduction

Although the calculated results from the approximate boundary layer analysis permitted a definition of some allowable operating conditions for low-density wind tunnels, detailed nozzle calculations are required to check on the accuracy of the approximate analysis and to provide final nozzle contours and system performance characteristics for the actual low-density wind tunnels. Three nozzle contours were designed, including appropriate boundary-layer corrections. The isentropic contours for these nozzles were obtained from two different sources, Refs. (50) and (51). Stagnation temperatures of 5500 R, 6730 R, and 12500 R were used. The exit Mach number for all three nozzles was about 10. The boundary layer correction method of Ref. (10) was used, since nozzles designed by this method had shown excellent results in previous experimental tests.

Nozzle Design Procedure

Isentropic contours were obtained from two sources. Reference (50) presents an isentropic contour with an exit Mach number of 10.068. In addition to this contour, nozzle coordinates were obtained from the Sandburg-Serrell Corporation, Ref. (51). The isentropic contour corresponding to an exit Mach number of 10 and a value of γ of 1.2 was used. The details of the boundary layer correction method are given in Ref. (10). Only the important details will be summarized here. The boundary layer thickness, δ, corresponding to flow conditions at any section along the isentropic contour, is made dimensionless using the axial distance between the nozzle throat section and the exit section.

This dimensionless ratio, δ^+, is thus defined as:

$$\delta^+ = \frac{\delta}{L_t} \tag{41}$$

Assuming that the boundary layer correction method has proceeded up to a Section n in the nozzle, the dimensionless boundary layer thickness for the next section is calculated from the following equation:

$$\delta^+_{n+1} = K_1 \delta^+_n - \frac{K_2}{\delta^+_n} \tag{42}$$

The constants K_1 and K_2 are defined by the following equations:

$$K_1 = \frac{(r_s^+ \rho_s^+ u_s^+)_n \left[u^+_{sn}(A_n - B_n - 1) + u^+_{s,n+1} \right]}{(r_s^+ \rho_s^+ u_s^+)_{n+1} \left[u^+_{s,n+1} A_{n+1} - u^+_{sn} B_{n+1} \right]} \tag{43}$$

$$K_2 = \frac{C'(r_s^+ u_s^+)_n \Delta x^+}{Re_{L_t} (r_s^+ \rho_s^+ u_s^+)_{n+1} \left[u^+_{s,n+1} A_{n+1} - u^+_{sn} B_{n+1} \right]} \tag{44}$$

Three of the dimensionless quantities in Eqs. (43) and (44) are defined as follows:

$$r_s^+ = \frac{r_s}{r^*} \tag{45}$$

$$\rho_s^+ = \frac{\rho_s}{\rho_e} \tag{46}$$

$$u_s^+ = \frac{u_s}{u_e} \tag{47}$$

The local radius of the isentropic contour has been made dimensionless using the radius of the isentropic contour at the nozzle throat section. The density and velocity at a given section of the isentropic contour have been made dimensionless based on the exit density and velocity, respectively. The length Reynolds number is defined as:

$$Re_{L_t} = \frac{\rho_e u_e L_t}{\mu_o} \tag{48}$$

Once more it will be noticed that the exit density and velocity have been used along with the viscosity evaluated at stagnation conditions. The dimensionless axial position parameter, x^+, is defined as:

$$\Delta X^+ = \frac{X_{n+1} - X_n}{L_t} \tag{49}$$

The remaining three quantities in Eqs. (43) and (44) are defined as follows:

$$A = \frac{\sqrt{1 + \frac{\gamma - 1}{2} M^2} - 1}{\frac{\gamma - 1}{2} M^2} \tag{50}$$

$$B = \frac{2}{\pi} \frac{\tan^{-1} \sqrt{\frac{\gamma - 1}{2}} M}{\sqrt{\frac{\gamma - 1}{2}} M} \tag{51}$$

$$C' = \frac{\pi}{2} \tag{52}$$

A sine-arch velocity profile in the boundary layer has been employed in solving the integral boundary layer equations.

In order to start the boundary layer calculation at the throat section of the nozzle, it is assumed that the boundary layer growth at this section is zero, or:

$$\frac{d\delta}{dx} = 0 \tag{53}$$

Using this condition and Eq. (42), it is possible to show that the boundary layer thickness at the first two sections along the isentropic contour is given by:

$$\delta_1^+ = \delta_o^+ = \sqrt{\frac{K_2}{K_1 - 1}} \tag{54}$$

Once the boundary layer thickness has been calculated at a given section, the boundary layer displacement thickness can be calculated from the following equation:

$$\delta_n^* = \delta_n^+ L_t (1 - B_n) \tag{55}$$

The actual calculation procedure is carried out as follows. In general the following quantities will have been selected prior to the design of the detailed nozzle contour; namely, the exit Mach number, an isentropic exponent for relating the exit conditions to the stagnation conditions, the stagnation temperature, and either a stagnation pressure or a nozzle exit pressure. The values of pressure will have been estimated through the use of charts similar to Figs. 4 or 5 and 13 or 14. The use of these charts will have given preliminary estimates

for the mean-free-path at the nozzle exit section and will have determined whether or not an isentropic core will exist at the nozzle exit section. The above information can then be used to calculate the following quantities at the nozzle exit plane; namely, static temperature, density, sonic velocity, actual velocity viscosity, Reynolds number per unit length, and mean-free-path.

Since the coordinates for most isentropic contours are given in a dimensionless form, it is necessary to pick at least one important dimension for the isentropic contour. This can be done through the use of the approximate boundary layer analysis and usually the exit diameter for the isentropic contour, D_{se}, will be chosen. Using this dimension, plus the area ratio for the isentropic contour, it is impossible to determine the throat radius and the quantity L_t. At this point all of the information is available for the dimensionless quantities which appear in Eqs. (43) and (44). In addition to the actual coordinates for the isentropic contour, usually values of Mach number are known along the wall of the isentropic contour. Since the flow field for the isentropic contour corresponds to an isentropic flow, these values of Mach number along with the stagnation pressure and temperature permit the calculation of the remaining quantities in Eqs. (43) and (44). A slightly different approach has been taken for the nozzle calculations which will be presented. Rather than employ a value of Mach number given along the wall of the isentropic contour, the radial coordinates at a given section for the isentropic contour have been used to calculate the area ratio, A/A*. The flow has been assumed to be one-dimensional and these area ratios have been used in conjunction with one-dimensional isentropic flow

tables to calculate the required density and velocities in Eqs. (43) and (44). Reference (52) has shown that this approximate method for calculating the isentropic flow parameters does not introduce serious errors into the calculations.

After the boundary layer growth along the nozzle had been calculated, the resulting contour was plotted on large-size graph paper and a smoothing process was employed to remove any bumps or waviness which had been introduced by the calculation procedure. Only the smooth nozzle contour information has been summarized in this report. A somewhat more detailed procedure for designing nozzles for low-density wind tunnels will be discussed later in this section after the calculated results for the detailed nozzle designs have been presented.

Nozzle Design I

The first detailed nozzle calculation was made based on the assumption that nitrogen would be used as the working fluid for a low-density wind tunnel. The stagnation temperature was also maintained at a fairly low value, namely, 5500 R. The use of nitrogen at this temperature led to a set of conditions such that dissociation of the nitrogen was not an important factor. Therefore, it would be possible to avoid non-equilibrium flow effects and to obtain data on rarefied gas flow phenomena without worrying about the complications of real-gas effects. An exit Mach number of 10 was selected, and an exit pressure for the nozzle of 40 microns was used. The pressure was selected based on a figure similar to Fig. 4. The approximate boundary layer analysis showed that there should be some isentropic flow region at the exit of the nozzle. These calculations are given below. At the time this nozzle design was made, only one isentropic con-

tour corresponding to a Mach number of 10 was available (50). The following information was specified:

Nitrogen

$M_e = 10$

$\gamma = 1.4$

$T_o = 5500$ R

$p_e = 40$ microns

For adiabatic flow of a perfect gas, the exit static temperature, T_e, can be calculated as follows:

$$\frac{T_o}{T_e} = 1 + \frac{\gamma-1}{2} M_e^2 = 1 + 0.2\ (10)^2 = 21$$

$$T_e = \frac{5500}{21} = 261.9 \text{ R}$$

Once the static temperature is known, the viscosity and sonic velocity can be calculated as follows:

$$\mu_e = \frac{0.073225 \times 10^{-5}\sqrt{T_e}}{1 + \frac{201.6}{T_e}} = \frac{0.073225 \times 10^{-5}\sqrt{261.9}}{1 + \frac{201.6}{261.9}}$$

$$\mu_e = 0.6695 \times 10^{-5} \text{ lbm/ft-sec}$$

$$a_e = \sqrt{g_o \gamma \frac{\bar{R}}{\bar{W}_o} T_e} = \sqrt{\frac{(32.174)(1.4)(1545.32)(261.9)}{(28)}}$$

$$a_e = 806.9 \text{ fps}$$

From a definition of Mach number the exit velocity, V_e, becomes:

$$V_e = M_e a_e = 8069 \text{ fps}$$

The exit density can be calculated from Eq. (7):

$$\rho_e = \frac{W_o p_e}{Z\bar{R}T_e}$$

The compressibility factor will be taken as 1, since at the temperature involved the amount of dissociation is negligible especially since nitrogen has been used. Therefore the density becomes:

$$\rho_e = \frac{(28)(40)(14.696)(144)}{(760,000)(1545.32)(261.9)} = 7.704 \times 10^{-6} \text{lbm/ft}^3$$

The Reynolds number per unit length can be calculated from the above quantities by the following equation:

$$Re/L = \frac{\rho_e V_e}{\mu_e} = \frac{(7.704 \times 10^{-6})(8069)}{(0.6695 \times 10^{-5})(12)}$$

$$= 773 \text{ inch}^{-1}$$

The mean-free-path at exit conditions is calculated from Eq. (8):

$$\lambda_e = \frac{8}{5}\sqrt{\frac{2\gamma}{\pi}}\frac{M_e}{Re/L} = \frac{8}{5}\sqrt{\frac{2(1.4)}{\pi}}\quad\frac{10}{773}$$

$$= 0.0195 \text{ inch}$$

The results from the approximate boundary layer analysis are as follows. An exit diameter for the isentropic contour, D_{se}, is selected as 4 inches. This value was selected based on the results shown in Fig. 12 since Re_{Dse} will be about 3090 using the calculated Reynolds number per unit length. This should produce a value of δ/r_e somewhat less than 0.9. A check on the isentropic contour (50) will also show that $\theta \sim 6°$ so that Fig. 12 could be used. From the isentropic contour (50) the quantity L_t becomes 38.28 inches. From Eq. (19) the exit boundary layer thickness is:

$$\frac{\delta_e}{L_t} = \frac{C}{\sqrt{\frac{\rho_e V_e L_t}{\mu_e}}}$$

The constant C in Eq. (19) was taken from Fig. 10 corresponding to the Van Driest solution for adiabatic-wall conditions. The value of the constant C is 31.8. Putting this information into the above equation, the boundary layer thickness becomes:

$$\delta_e = \frac{(31.8)(38.28)}{\sqrt{773 \times 38.28}} = \frac{(31.8)(38.28)}{\sqrt{29,600}} = 7.06 \text{ inches}$$

Also, the displacement thickness at the nozzle exit section becomes:

$$\delta_e^* = (1 - B_e)\delta_e$$

$$\delta_e^* = (1 - 0.192)7.06 = 5.70 \text{ inches}$$

TABLE III - CALCULATED RESULTS FOR NOZZLE DESIGN I

T_o = 5500 R Gas-Nitrogen

M_e = 10.068 Isentropic Contour From Reference (50)

p_e = 40 microns γ = 1.4

x(in.)	r_s(in.)	δ^*(in.)	r(in.)	M	u_s^+	ρ_s^+	A	B
0.0000	0.0850	21.920×10^{-4}	0.0872	1.000	0.4182	1323.00	0.4770	0.59861
.0766	.0876	51.911	.0928	1.288	.5114	1019.80	.4641	.57754
.1531	.0927	34.545	.0962	1.518	.5754	809.17	.4527	.55923
.2297	.1003	64.727	.1068	1.756	.6328	628.01	.4402	.53988
.3062	.1105	74.197	.1179	2.002	.6834	479.20	.4269	.51919
.3828	.1224	95.003	.1319	2.238	.7247	368.17	.4141	.49986
.4594	.1360	119.71	.1480	2.469	.7593	284.47	.4017	.48133
.5359	.1513	151.44	.1664	2.695	.7884	221.59	.3897	.46387
.6125	.1658	186.76	.1845	2.887	.8100	179.68	.3797	.44958
.6890	.1811	218.75	.2030	3.073	.8283	147.18	.3704	.43624
.7656	.1964	269.37	.2233	3.244	.8434	122.89	.3630	.42710
.8422	.2108	324.98	.2433	3.394	.8554	105.20	.3549	.41450
.9187	.2253	370.27	.2623	3.536	.8658	91.036	.3483	.40537
0.9953	.2440	426.57	.2867	3.709	.8773	76.567	.3405	.39467
1.072	.2559	479.10	.3038	3.814	.8837	69.065	.3359	.38835
1.148	.2746	541.33	.3287	3.970	.8925	59.407	.3292	.37933
1.225	.2899	669.78	.3569	4.092	.8989	52.919	.3241	.37248
1.378	.3188	821.67	.4010	4.309	.9092	43.266	.3153	.36079
1.531	.3502	1145.1	.4647	4.529	.9185	35.488	.3068	.34958
1.914	.4259	1781.9	.6041	5.005	.9353	23.570	.2897	.32726
2.297	.4998	2425.3	.7423	5.415	.9468	16.905	.2762	.31000
2.680	.5738	3133.7	.8872	5.785	.9555	12.713	.2650	.29579
3.062	0.6443	3902.2	1.0345	6.109	0.9620	10.013	0.2558	0.28426

TABLE III (continued)

x(in.)	r_s(in.)	δ^*(in.)	r(in.)	M	u_s^+	ρ_s^+	A	B
3.445	0.7140	4917.0×10^{-4}	1.2057	6.407	0.9672	8.1079	0.2478	0.27439
3.828	.7778	5737.7	1.3516	6.662	.9711	6.8061	.2414	.26636
4.211	.8381	6618.6	1.5000	6.892	.9744	5.8392	.2358	.25965
4.594	.8942	7555.6	1.6498	7.096	.9770	5.1176	.2310	.25387
4.976	.9486	8524.1	1.8010	7.286	.9793	4.5372	.2268	.24872
5.359	1.0013	9502.9	1.9516	7.463	.9813	4.0638	.2230	.24408
5.742	1.0506	10481	2.0987	7.624	.9830	3.6844	.2196	.24002
6.125	1.0965	11580	2.2545	7.770	.9844	3.3779	.2166	.23645
6.508	1.1416	12592	2.4008	7.909	.9857	3.1116	.2139	.23314
6.890	1.1858	13704	2.5562	8.041	.9869	2.8813	.2113	.23005
7.273	1.2274	14746	2.7020	8.163	.9880	2.6861	.2090	.22730
7.656	1.2691	18635	3.1326	8.283	.9890	2.5099	.2067	.22464
9.570	1.445	25195	3.9645	8.763	.9926	1.9285	.1982	.21458
11.48	1.5785	31216	4.7001	9.102	.9948	1.6131	.1926	.20800
13.40	1.6847	37121	5.3968	9.360	.9963	1.4136	.1885	.20324
15.31	1.774	42541	6.0281	9.568	.9975	1.2738	.1854	.19954
17.23	1.8428	47864	6.6112	9.725	.9983	1.1792	.1831	.19685
19.14	1.8981	52991	7.1972	9.848	.9989	1.1109	.1813	.19478
21.05	1.9406	57357	7.6763	9.941	.9994	1.0621	.1800	.19325
22.97	1.9686	61467	8.1153	10.000	.9997	1.0327	.1791	.19229
24.88	1.9848	65511	8.5359	10.035	.9998	1.0158	.1786	.19174
26.80	1.9941	69047	8.8988	10.055	.9999	1.0060	.1784	.19142
28.71	2.0000	72454	9.2454	10.068	1.0000	0.9999	.1782	.19119
30.62	"	75688	9.5688	"	"	1.0000	"	"
32.54	"	78789	9.8789	"	"	"	"	"
34.45	"	81771	10.1771	"	"	"	"	"
36.37	"	84649	10.4649	"	"	"	"	"
38.28	"	87433	10.7433	"	"	"	"	"

The actual exit radius for the corrected nozzle contour can be calculated from Eq. (34):

$$r_e = r_{se} + \delta^* = 2 + 5.70 = 7.70 \text{ inches}$$

The radius of the isentropic contour is determined by Eq. (35):

$$r'_{se} = r_e - \delta = 7.70 - 7.06 = 0.64 \text{ inch}$$

This means that an isentropic flow region with a diameter of approximately 1.28 inches will be available for test purposes. It will be seen from the actual nozzle calculation that this estimate was over-optimistic.

Table III summarizes the important information for the final nozzle calculation. The radius of the isentropic contour, the displacement thickness, and the radius of the actual contour are given. Values for several flow parameters are also presented including the Mach number distribution for the nozzle. The actual boundary layer displacement thickness at the exit plane of the nozzle is about 8.74 inches. Since the radius at the exit section of the isentropic contour was taken as 2 inches, the actual exit radius for the final nozzle is 10.74 inches. Using Eq. (23) to convert the boundary layer displacement thickness to a boundary thickness, yields a value of the boundary layer thickness of 10.82 inches. The detailed nozzle calculation indicates that there is no isentropic flow region at the exit plane of the nozzle. Therefore, the approximate boundary layer analysis predicted an exit diameter for the isentropic contour which was too small. It is interesting to observe that the boundary layer growth at Mach numbers close to the exit Mach number is extremely rapid. At a position in

the nozzle located halfway between the nozzle throat and the nozzle exit plane, the Mach number is already 9.85, and the boundary layer displacement thickness is 5.3 inches. This value of the displacement thickness should be compared with that given by the approximate boundary layer analysis above. In the downstream half of the divergent section of the nozzle, the Mach number changes from 9.85 to 10.068, a 2 percent change, while the boundary layer displacement thickness changes from 5.3 to 8.74 inches, a 40 percent change. It is worthwhile and important to determine a value of C from the detailed nozzle calculation. This can be done using the equation which defines C:

$$\frac{\delta}{L_t} = \frac{C}{\sqrt{\rho_e V_e L_t / \mu_e}}$$

The value of δ from the detailed boundary layer analysis is used. For the first nozzle design C is 48.8. A later section is devoted to further comments on this value of C, which is considerably higher than that given by the Van Driest results for adiabatic flow shown in Fig. 10.

If this nozzle contour were used in an actual low-density wind tunnel, under the conditions assumed, there would be no region of uniform isentropic flow in which to place a model.

Nozzle Design II

The second detailed nozzle calculation was performed using air as the working fluid. The stagnation temperature and pressure were 6730 R and 17.7 atm, respectively. The exit Mach number for the nozzle was assumed to be 10. Additional isentropic nozzle contours were obtained from the Sandberg-Serrell

Corporation (51). A nozzle contour corresponding to a value of 1.2 was used for the second nozzle calculation. Calculations pertaining to the second nozzle contour were made in a manner identical to those for the first nozzle. The results are summarized in Tables VI and VII.

Table IV gives the nozzle coordinates for the second contour. The boundary layer displacement thickness at the nozzle exit is 14.54 inches. The corresponding boundary layer thickness is 19.50 inches. Since the exit radius for the isentropic contour is only 2 inches, there is no isentropic core region for this second contour. This situation was anticipated by the approximate analysis as can be seen in Table VII. The values for the displacement thickness from the detailed and approximate analyses are 14.54 and 17.42 inches, respectively. For the approximate analysis, a value of C of 25.9 was obtained from the Howarth result, Eq. (36), using a value of ν of 1.2. This value of C predicted values for the boundary layer thicknesses which were too large in comparison to the values from the detailed analyses. The value of C for the detailed analyses was only 21.6. However, the results were sufficiently close enough to each other so that the use of the approximate analyses can be justified.

TABLE IV - CALCULATED RESULTS FOR NOZZLE DESIGN II

T_o = 6730 R Gas-Air

M_e = 10 Isentropic Contour from Reference (51)

p_o = 17.7 atm γ = 1.2

x(in.)	r_s(in.)	δ^*(in.)	r(in.)	M	u_s^+	ρ_s^+	A	B
0	0.0112	0.0006	0.011	1.00	0.3162	100,000	0.4880	0.6166
0.2	.0134	.0013	.014	1.71	.4989	44,660	.4678	.5836
0.4	.0197	.0028	.023	2.41	.6358	16,320	.4430	.5440
0.6	.0298	.0170	.047	3.03	.7256	6,204	.4192	.5076
0.8	.0437	.0200	.064	3.57	.7851	2,646	.3987	.4770
1.0	.0608	.0295	.09	4.03	.8251	1,293	.3817	.4523
1.2	.0811	.0439	.13	4.42	.8530	717	.3678	.4326
1.4	.1043	.0637	.16	4.78	.8747	421	.3556	.4155
1.6	.1300	.0863	.21	5.12	.8924	259	.3445	.4001
1.8	.1579	.1153	.27	5.40	.9050	175	.3357	.3882
2.0	.1878	.1470	.34	5.67	.9160	121	.3275	.3771
2.2	.2194	.1840	.41	5.90	.9244	89	.3209	.3681
2.4	.2523	.2228	.48	6.12	.9318	67	.3146	.3598
2.6	.2863	.2689	.56	6.30	.9374	53	.3097	.3533
2.8	.3210	.3199	.65	6.48	.9426	42	.3049	.3470
3.0	.3562	.3729	.74	6.65	.9472	34	.3004	.3411
3.2	.3914	.4538	.84	6.82	.9515	28	.2961	.3355
3.4	.4266	.5278	.94	6.97	.9551	23	.2924	.3307
3.6	.4616	.5776	1.06	7.13	.9588	19	.2885	.3257
3.8	.4962	.6559	1.18	7.25	.9613	17	.2856	.3219
4.0	.5303	.7320	1.30	7.37	.9639	14.64	.2828	.3184
4.2	.5639	.8069	1.42	7.48	.9661	12.91	.2803	.3151
4.4	0.5968	0.8879	1.56	7.58	.9680	11.53	0.2780	0.3122

TABLE IV (continued)

x(in.)	r_s(in.)	δ^*(in.)	r(in.)	M	u_s^+	ρ_s^+	A	B
4.6	0.6292	0.9700	1.70	7.68	0.9698	10.31	0.2758	0.3094
4.8	.6608	1.0500	1.82	7.77	.9715	9.325	.2738	.3069
5.0	.6918	1.1435	1.96	7.85	.9729	8.544	.2720	.3046
5.2	.7222	1.2282	2.10	7.94	.9744	7.744	.2701	.3022
5.4	.7519	1.3103	2.26	8.01	.9756	7.181	.2686	.3003
5.6	.7810	1.3932	2.40	8.08	.9767	6.659	.2671	.2985
5.8	.8095	1.4980	2.56	8.14	.9776	6.244	.2658	.2969
6.0	.8374	1.5901	2.70	8.21	.9787	5.796	.2644	.2950
6.2	.8648	1.6865	2.86	8.27	.9796	5.440	.2632	.2935
6.4	.8915	1.7685	3.00	8.33	.9805	5.107	.2619	.2919
6.6	.9177	1.8480	3.16	8.38	.9813	4.847	.2609	.2907
6.8	.9433	1.9422	3.30	8.42	.9819	4.649	.2601	.2897
7.0	.9684	2.0394	3.46	8.47	.9826	4.413	.2591	.2884
7.8	1.0638	2.7628	4.04	8.68	.9855	3.56	.2550	.2833
8.6	1.1516	3.2060	4.62	8.83	.9874	3.05	.2522	.2798
9.4	1.2325	3.6423	5.16	8.97	.9892	2.66	.2495	.2764
10.2	1.3071	4.0889	5.70	9.09	.9906	2.36	.2473	.2737
11.0	1.3758	4.6796	6.22	9.20	.9919	2.12	.2453	.2713
11.8	1.4392	5.0403	6.70	9.33	.9933	1.86	.2430	.2685
12.6	1.4976	5.3982	7.18	9.40	.9941	1.75	.2418	.2670
13.4	1.5513	5.7757	7.65	9.45	.9946	1.66	.2409	.2659
14.2	1.6008	6.1765	8.10	9.51	.9952	1.57	.2398	.2646
15.0	1.6462	6.6660	8.54	9.57	.9959	1.49	.2388	.2634
15.8	1.6878	7.1229	8.96	9.63	.9965	1.41	.2378	.2620
16.6	1.7259	7.5074	9.36	9.68	.9970	1.34	.2370	.2610
17.4	1.7606	7.7843	9.76	9.73	.9975	1.28	.2361	.2600
18.2	1.7923	8.1035	10.16	9.75	0.9977	1.26	0.2358	0.2596

TABLE IV (continued)

x(in.)	r_s(in.)	δ^*(in.)	r(in.)	M	u_s^+	ρ_s^+	A	B
19.0	1.8210	8.3669	10.54	9.77	0.9979	1.23	0.2354	0.2592
19.8	1.8469	8.9288	10.90	9.82	.9983	1.18	.2346	.2581
20.6	1.8703	9.2511	11.28	9.85	.9986	1.15	.2341	.2576
21.4	1.8912	9.6431	11.63	9.87	.9988	1.13	.2338	.2572
22.2	1.9098	9.9186	11.97	9.89	.9990	1.11	.2335	.2567
23.0	1.9263	10.2494	12.30	9.91	.9992	1.09	.2332	.2563
23.8	1.9408	10.6730	12.62	9.93	.9994	1.07	.2328	.2559
24.6	1.9533	10.9103	12.92	9.95	.9996	1.05	.2325	.2555
25.4	1.9641	11.2085	13.22	9.96	.9996	1.04	.2323	.2554
26.2	1.9733	11.5000	13.50	9.97	.9997	1.03	.2322	.2552
27.0	1.9809	11.7806	13.78	9.98	.9998	1.02	.2320	.2549
27.8	1.9872	12.1695	14.04	9.984	.9999	1.015	.2319	.2547
28.6	1.9922	12.3004	14.30	9.988	.9999	1.01	.2319	.2547
29.4	1.9961	12.4750	14.54	9.992	.9999	1.01	.2318	.2547
30.2	1.9990	12.7650	14.76	9.996	1.0000	1.005	.2317	.2546
31.0	2.0010	13.0074	15.00	10.0	"	1.000	"	"
31.8	2.0023	13.2481	15.24	"	"	"	"	"
32.6	2.0031	13.4874	15.48	"	"	"	"	"
33.4	2.0035	13.7246	15.72	"	"	"	"	"
34.2	2.0037	13.4596	15.95	"	"	"	"	"
35.0	2.0038	14.1912	16.19	"	"	"	"	"
35.8	2.0038	14.4194	16.42	"	"	"	"	"
36.2	2.0038	14.5417	16.54	"	"	"	"	"

Nozzle Design III

The third detailed nozzle calculation was made using air as a working fluid. The stagnation temperature and pressure were 12500 R and 89 atm, respectively. An exit Mach number of 10 was selected, and an isentropic contour corresponding to a value of γ of 1.2 was used (51). The calculations for the third nozzle were made as shown for the first nozzle and the results are given in Tables VI and VII.

Table V summarizes the nozzle coordinates for this third nozzle. It will be seen that the exit displacement thickness and the boundary layer thickness from the detailed calculation are 9.47 and 12.72 inches, respectively. Since the exit radius for the isentropic contour was taken as 2 inches, once more the isentropic flow area does not exist at the exit of the nozzle. For this third contour the approximate boundary layer analysis also predicted the absence of the isentropic flow region. However, as previously encountered in the second nozzle design, values for the displacement thickness from the approximate and the detailed calculations are very close to each other. The value of the displacement thickness from the approximate analysis at the nozzle exit plane was 11.27 inches while the detailed calculation gave a value of 9.47 inches. The value of the constant C corresponding to the detailed calculation was 21.9 as compared to the Howarth value of 25.9. Note that the values of C from the detailed analyses of the second and third nozzles are approximately equal.

Summary

Some of the important results from the three detailed nozzle calculations have been summarized in Tables VI and VII. The

general operating characteristics for the low-density wind tunnels using the three nozzles are given in Table VI, where the important test section conditions have been presented along with some of the tunnel requirements such as flow rate, heating requirements, and so forth. The equations and discussion of these requirements are given in the section of this report entitled, "Components for Low-Density Wind Tunnels". As the stagnation temperature was increased, at a constant value of Mach number, the exit velocity increased from about 8000 to 15000 ft/sec. Since a different value of γ was used for two of three nozzles, the static pressure requirements do not follow a regular pattern. In general, static pressures between 7 and 40 microns are required. The mean free path at test section conditions varies between approximately 0.01 and 0.313 inch.

Table VII summarizes the boundary layer calculations from the approximate and from the detailed calculations. Consider the first detailed nozzle design for a value of ν of 1.4. It will be seen that the use of the Van Driest value of C for adiabatic-flow conditions resulted in a value of the boundary layer thickness which was only 65 per cent of that obtained from the accurate boundary layer analysis. Instead of the Van Driest value of C of 31.8, a value of C of 48.8 would be required to explain the value of boundary layer thickness from the detailed analysis. An indication that such a large difference might be expected was given by the information in Table II, where values of C from existing low-density wind tunnels were compared with the values from the Van Driest adiabatic-wall solution. Although the experimental data only extend up to a Mach number of 6, at this Mach number the experimental

value was about 1.5 times larger. The values for C from Table II and from the first nozzle design at a Mach number of 10 have been plotted in Fig. 26, together with values from the Van Driest adiabatic-wall solutions and the Howarth solution It will be seen that the suggested use of the Van Driest solution is fairly accurate at Mach numbers of about 2, whereas as the Mach number is gradually increased into the hypersonic range, the difference between the Van Driest solution and the average curve through the existing experimental and theoretical data for a value of γ of 1.4 continues to increase until at a Mach number of 10, the difference is about 60 percent. It will be seen that the predictions from the Howarth solution for a value of γ of 1.4 are in much better agreement with the mean curve for this same value of γ than those from the Van Driest solution. Thus the mean curve is available for values of C when γ is 1.4 and the Howarth solution may be used as a close approximation.

The values of C from the second and third detailed nozzle designs are also shown in Fig. 26. Since these designs correspond to a value of γ of 1.2 the Howarth solution for this value has also been shown. The closeness of the results at a Mach number of 10 add support to the use of the Howarth solution for obtaining values of C for the approximate boundary layer analysis when experimental data or detailed calculations are absent.

TABLE V - CALCULATED RESULTS FOR NOZZLE DESIGN III

T_o = 12500 R Gas-Air

M_e = 10 Isentropic Contour from Reference (51)

p_o = 89 atm. γ = 1.2

x(in.)	r_s(in.)	δ^*(in.)	r(in.)	M	u_s^+	ρ_s^+	A	B
0	0.0112	0.0004	0.011	1.00	0.3162	100,000	0.4880	0.6166
0.2	.0134	.0009	.013	1.70	.4966	45,260	.4682	.5842
0.4	.0197	.0018	.024	2.42	.6374	16,068	.4426	.5434
0.6	.0298	.0120	.038	3.03	.7256	6,204	.4192	.5076
0.8	.0437	.0132	.058	3.57	.7851	2646	.3987	.4770
1.0	.0608	.0193	.083	4.03	.8251	1293	.3817	.4523
1.2	.0811	.0287	.112	4.42	.8530	717	.3678	.4326
1.4	.1043	.0416	.146	4.78	.8747	421	.3556	.4155
1.6	.1300	.0563	.186	5.12	.8923	259	.3445	.4001
1.8	.1579	.0752	.232	5.40	.9050	175	.3357	.3882
2.0	.1878	.0959	.290	5.67	.9159	121	.3275	.3771
2.2	.2194	.1196	.360	5.90	.9244	89	.3209	.3681
2.4	.2523	.1448	.420	6.12	.9318	67	.3146	.3598
2.6	.2863	.1747	.480	6.30	.9373	53	.3097	.3533
2.8	.3210	.2079	.540	6.48	.9426	42	.3049	.3470
3.0	.3562	.2423	.620	6.65	.9472	34	.3004	.3411
3.2	.3914	.2948	.690	6.82	.9515	28	.2961	.3355
3.4	.4266	.3304	.760	6.97	.9551	23	.2924	.3307
3.6	.4616	.3636	.850	7.13	.9588	19	.2885	.3257
3.8	.4962	.4135	.930	7.25	.9614	17	.2856	.3219
4.0	.5303	.4666	1.02	7.37	.9638	14.64	.2828	.3184
4.2	.5639	.5148	1.11	7.48	.9660	12.91	.2803	.3151
4.4	0.5968	0.5670	1.20	7.58	0.9679	11.53	0.2780	0.3122

TABLE V (continued)

x(in.)	r_s(in.)	δ^*(in.)	r(in.)	M	u_s^+	ρ_s^+	A	B
4.6	0.6292	0.6172	1.29	7.68	0.9698	10.31	0.2758	0.3094
4.8	.6608	.6724	1.38	7.77	.9714	7.325	.2738	.3069
5.0	.6918	.7326	1.48	7.85	.9728	8.544	.2720	.3046
5.2	.7222	.8028	1.57	7.94	.9744	7.744	.2701	.3022
5.4	.7519	.8630	1.67	8.01	.9755	7.181	.2686	.3003
5.6	.7810	.9293	1.76	8.08	.9767	6.659	.2671	.2985
5.8	.8095	.9935	1.86	8.14	.9776	6.244	.2658	.2969
6.0	.8374	1.0637	1.96	8.21	.9787	5.796	.2644	.2950
6.2	.8648	1.1340	2.06	8.27	.9796	5.440	.2632	.2935
6.4	.8915	1.2072	2.16	8.33	.9805	5.107	.2619	.2919
6.6	.9177	1.2805	2.27	8.38	.9813	4.847	.2609	.2907
6.8	.9433	1.3548	2.37	8.42	.9818	4.649	.2601	.2897
7.0	.9684	1.4300	2.47	8.47	.9826	4.413	.2591	.2884
7.8	1.0638	1.7311	2.86	8.68	.9854	3.56	.2550	.2833
8.6	1.1516	2.0321	3.27	8.83	.9873	3.05	.2522	.2798
9.4	1.2325	2.3332	3.68	8.97	.9890	2.66	.2495	.2764
10.2	1.3071	2.6393	4.06	9.09	.9905	2.36	.2473	.2737
11.0	1.3758	3.0376	4.43	9.20	.9917	2.12	.2453	.2713
11.8	1.4392	3.2719	4.79	9.33	.9932	1.86	.2430	.2685
12.6	1.4976	3.5047	5.13	9.40	.9940	1.75	.2418	.2670
13.4	1.5513	3.7499	5.46	9.45	.9945	1.66	.2409	.2659
14.2	1.6008	4.0103	5.77	9.51	.9952	1.57	.2398	.2646
15.0	1.6462	4.3290	6.07	9.57	.9958	1.49	.2388	.2634
15.8	1.6878	4.6260	6.36	9.63	.9964	1.41	.2378	.2620
16.6	1.7259	4.8760	6.64	9.68	.9969	1.34	.2370	.2610
17.4	1.7606	5.0559	6.90	9.73	.9974	1.28	.2361	.2600
18.2	1.7923	5.2665	7.16	9.75	.9976	1.26	.2358	.2596
19.0	1.8210	5.5739	7.42	9.77	0.9977	1.23	0.2354	0.2592

TABLE V (concluded)

x(in.)	r_s(in.)	δ^*(in.)	r(in.)	M	u_s^+	ρ_s^+	A	B
19.8	1.8469	5.7975	7.68	9.82	0.9982	1.18	0.2346	0.2581
20.6	1.8703	6.0011	7.90	9.85	.9985	1.15	.2341	.2576
21.4	1.8912	6.2557	8.15	9.87	.9986	1.13	.2338	.2572
22.2	1.9098	6.4352	8.39	9.89	.9988	1.11	.2335	.2567
23.0	1.9263	6.6499	8.62	9.91	.9990	1.09	.2332	.2563
23.8	1.9408	6.9251	8.84	9.93	.9992	1.07	.2328	.2559
24.6	1.9533	7.0797	9.05	9.95	.9993	1.05	.2325	.2555
25.4	1.9641	7.2733	9.26	9.96	.9994	1.04	.2323	.2554
26.2	1.9733	7.4630	9.46	9.97	.9996	1.03	.2322	.2552
27.0	1.9809	7.6451	9.64	9.98	.9997	1.02	.2320	.2550
27.8	1.9872	7.9250	9.92	9.984	.9997	1.015	.2319	.2549
28.6	1.9922	8.0097	9.98	9.988	.9997	1.01	.2319	.2547
29.4	1.9961	8.1225	10.15	9.992	.9998	1.01	.2318	"
30.2	1.9990	8.3195	10.32	9.996	.9999	1.005	.2317	"
31.0	2.0010	8.4762	10.47	10.0	1.0000	1.000	"	"
31.8	2.0023	8.6323	10.63	"	"	"	"	"
32.6	2.0031	8.7874	10.79	"	"	"	"	"
33.4	2.0035	8.9410	10.95	"	"	"	"	"
34.2	2.0037	9.0931	11.10	"	"	"	"	"
35.0	2.0038	9.2434	11.25	"	"	"	"	"
35.8	2.0038	9.3912	11.40	"	"	"	"	"
36.2	2.0038	9.4662	11.47	"	"	"	"	"

TABLE VI - TUNNEL REQUIREMENTS AND TEST SECTION CONDITIONS FOR DETAILED NOZZLE DESIGNS

Nozzle	Gas	γ	p_o atm	T_o R	M_e -	p_e microns	T_e R	V_e fps	λ_e inch	R_e/L
I	Nitrogen	1.4	2.2	5500	10	40	262	8070	0.0195	773
II	Air	1.2	17.7	6730	10	7.6	612	11,200	0.313	44.6
III	Air	1.2	89.0	12,500	10	38	1136	15300	0.131	106

Nozzle	D_{se} inch	D^* inch	D_e inch	w lbm/sec	q kw	S_p liters/sec
I	4	0.1744	10.7433	0.00540	9.2	20,000
II	4	0.022	16.54	0.00061	1.4	27,000
III	4	0.022	11.47	0.00200	10.0	32,000

TABLE VII - EXIT SECTION BOUNDARY LAYER RESULTS FROM APPROXIMATE AND DETAILED CALCULATIONS

Nozzle	D_{se} Inch	δ^* Inch	D_e Inch	δ Inch	D'_{se} Inch	C -
DETAILED CALCULATIONS:						
I	4	8.74	21.48	10.82	-0.16	48.8[3]
II	4	14.54	33.08	19.50	-5.92	21.6[3]
III	4	9.47	22.94	12.72	-2.50	21.9[3]
APPROXIMATE CALCULATIONS:						
I	4	5.70	15.40	7.06	+1.28	31.8[1]
II	4	17.42	38.84	23.35	-7.86	25.9[2]
III	4	11.27	26.54	15.12	-3.70	25.9[2]

1. From Fig. 10, Van Driest Adiabatic-Wall Values
2. From Howarth, Eq. (36)
3. Values from $(\delta/L_t) = C/\sqrt{\rho_e V_e L_t/\mu_e}$ using values of δ from detailed calculation

SUGGESTED DESIGN PROCEDURE FOR LOW-DENSITY WIND TUNNELS

In view of the results of the approximate and detailed analysis, it is possible to identify a design procedure for low-density wind tunnels. It is assumed that at the start of the design two quantities are specified:

T_o - stagnation temperature

M_e - nozzle exit Mach number

Equation (27) should be used to determine values of Re_{Dse} as a function of δ/r_e.

$$Re_{Dse} = 2B^2C^2\cot\frac{\theta}{2}\left[\frac{\sqrt{A/A^*}-1}{\sqrt{A/A^*}}\right]\left[\frac{1}{B}\left(\frac{1}{\delta/r_e}-1\right)+1\right]^2 \quad (27)$$

Starting with a value of δ/r_e of unity and selecting subsequent values based on a fine increment, i.e., 0.98, 0.96, etc., a series of values of Re_{Dse} can be obtained. There are two reasons for using a fine increment. First, the size of the nozzle grows very rapidly as the increment is increased and the sizes, therefore, may become ridiculous. Secondly, the use of a fine increment will yield a sufficient amount of data on the expected isentropic flow diameter, D'_{se}, so that a decision can be made when this region has achieved a size so that uncertainties in the approximate analysis will not cause it to vanish when the detailed calculation is made. The remaining quantities in Eq. (27) are to be selected as follows:

1. Isentropic Exponent, γ - The value of γ in Eq. (27) is used to relate thermodynamic properties at the Mach number M_e to stagnation conditions. Thus from the various plots given in this report on nozzle

expansion processes it is obvious that the values of γ will vary between 1.1 and 1.67. Limiting the discussion to expansions to high Mach numbers, i.e. 10 or greater, it appears that for tunnels using air at stagnation pressures in the range from 1 to 100 atmospheres and stagnation temperatures around 5000K, a value of γ of about 1.4 should be used in Eq. (27). For a diatomic gas, the ease with which the gas can be dissociated will exert a strong influence on the value of γ. At a given pressure and temperature, oxygen may be in a monatomic form while nitrogen may be mostly in a diatomic form. In the general case it will be necessary to make calculations on the real expansion processes and from these deduce a value of γ.

2. B - Equation (24) should be used with the known values of γ and M_e.

3. θ - A value of 6° seems representative for most isentropic contours.

4. A/A* - Values of the area ratio follow immediately from the known values of γ and M_e.

5. C - The average curve given in Fig. 26 should be used for low-density wind tunnels using air in the range of stagnation pressures and temperatures mentioned. For other gases, detailed nozzle designs must be done before the values of C are available. Based on the results shown in Fig. 26, it appears that the Howarth solution, Eq. (36), will predict reasonable values for C.

Values of the Reynolds number per unit length should now be selected and the actual diameters and boundary layer thicknesses should be calculated from the following results:

$$D_{se} = Re_{Dse}/(Re/L) \tag{33}$$

$$\delta_e = \frac{BC^2 \cot\frac{\theta}{2}\left[\frac{\sqrt{A/A^*}-1}{\sqrt{A/A^*}}\right]}{(Re/L)} \cdot \left[\frac{1}{B}\left(\frac{1}{\delta/r_e}-1\right)+1\right] \tag{30}$$

$$\delta_e^* = \delta_e(1 - B_e) \tag{23}$$

$$D_e = D_{se} + 2\delta_e^* \tag{34}$$

$$D'_{se} = D_e - 2\delta_e \tag{35}$$

The results should then be inspected in order to obtain the lowest possible value of Re/L. This minimum value will yield the largest mean-free-path and will allow the use of the largest model at a given Knudsen number. In general, the largest nozzle size will be selected. The isentropic flow region must be sufficiently large and the nozzle must be compatible with facility supply systems and budgets.

The test section pressure and mean-free-path and the stagnation pressure can now be calculated from the following results:

$$\frac{Re}{L} = \frac{M_e}{\mu_e} p_e \sqrt{\frac{W_o}{\bar{R} T_e} \cdot \frac{\gamma}{Z_e}} \tag{11}$$

$$p_o = p_e \left[1 + \frac{\gamma-1}{2} M_e^2\right]^{\frac{\gamma}{\gamma-1}} \tag{56}$$

$$\lambda_e = \frac{8}{5}\sqrt{\frac{2\gamma}{\pi}} \cdot \frac{M_e}{(Re/L)} \tag{8}$$

The facility requirements can be calculated from Eqs. (57), (58), and (61).

Detailed calculations for the nozzle can now be made. Due to the variation of the isentropic exponent in the frozen-flow expansion from the nozzle throat, an isentropic contour for the nozzle should be calculated taking into account the variation of thermodynamic properties. Once this contour has been determined, it is possible to calculate the actual nozzle expansion process for this particular contour using present data on the dissociation and recombination rates. This check on the isentropic contour design will reveal the point in the expansion process at which freezing actually occurs and will indicate whether a new isentropic contour should be designed. The boundary layer corrections can then be calculated using either the method of this report or based on the results of several papers which appeared in the literature after this study had been completed; namely, Refs. (53), (54), and (55). In the event that the approximate analysis had been overoptimistic, in the prediction of the boundary layer thicknesses, it may be necessary to repeat the isentropic contour and boundary layer calculations until a sufficiently large core of isentropic uniform flow is produced at the nozzle exit section.

COMPONENTS FOR LOW-DENSITY WIND TUNNELS

There are three important components for low-density wind tunnels which have not been considered thus far in this report. These components are the heater, the precooler, and the low-pressure vacuum source for the wind tunnel. Although time was not available for a complete study of these components, some comments can be made based on some rather simple and accurate calculations.

Mass Flow Rate Requirements

The calculations of nozzle expansion processes for air over the stagnation temperature and pressure ranges of interest indicate that the expansion process from the stagnation state to the nozzle throat will be an equilibrium-flow process. The isentropic exponent for these processes will have values of about 1.2 or less. The compressibility factor will be about 1.25 for stagnation pressures between 1 and 100 atmospheres if the stagnation temperatures do not exceed about 6500 K. (See Fig. 1, Ref. 5) The choked flow rate can be calculated using the usual expression for one-dimensional flow of a perfect gas:

$$\frac{w}{A^*} = \sqrt{\frac{g_o W_o}{\bar{R} Z_o}} \sqrt{\gamma \left(\frac{2}{\gamma+1}\right)^{\frac{\gamma+1}{\gamma-1}}} \quad \frac{14.7\, p_o}{\sqrt{T_o}} \qquad (57)$$

where
- w - lbm/sec
- A^* - in^2
- g_o - 32.174 lbm ft/lbf sec^2
- $\bar{R}$ - 1545.32 ft lbf/lbm-mole R
- p_o - atmospheres
- T_o - R

The differences between the choked flow rates from the equilibrium-air calculations and those from Eq. (57) using "appropriate" values for γ and Z_o will not exceed a few percent. Choked flow rates were calculated for values of γ of 1.1, 1.2, 1.3 and 1.4. Values of T_o and p_o were selected and then the corresponding value of Z_o was obtained from Reference (56).

The results are shown in Fig. 27 for $\gamma = 1.2$. It was found that for other values of γ, the choked flow rates were about 6% higher for $\gamma = 1.4$ and 3% lower for $\gamma = 1.1$. The mass flow rate per unit throat area has been given for an obvious reason. At a stagnation temperature of 3000R the mass flow rate varies between 0.135 and 135 lbm/sec-in^2 over the stagnation pressure range from 1 to 1000 atmospheres. At a higher stagnation temperature of 14000R the flow rates are lower by a factor of about two. At a constant value of stagnation pressure, the mass flow rate should not depend on $T_o^{1/2}$ since Z_o is also a function of stagnation temperature. For a similar reason the mass flow rate should not necessarily be a linear function of p_o although for the range of variables shown in Fig. 27, the predicted linear behavior is observed at all but highest values of stagnation temperature.

In order to use the results shown in Fig. 27 specific operating conditions for the wind tunnel must be selected. From Fig. 13 the exit diameter for the isentropic contour is 1.36 inches if an exit Mach number of 10 is required. Since a value of γ of 1.4 was used to relate the nozzle exit state to the stagnation conditions, the area ratio of the nozzle, A/A*, is 536, D* is 0.0587 inch and the throat area is 0.00271 inch^2. This diameter corresponds to the minimum exit diameter of the isentropic contour or the closing of the boundary layers at the

exit of the nozzle, i.e., $\delta/r_e = 1$. Since it was based on the Van Driest values for the boundary layer growth constant, C, some adjustment should be made for the differences in C shown in Fig. 26. From Eqs. (28) and (33) it will be seen that the diameter depends on C^2. At a Mach number of 10 the Van Driest value for C is about half the recommended value shown in Fig. 26. The throat diameter should be increased by a factor of 4 and the throat area should be increased by a factor of 16. The new values of these quantities then become 0.235 inch and 0.0434 $inch^2$. These dimensions must now be related to other tunnel conditions. A value of the Reynolds number per unit length of 10^3 $inch^{-1}$ from Fig. 13 must be retained. For a stagnation temperature of 12,000R (Fig. 5) the static pressure at the nozzle exit is about 170 microns. This value was fixed by the specified values of M, Re/L and γ. From Fig. 6 the stagnation pressure must be 9.35 atmospheres. Finally, the values of p_o and T_o fix the mass flow rate in Fig. 27 at about 0.55 lbm/sec-in^2. The required mass flow rate is 0.0238 lbm/sec.

Requirements for Heater

The minimum power requirements for the heater can be calculated from the steady-flow energy equation:

$$\frac{q}{A^*} = \left(\frac{w}{A^*}\right) \quad (h_o - h_a) \tag{58}$$

The mass flow rates per unit area were taken from Fig. 27. The values of h_o were taken from Reference (56). The term h_a was evaluated at 70F. The results are shown in Fig. 28 where the heater power is given as kw/in^2.

At the highest stagnation temperatures and pressures, the heater power is about 100,000 kw/in^2. Since throat areas between 0.01 and 0.1 in^2 are to be expected, the heater power requirements are probably in the range from 1000 to 10,000 kilowatts. For the example given in the first section, the stagnation conditions of 9.35 atmospheres and 12,000 R require a heater power per square inch of about 3000 kw/in^2 and the throat area of 0.0434 in^2 results in a heater power of about 130 kilowatts.

Requirements for Precooler

The exact requirements for the precooler will be determined by the specific type of exhaust system which is employed. The use of a cryogenic pumping system does impose some obvious restrictions. Presently, the largest cryogenic unit being built has a capacity of 1300 watts. The lowest heater requirements (for the use of air) are about 100 kw/in^2 (Fig. 29) and for throat areas between 0.01 and 0.10 in^2, the heater power inputs become 1000 to 10,000 watts. These results indicate that the precooler for a low-density wind tunnel using a single cryogenic pumping unit must have a capacity equal to the heater power input and any compressor power which is involved. Calculations were made for air which showed that the compressor power was several orders of magnitude smaller than the heater power. In view of the heater requirements and the capacity of future cryogenic pumping units, it appears that the precooler must always have the capacity just mentioned. The design of the precooler must also be such that the pressure drop is made compatible with the cryogenic unit.

If a steam-ejector system is used, then the specifications for the precooler are indeterminate until the characteristics of the ejector system are known. The precooler could be a surface-to-gas heat exchanger whose capacity was adjusted to yield satisfactory operation of the ejector. The operating point would be determined when enough heat was removed from the gas stream so that the ejector performance was still acceptable and when the precooler pressure drop was matched with the wind tunnel and ejector characteristics. The design of a precooler with a sufficiently low pressure drop may be difficult or impossible to achieve. The precooler might also be a spray-tube cooler in which cooling water is introduced into the gas stream. In this case a suitable operating point is achieved when the total flow rate of gas and coolant is matched to the ejector characteristics and any pressure drop restrictions have been met.

Requirements for Exhaust System

Some remarks have already been made on the exhaust systems. The cryogenic system cannot tolerate any heat load other than that required to condense the gas. The maximum capacity of a single unit is about 1300 watts. Since the enthalpy change for air between the saturated vapor and saturated solid states at low temperatures is about 9 Btu/lbm, the mass flow rate capacity of a single unit, with no additional heat load, is about 0.14 lbm/sec. This number, together with the information given in Fig. 27, then define the allowable throat sizes for low-density wind tunnels using this single cryogenic unit.

A final quantity of interest is the volume flow rate at nozzle exit density. This quantity is:

$$\frac{S_p}{A^*} = \frac{(w/A^*)}{\rho_e} \tag{59}$$

$$= \left(\frac{w}{A^*}\right) \frac{Z_e \bar{R} T_e}{p_e W_o} \tag{60}$$

Using Eq. (57) the following expression is obtained:

$$\frac{S_p}{A^*} = \sqrt{\gamma \left(\frac{2}{\gamma+1}\right)^{\frac{\gamma+1}{\gamma-1}}} \sqrt{\frac{g_o \bar{R}}{Z_o W_o}} \quad Z_e \cdot \frac{\rho_o}{\rho_e} \cdot \sqrt{T_o} \tag{61}$$

For the calculations the following values were used:

$$\gamma = 1.2$$
$$Z_o = 1.1$$
$$Z_e = 1.0$$

The volume flow rate depends on the stagnation temperature and the exit Mach number through the density ratio. A value of γ of 1.4 was used to determine the density ratio since this value is more characteristic of the overall nozzle expansion process. The value of γ of 1.2 was used for the process between the stagnation state and the nozzle throat. The results are shown in Fig. 29. At the higher Mach numbers the volume flow rates approach one million liters per second per square inch. Whether viewed from a mass flow rate or a volume flow rate basis, the requirements for a steam-ejector system are enormous.

CONCLUSIONS

The most critical component in future low-density wind tunnels which are designed to operate at high stagnation temperatures is the nozzle. These nozzles will be operated with stagnation temperatures between 3000 and 10000 K and with stagnation pressures between 0.1 and 100 atmospheres. Due to this combination of pressures and temperatures, the actual expansion process in the nozzle will consist of three regions: the expansion process from the stagnation state to some section downstream of the throat will be an equilibrium-flow process in which the chemical reaction rates may be considered as infinite. For some distance downstream of the throat a second region will be encountered in which the rates of dissociation and recombination are important. This will be a nonequilibrium-flow region in which the chemical kinetic processes must be considered. The last stage of the nozzle expansion process will be a frozen flow process in which the composition of the gas mixture will be constant but in which the thermodynamic properties may be either variable or constant. It will be found that a particular value of the isentropic exponent will be required to relate the nozzle exit section conditions to the nozzle stagnation conditions, while an average or varying value of the isentropic exponent will be required to describe the actual nozzle expansion process.

An approximate boundary layer analysis has been developed which can be used to predict feasible operating ranges for low-density wind tunnels. The results of this analysis lead to information on the nozzle stagnation pressure, temperature, and

nozzle sizes for isentropic contours which will produce various sizes of uniform isentropic flow at the nozzle exit section. In order to utilize the approximate boundary layer analysis, it is necessary to have a knowledge of the boundary layer velocity profile, a value of γ to describe the expansion process between the nozzle stagnation state and the nozzle exit section, and a value of boundary layer growth constant, C. The sine-arch velocity profile has been used previously in the design of low-density wind tunnel nozzles and was used in this report. The actual nozzle expansion processes which will be encountered in low-density wind tunnels are such that values of the isentropic exponent between 1.1 and 1.67 are to be expected. Values of the boundary layer growth constant, C, have been obtained from existing experimental data for low-density wind tunnels up to a Mach number of about 6, while beyond this Mach number an extrapolated curve is available (Fig. 26). Values of C at a Mach number of 10 were determined by detailed calculations during this study.

Based on the approximate boundary layer analysis, it is possible to determine the required static pressure at the exit of the nozzle and hence the stagnation pressure for the wind tunnel. The mean-free-path at the exit of the nozzle can also be calculated, and this information can be used to determine the allowable ranges of model size and Knudsen number which can be produced by the tunnel. It is also possible to calculate the power requirements, mass flow rates, and exhaust system requirements for the tunnel.

After the approximate analyses have been completed, a detailed nozzle design must be made in which an isentropic contour is generated using the variable thermodynamic properties which

characterize the actual nozzle expansion process. The boundary layer correction calculations can then be made based on the analysis given in this report or upon publications which were made after the completion of this study.[53],[54],[55]

One of the most important conclusions of this study is related to the future applications of low-density wind tunnels. It does not appear that it will ever be possible to utilize "large" models in low-density wind tunnels under conditions such that Knudsen numbers corresponding to free-molecular-flow conditions can be generated. Such conditions are deemed as being impossible due to the huge size of a low-density wind tunnel which would be required. A large model is considered to be one whose characteristic dimension is approximately 1 inch. The future of low-density wind tunnels should be devoted to testing the largest possible models which can be used under conditions in the slip and transition flow regimes. The use of large models will permit the highest possible accuracy for measurements in these flow regimes. Such accuracy is required in the development of the theoretical bases for these flow regimes. The main effort on research in the free-molecular-flow regime should be devoted to basic studies of the surface-particle interaction phenomena. Once more a large amount of highly accurate data is required for the surface-particle interaction phenomena in order to improve the theoretical bases for these phenomena which are presently in poor condition. This study has also pointed out the need for the use of gases other than air in high-stagnation hypervelocity low-density wind tunnels. An understanding of the basic processes which are involved between a rarefied gas stream and a model in the

slip, transition and free-molecular-flow regions is difficult enough to obtain without the complications which arise from effects such as a nonequilibrium flow condition. The use of gases other than air or other dissociating gases would allow a research effort to separate out those effects which are peculiar to rarefied gas dynamics and those effects which are peculiar to high-temperature physical phenomena.

RECOMMENDATIONS

Based on the results of this study, it is possible to make the following recommendations for future work on the design of low-density wind tunnels.

Additional calculations should be made on the actual nozzle processes which will be encountered in low-density wind tunnels, since present calculations of this type exist only down to stagnation pressures of 100 atmospheres. The calculations should be extended to stagnation pressures in the range from 0.1 to 100 atm. The stagnation temperature range should be between 3000 and 10000 K. A survey of available data on the dissociation and recombination rates for air and for the gases of which air is comprised should be made. Such a survey is required, since considerable effort is being made at the present time to determine these rates, and new data are becoming available at a high rate. In addition to air, other gases should be investigated; particularly those which will not show large effects of non-equilibrium-flow phenomena.

Isentropic nozzle contours for low-density wind tunnels should be designed based on a variable isentropic exponent. Some procedures already exist to account for this effect; however, they have not been developed to the point where they are readily usable for rapid calculations. Some consideration should also be given to the design of nozzle contours when non-equilibrium-flow conditions are encountered.

A review should be made of accurate boundary layer correction techniques for use in high-temperature, low-density nozzles. The method of Reference 10 was used in this report; however, additional work (53), (54), (55), came out after the completion

of this study and these new methods should be investigated. Comparisons should be made between the results predicted by the different methods and some conclusions drawn as to whether the state of the art is now acceptable or whether further work is required. In relation to the accurate boundary layer correction techniques, it should be mentioned that a study should also be made of the integral boundary layer equations when dissociation, ionization, and so forth, are present. Although a solution of the boundary layer equations using the integral method are highly developed for incompressible and low-speed flows, additional work is required when dissociation effects, etc., are present. Existing data and theoretical predictions for boundary layer separation in low-density wind tunnel nozzles should be incorporated into the design of nozzles.

The approximate boundary layer analysis which was developed in this report is an extremely useful tool for determining feasible operating ranges for low-density wind tunnels. It is also useful in preliminary nozzle design estimates. However, it is obviously lacking one important ingredient; namely, information on the boundary layer growth constant, C. Additional experimental data at the higher Mach numbers was presented in References (53) and (55), but at a time so that they could not be used in this report. These new experimental data should be incorporated into Fig. 26 as a check against the detailed boundary layer calculations which were made in this study to see how the new data fall relative to the low-stagnation temperature data taken at low Mach numbers. The above studies on non-equilibrium flows, isentropic contours, and boundary layer correction techniques will also provide information on the constant, C, and the entire concept of the approximate boundary layer analysis.

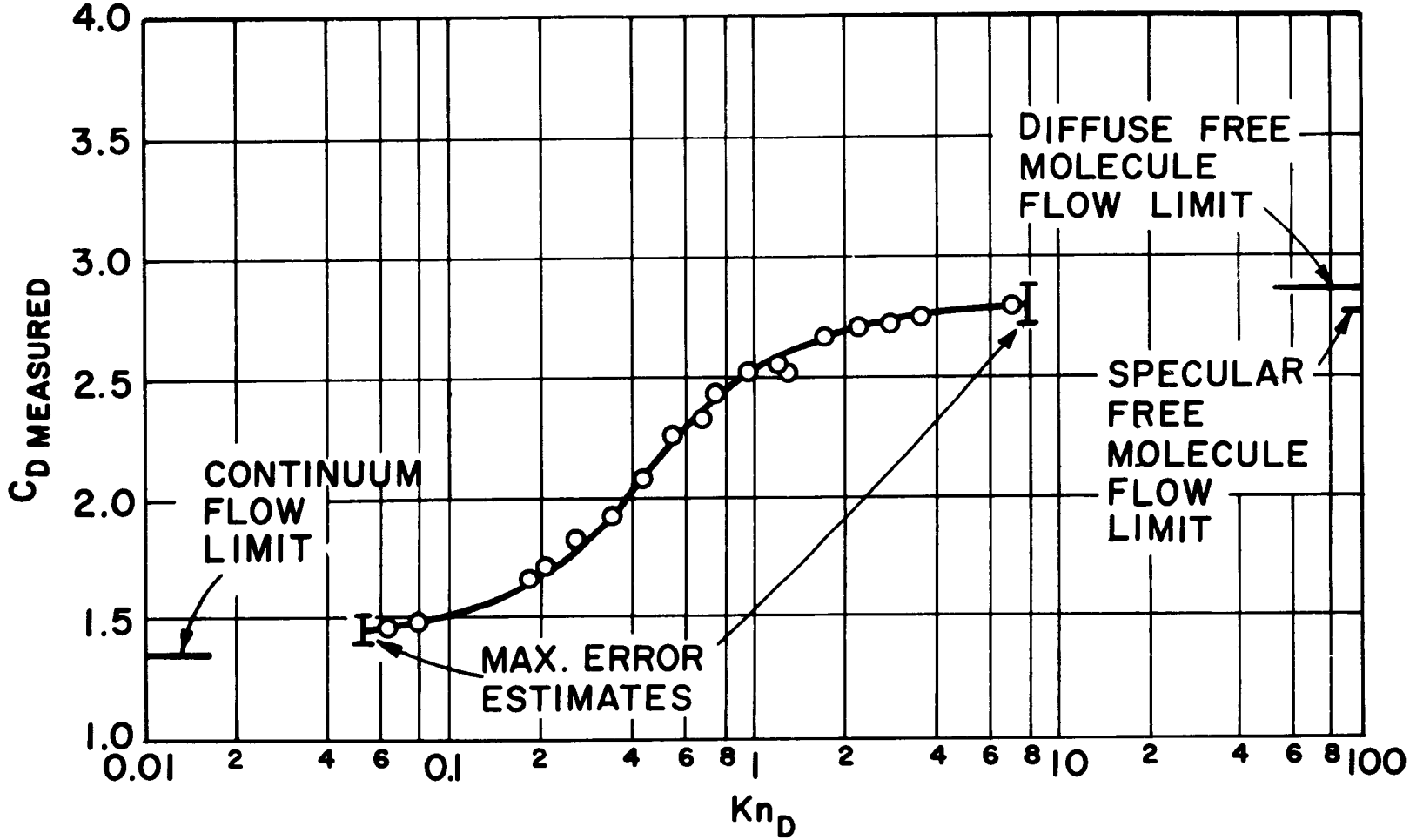

FIG. 1 - DRAG COEFFICIENT ON A CYLINDER AT M=5.92 UNDER RAREFIED GAS FLOW CONDITIONS (FIG. 4 OF REFERENCE 2)

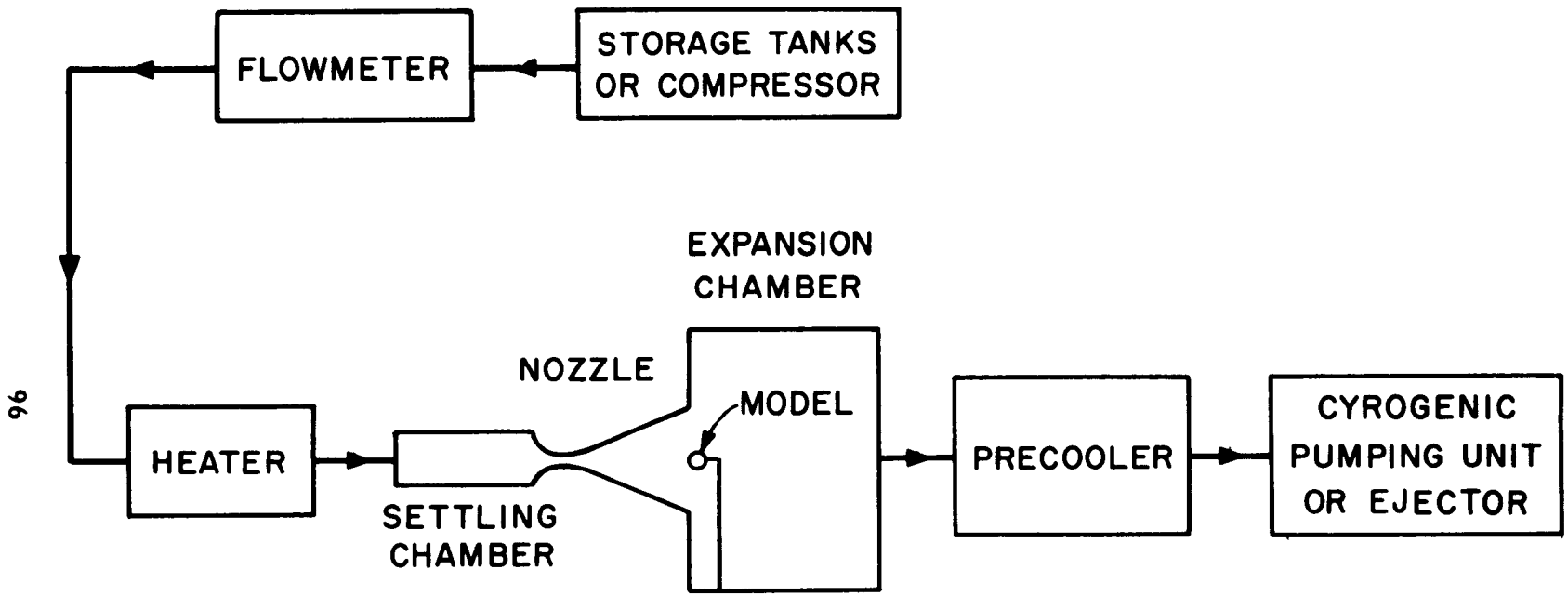

FIG. 2 - SCHEMATIC OF LOW-DENSITY WIND TUNNEL

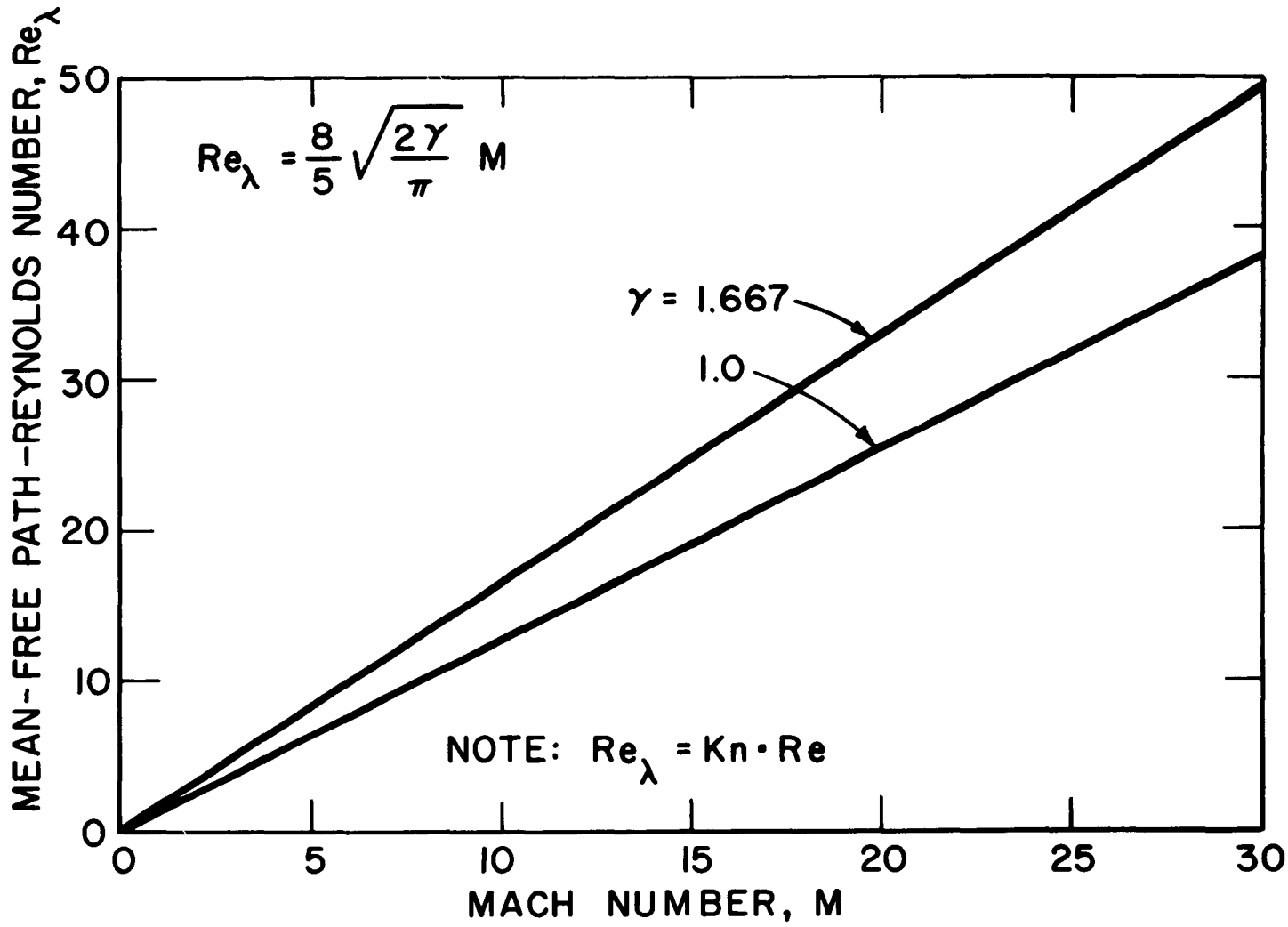

FIGURE 3 REYNOLDS NUMBER REQUIREMENTS FOR LOW-DENSITY WIND TUNNELS

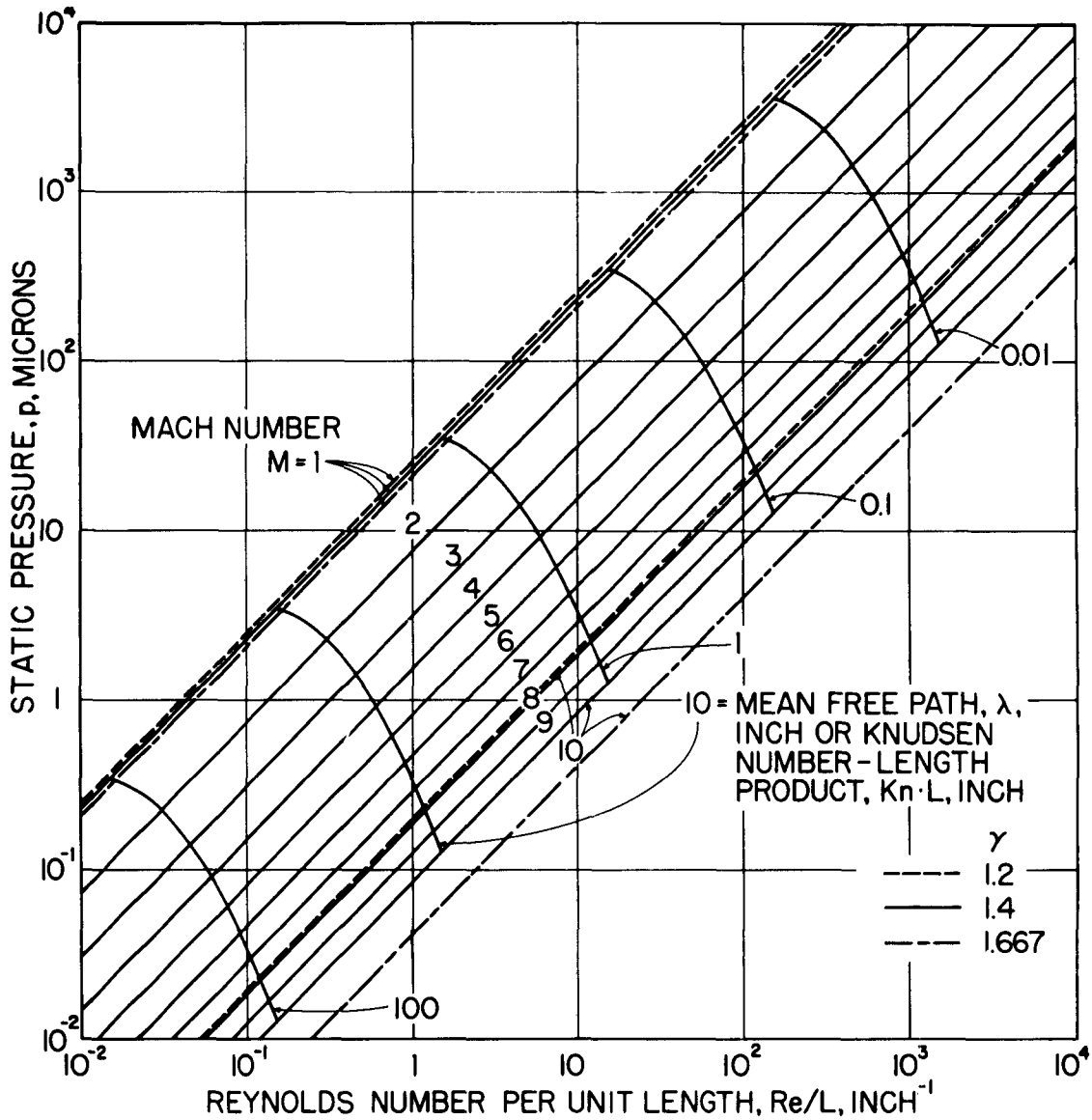

FIGURE 4 - VARIATION OF PRESSURE WITH MACH NUMBER, REYNOLDS NUMBER AND KNUDSEN NUMBER FOR AIR, $T_o = 700^0R$

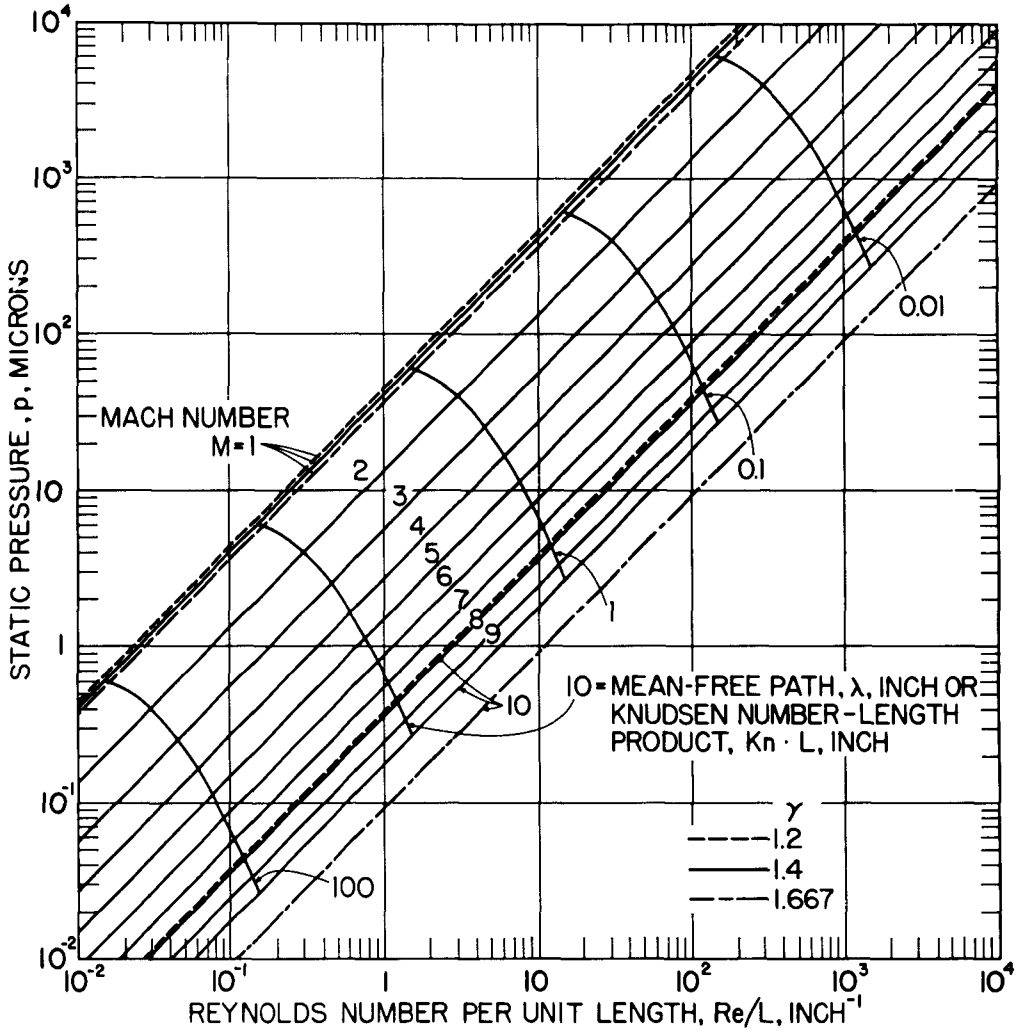

FIGURE 5 - VARIATION OF STATIC PRESSURE WITH MACH NUMBER, REYNOLDS NUMBER AND KNUDSEN NUMBER FOR AIR, T_o = 12000R

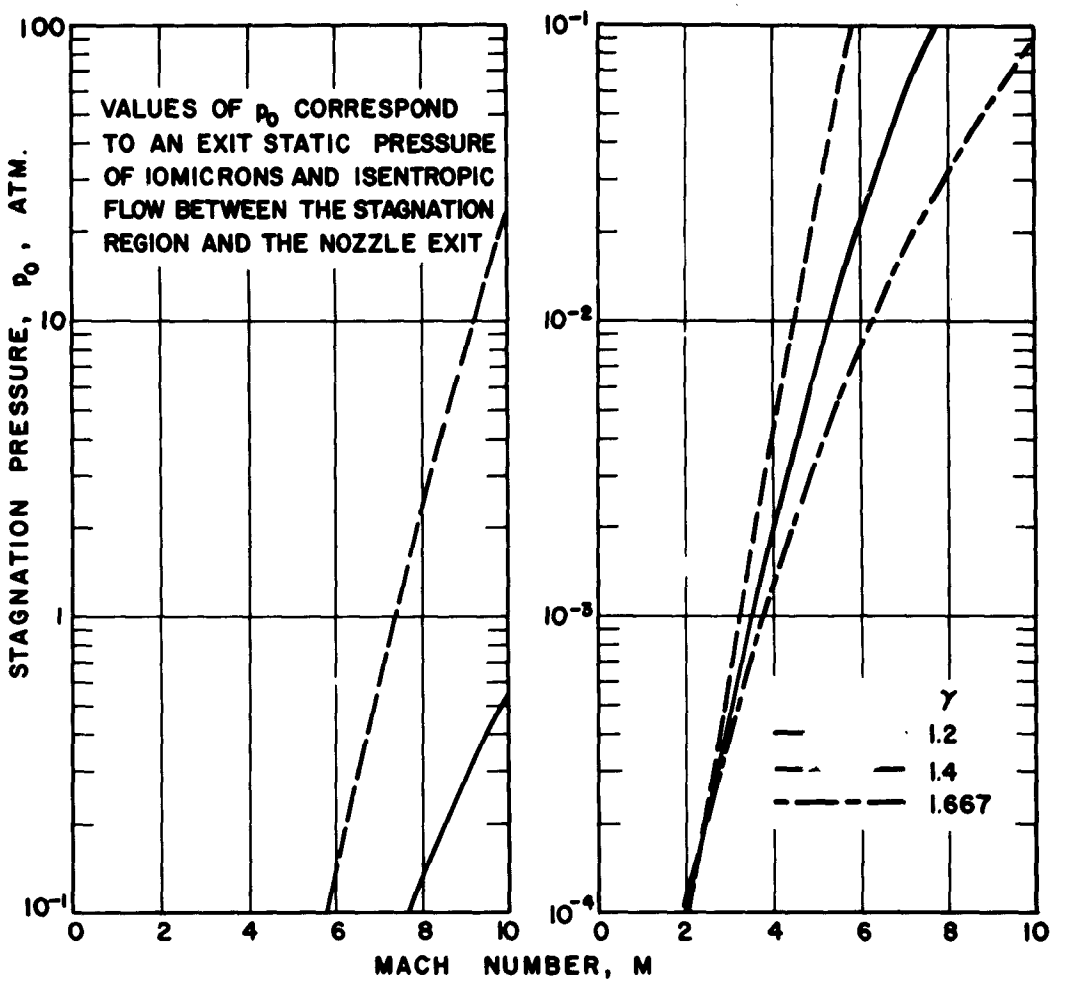

FIGURE 6 NOZZLE STAGNATION PRESSURE REQUIREMENTS

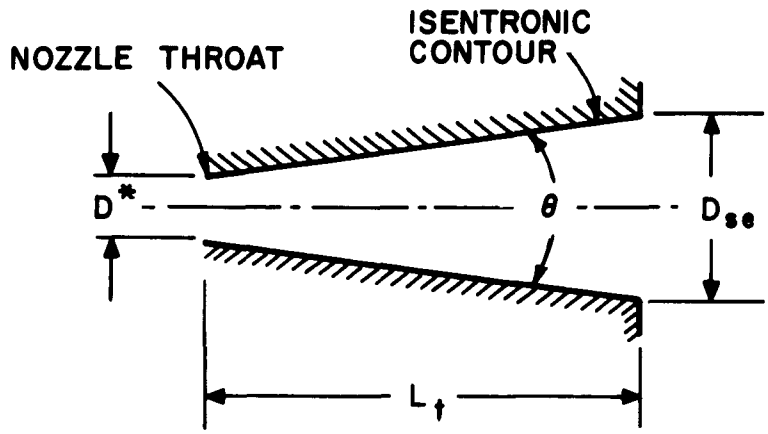

(a) ISENTROPIC NOZZLE CONTOUR

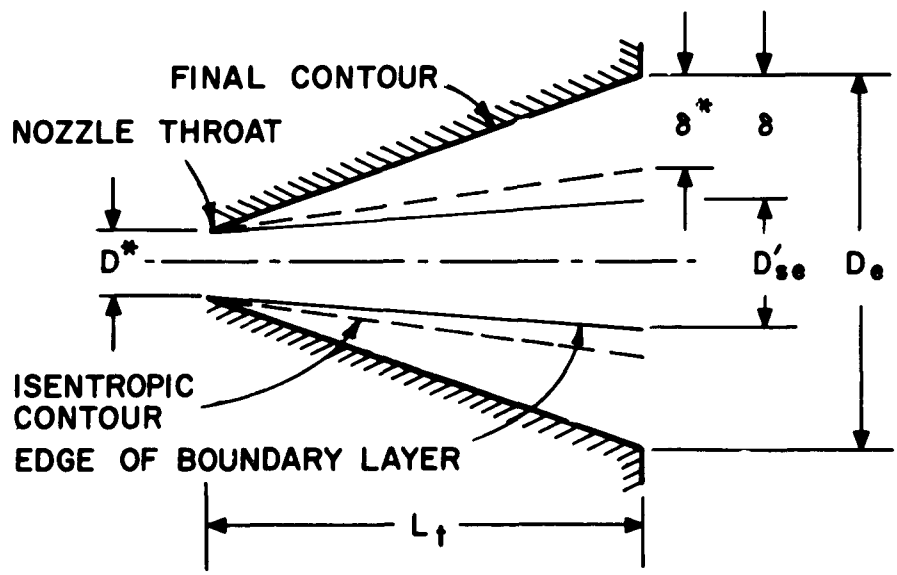

(b) FINAL NOZZLE CONTOUR - CORRECTED FOR BOUNDARY LAYER GROWTH

δ^* - BOUNDARY LAYER DISPLACEMENT THICKNESS
δ - BOUNDARY LAYER THICKNESS (99% OF FREE-STREAM VELOCITY)
D_{se} - EXIT DIAMETER OF ISENTROPIC CONTOUR
D'_{se} ACTUAL EXIT DIAMETER OF ISENTROPIC CORE
D_e - ACTUAL EXIT DIAMETE OF FINAL CONTOUR
D^* - THROAT DIAMETER

FIG. 7 - NOMENCLATURE FOR APPROXIMATE BOUNDARY LAYER ANALYSIS

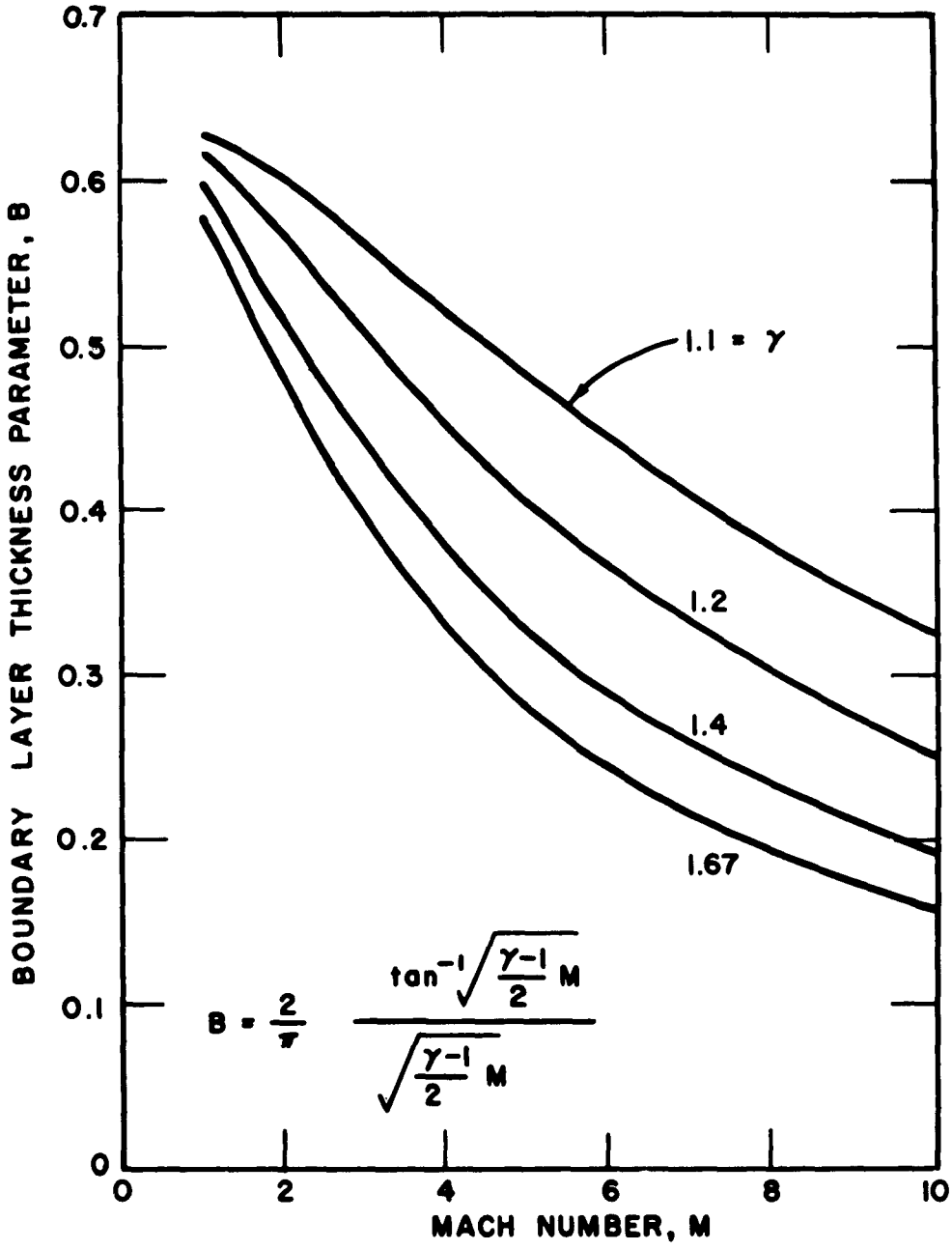

FIGURE 8 BOUNDARY LAYER THICKNESS PARAMETER FOR A SINE-ARCHVELOCITY PROFILE

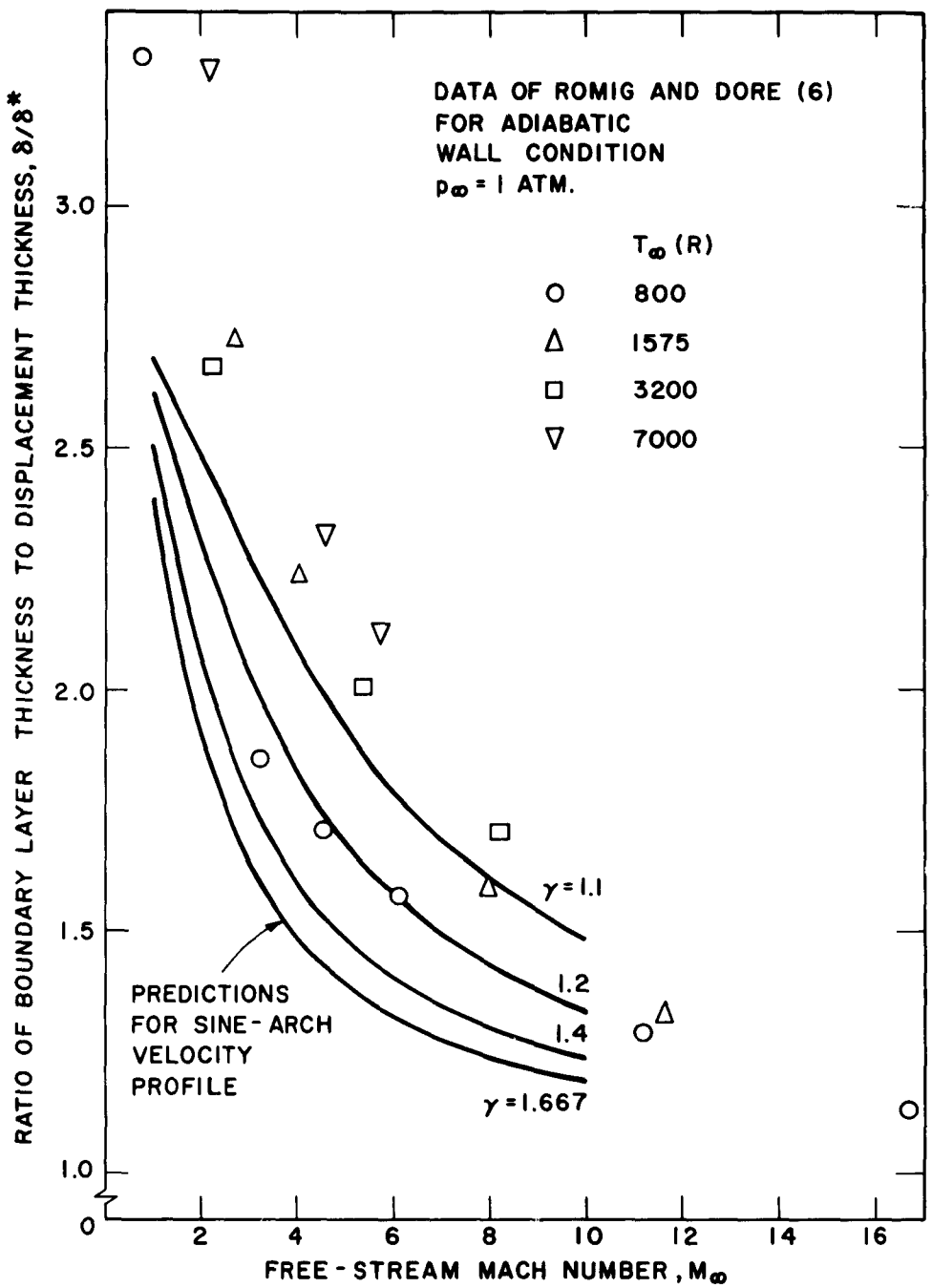

FIG. 9 - COMPARISON OF LAMINAR BOUNDARY LAYER THICKNESS FOR SINE-ARCH VELOCITY PROFILE AND FLAT PLATE SOLUTIONS

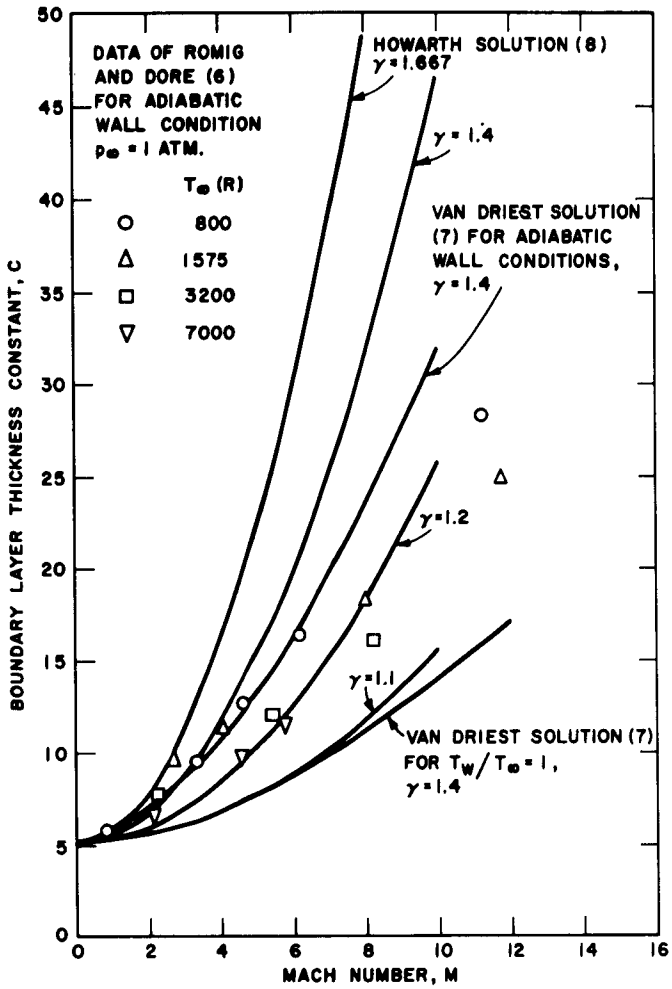

FIG. 10 - LAMINAR BOUNDARY LAYER THICKNESS CONSTANT FOR COMPRESSIBLE FLOW OVER A FLAT PLATE

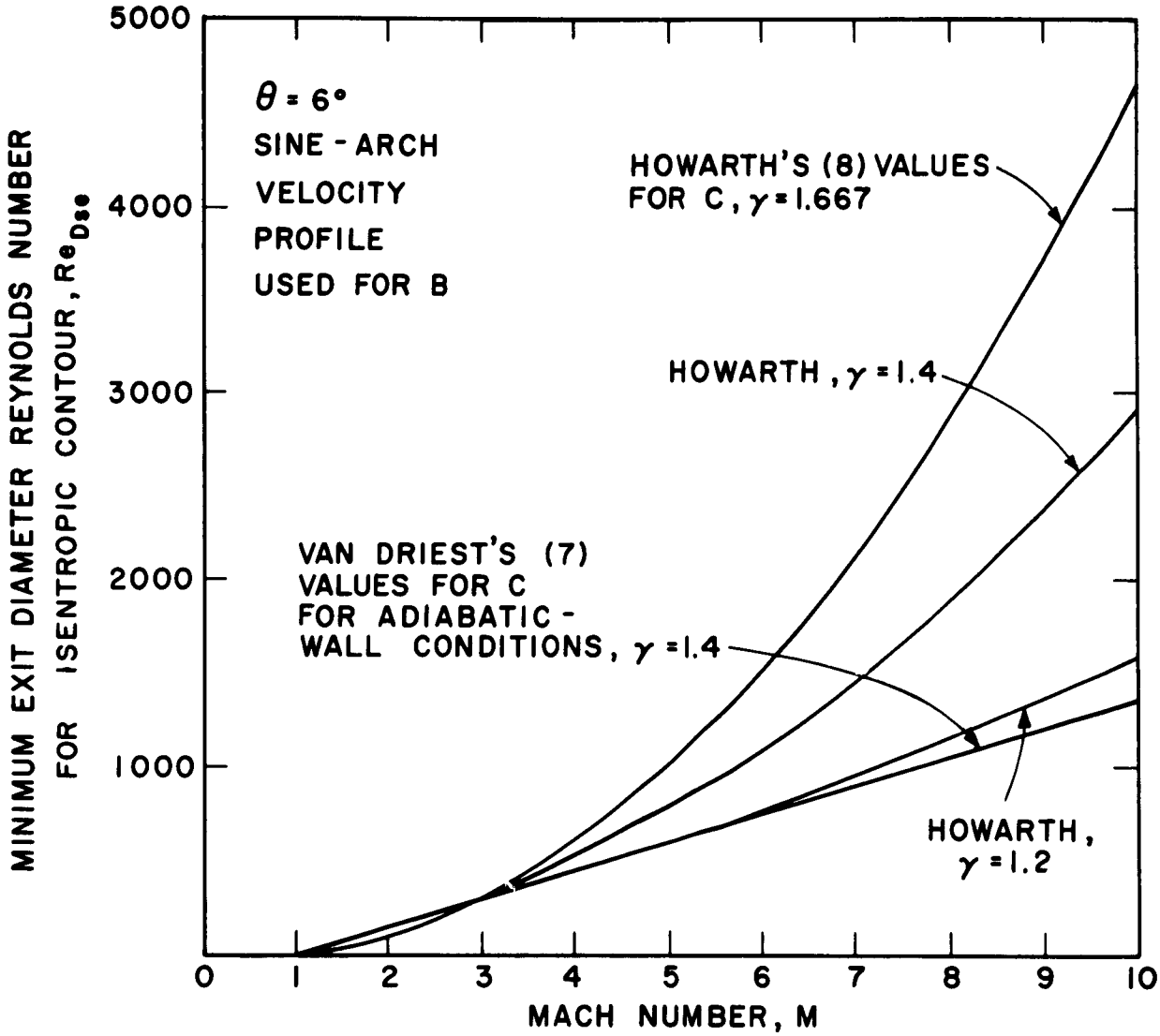

FIG. 11 - MINIMUM EXIT DIAMETER REYNOLDS NUMBER (ISENTROPIC CONTOUR) FOR $\delta/r_e = 1$ AT EXIT OF ACTUAL NOZZLE

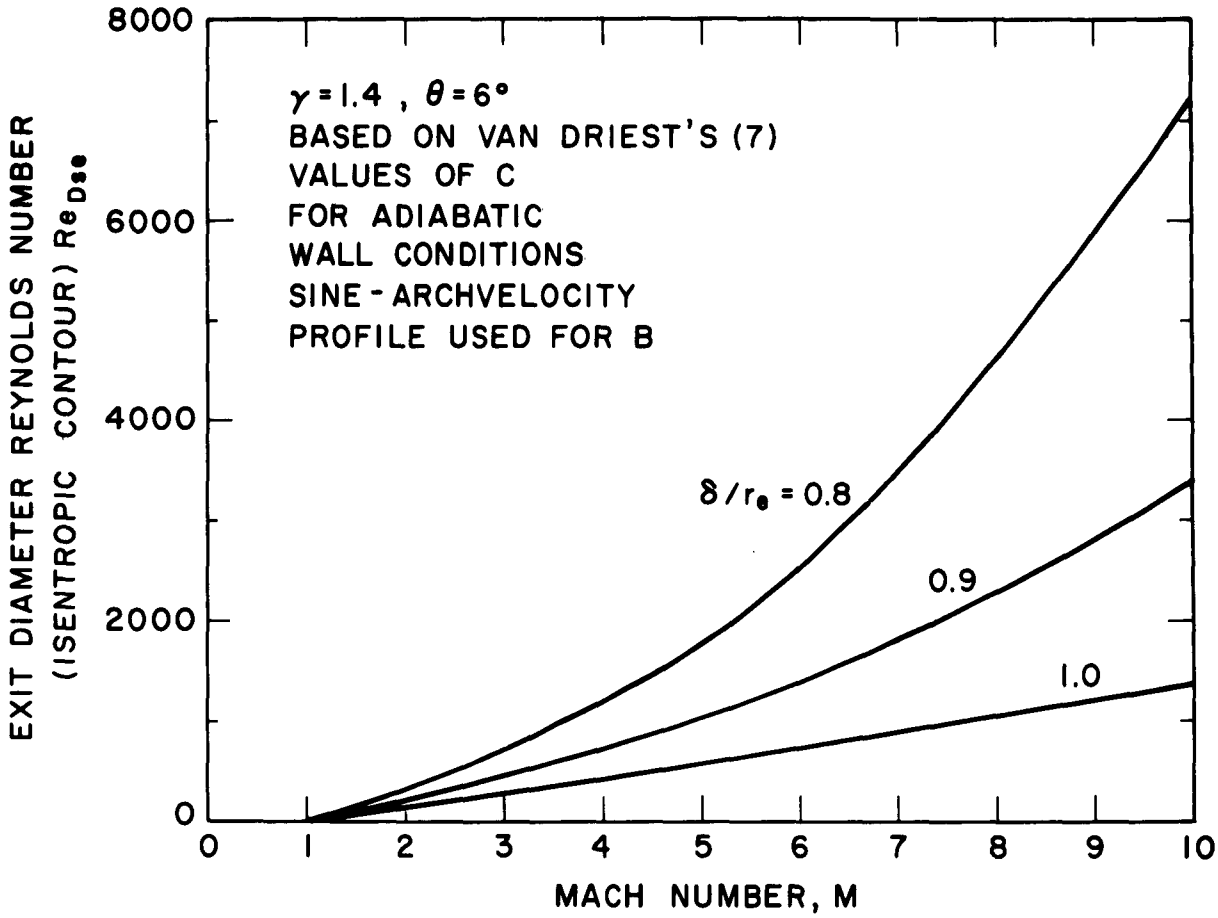

FIG. 12 - DEPENDENCE OF EXIT DIAMETER REYNOLDS NUMBER (ISENTROPIC CONTOUR) ON ISENTROPIC CORE SIZE AT EXIT OF ACTUAL NOZZLE

$\gamma = 1.4$

$\theta = 6°$

$Re/L = 10^3\ INCH^{-1}$

VALUES OF C FROM VAN DRIEST (7) CORRESPOND TO ADIABATIC-WALL CONDITIONS. SINE-ARCH VELOCITY PROFILE USED FOR B.

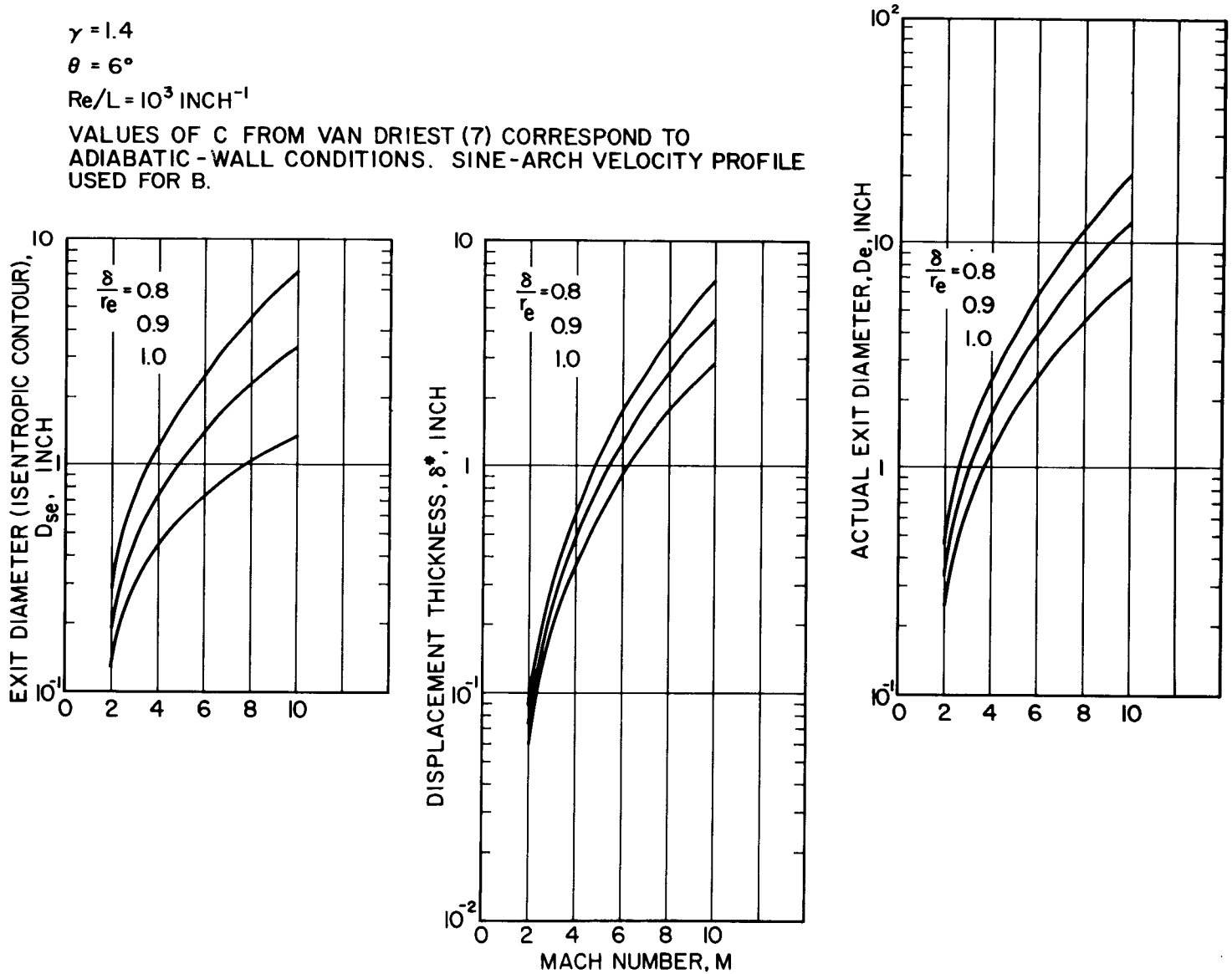

FIGURE 13 ISENTROPIC CONTOUR EXIT DIAMETER, DISPLACEMENT, THICKNESS AND ACTUAL EXIT DIAMETER FOR A LOW-DENSITY WIND TUNNEL NOZZLE

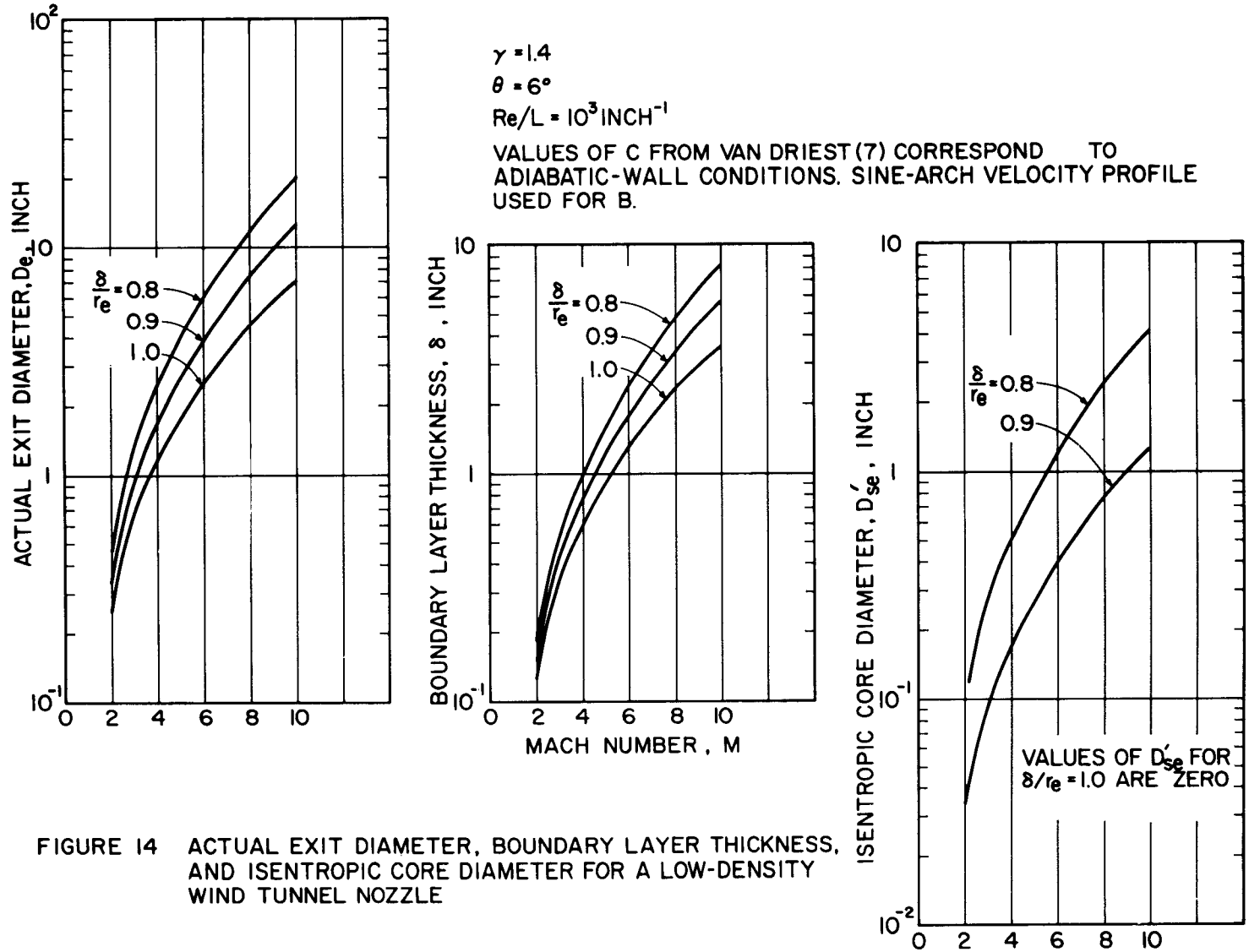

FIGURE 14 ACTUAL EXIT DIAMETER, BOUNDARY LAYER THICKNESS, AND ISENTROPIC CORE DIAMETER FOR A LOW-DENSITY WIND TUNNEL NOZZLE

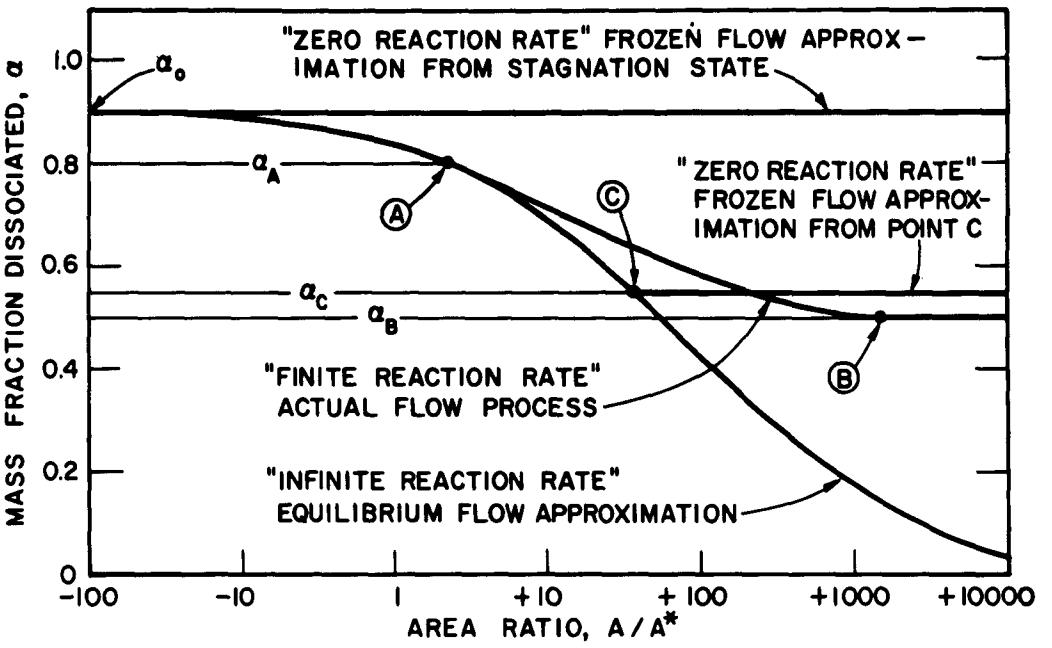

(a) COMPOSITION VARIATIONS.

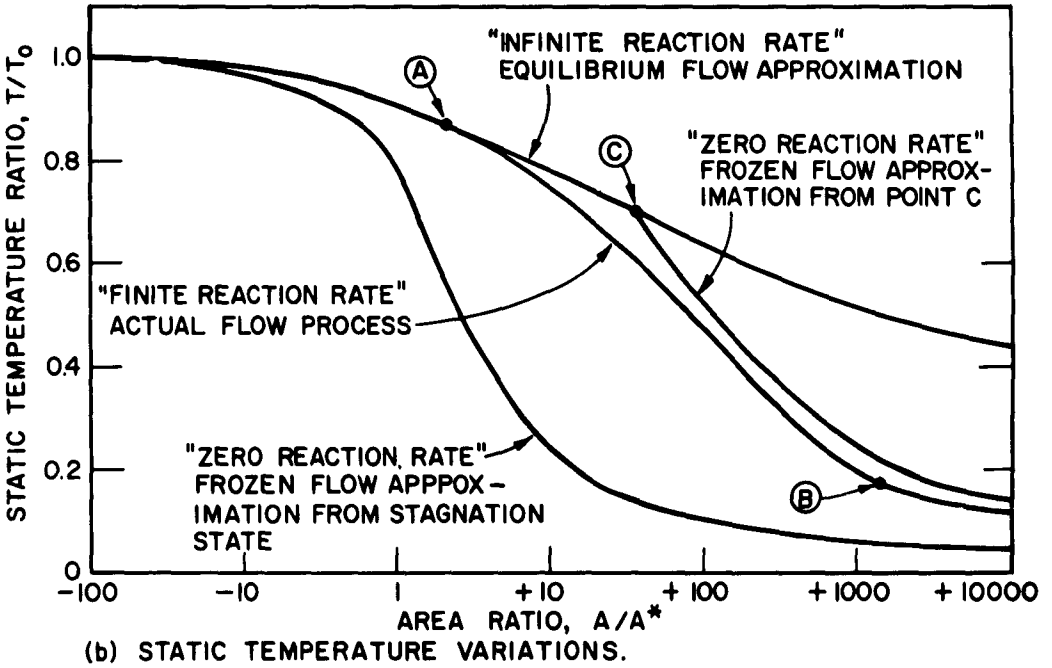

(b) STATIC TEMPERATURE VARIATIONS.

FIGURE 15 ACTUAL AND APPROXIMATE NOZZLE EXPANSION PROCESSES.

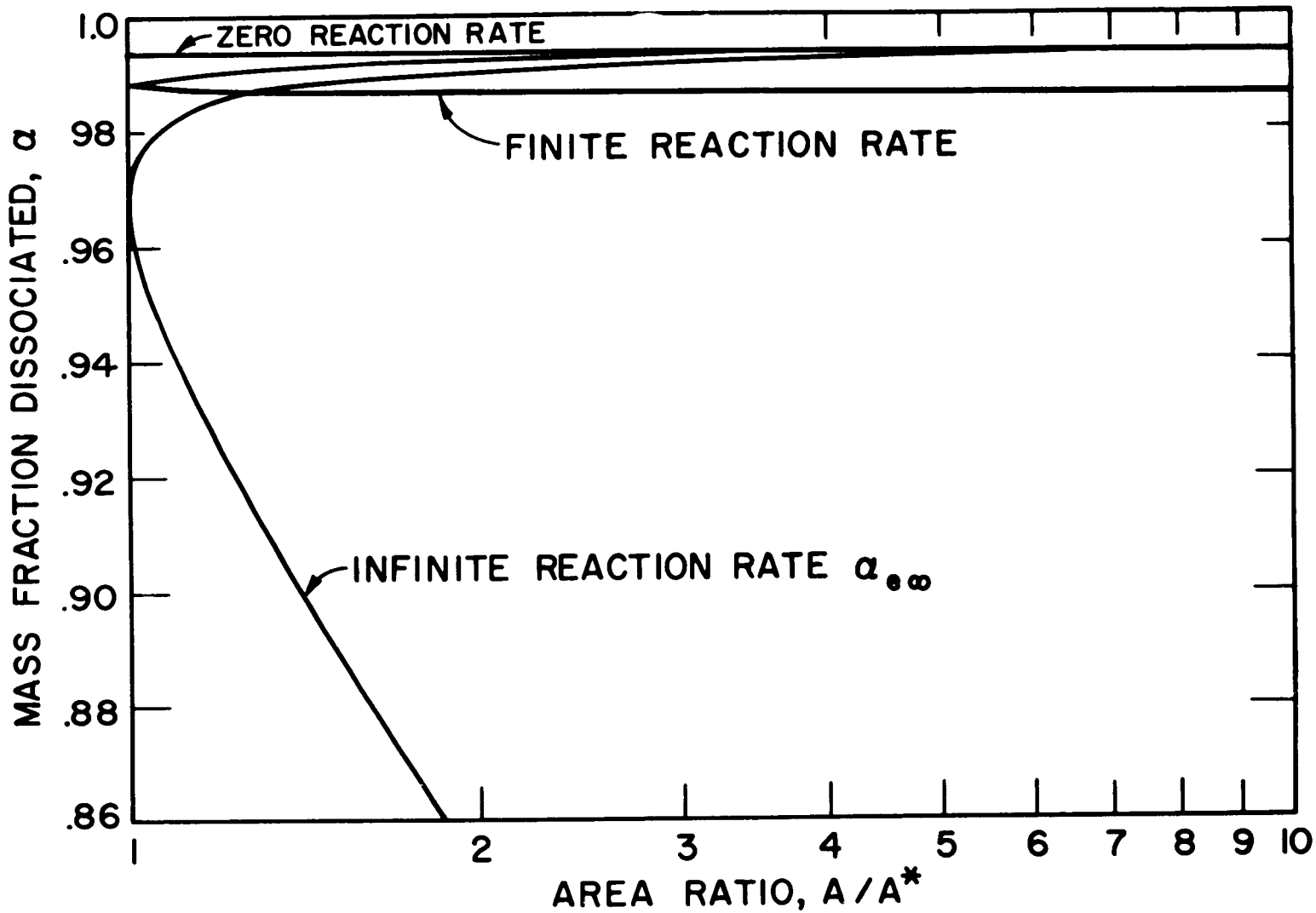

FIGURE 16 VARIATION OF COMPOSITION FOR THE EXPANSION OF OXYGEN IN A 15° HYPERBOLIC NOZZLE, T_0 =5900K, p_0 = 0.965 ATM. (FIG. 1 OF REF. 35)

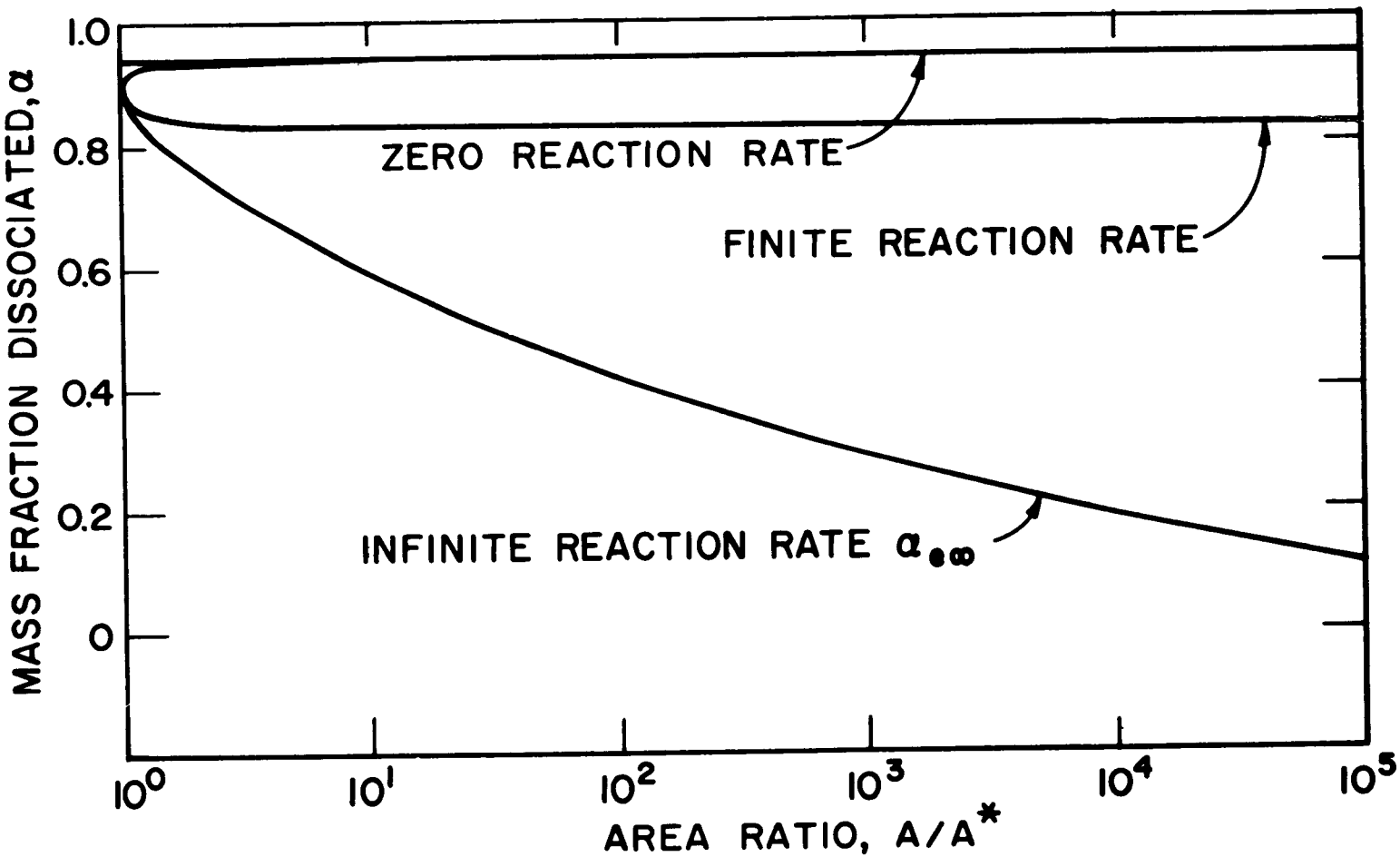

FIGURE 17 VARIATION OF COMPOSITION FOR THE EXPANSION OF OXYGEN IN A 15° HYPERBOLIC NOZZLE, $T_0 = 5900$ K, $p_0 = 9.4$ ATM. (FIG. 1 OF REF. 35)

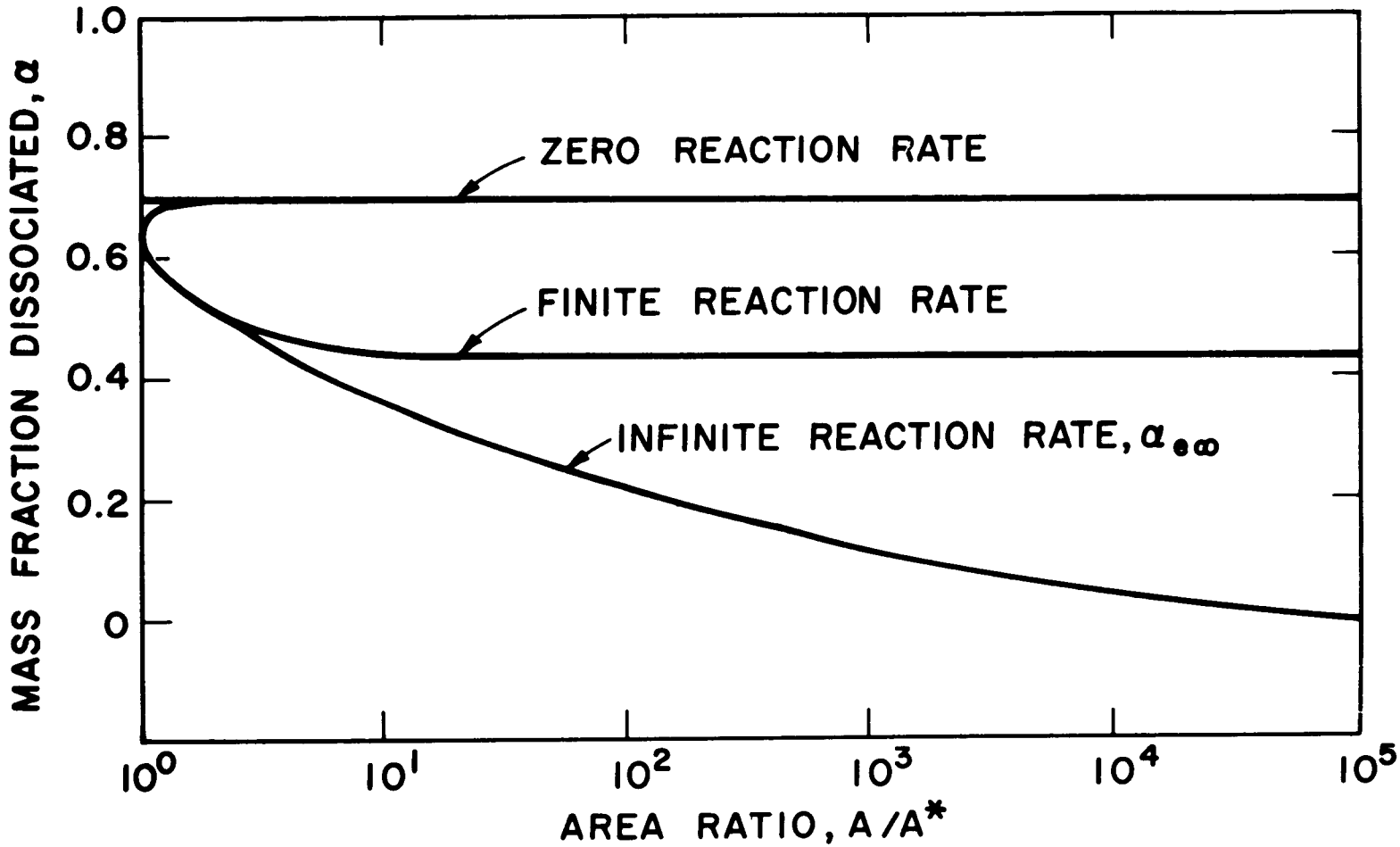

FIG. 18 - VARIATION OF COMPOSITION FOR THE EXPANSION OF OXYGEN IN A 15° HYPERBOLIC NOZZLE, $T_0 = 5900$ K, $p_0 = 82$ ATM. (FIG. 1 OF REF. 35)

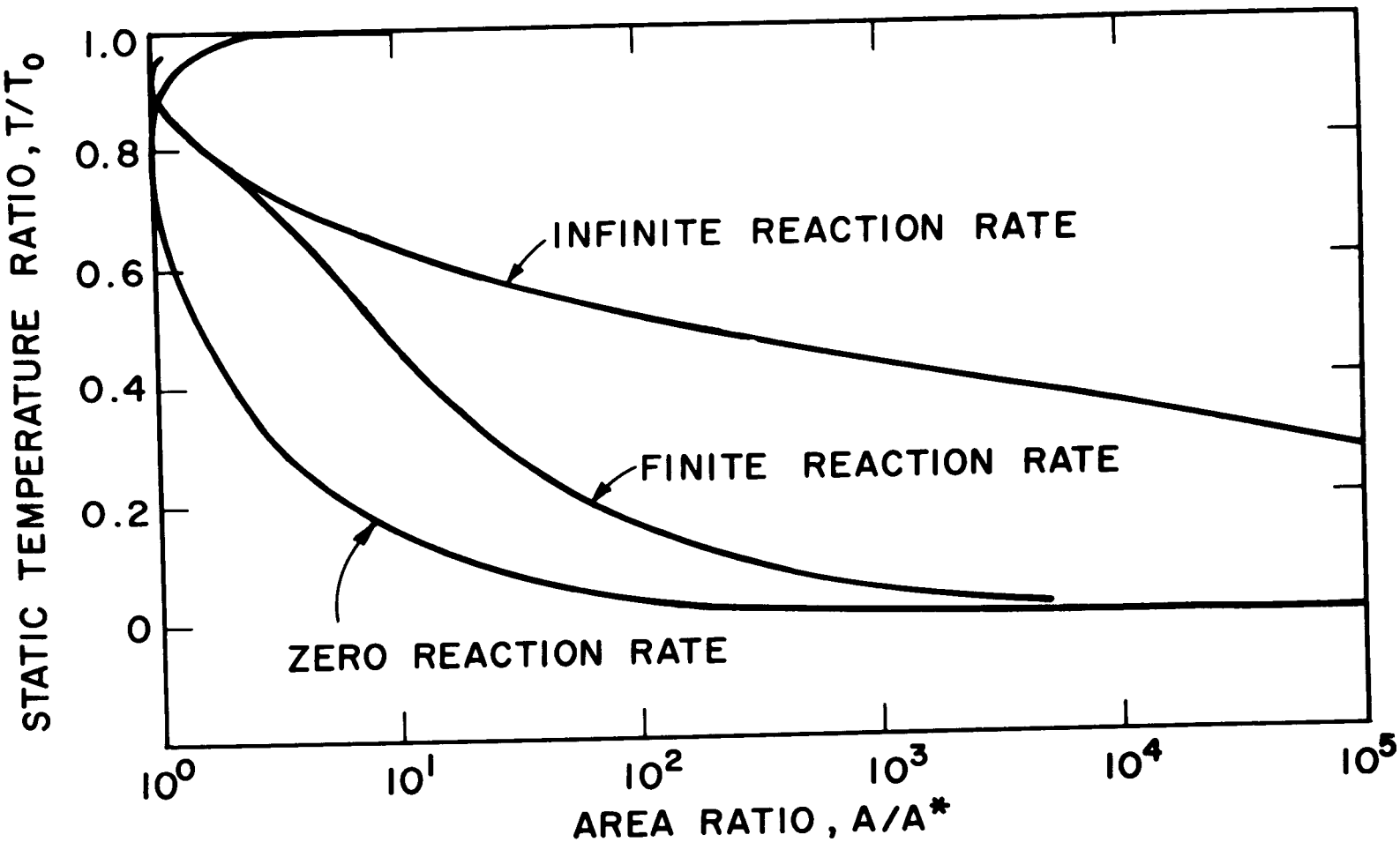

FIG. 19 - VARIATION OF STATIC TEMPERATURE FOR THE EXPANSION OF OXYGEN IN A 15° HYPERBOLIC NOZZLE, $T_0 = 5900$ K, $p_0 = 82$ ATM. (FIG. 2a OF REF. 35)

APPENDIX A

STATIC PRESSURE REQUIREMENTS FOR LOW DENSITY WIND TUNNELS

The Knudsen number is defined as:

$$Kn = \frac{\lambda}{L} \tag{A-1}$$

Multiplication of Eq. (A-1) by several ratios yields:

$$Kn = \frac{\rho \lambda a}{\mu} \cdot \frac{\frac{V}{a}}{\frac{\rho V L}{\mu}} \tag{A-2}$$

Substituting the definitions for the Mach and Reynolds numbers into Eq. (A-2) yields:

$$Kn = \frac{\rho \lambda a}{\mu} \cdot \frac{M}{Re} \tag{A-3}$$

For the pressures and temperatures of interest, the viscosity can be calculated from the following equation (5):

$$\mu = \frac{5\pi}{32} \rho \bar{V} \lambda \tag{A-4}$$

where

$$\bar{V} = \sqrt{\frac{8}{\pi} \frac{k T}{m}} \tag{A-5}$$

or

$$\bar{V} = \sqrt{\frac{8}{\pi} \frac{\bar{R}\,T}{W}} \tag{A-6}$$

Substituting Eqs. (A-4) and (A-6) into Eq. (A-3) yields:

$$Kn = \frac{8}{5} \sqrt{\frac{2}{\pi} \frac{W}{\bar{R}\,T}} \cdot a \cdot \frac{M}{Re} \tag{A-7}$$

A speed of sound parameter, τ , is defined as:

$$\tau = \frac{a^2 \rho}{p} \tag{A-8}$$

The compressibility factor, Z, is defined as:

$$Z = \frac{p}{\rho T} \cdot \frac{W_o}{\bar{R}} \tag{A-9}$$

and

$$ZW = W_o \tag{A-10}$$

Combining Eqs. (A-7) through (A-10) yields:

$$Kn = \frac{8}{5} \sqrt{\frac{2}{\pi} \tau} \cdot \frac{M}{Re} \tag{A-11}$$

For flows in which the gas composition is frozen:

$$\tau = \gamma \tag{A-12}$$

and Eq. (A-11) becomes:

$$Kn = \frac{8}{5}\sqrt{\frac{2}{\pi}\gamma} \cdot \frac{M}{Re} \qquad \text{(A-13)}$$

The Reynolds number per unit length is defined as:

$$\frac{Re}{L} = \frac{\rho V}{\mu} \qquad \text{(A-14)}$$

Using the definition of the Mach number, Eq. (A-14) becomes:

$$\frac{Re}{L} = \frac{\rho M a}{\mu} \qquad \text{(A-15)}$$

Substituting Eqs. (A-8) and (A-9) into Eq. (A-15) yields:

$$\frac{Re}{L} = \frac{M}{\mu} p \sqrt{\frac{\gamma}{R T_o}\frac{\gamma}{T}} \qquad \text{(A-16)}$$

The temperature T is calculated from:

$$\frac{T_o}{T} = 1 + \frac{\gamma - 1}{2} M^2 \qquad \text{(A-17)}$$

and the viscosity can be calculated from:

$$\mu = 0.073225 \times 10^{-5} \frac{\sqrt{T}}{1 + \frac{201.6}{T}} \qquad \text{(A-18)}$$

Specific units are involved in Eq. (A-18), namely,

μ - lbm/ft-sec

T - °R

APPENDIX B

APPROXIMATE BOUNDARY LAYER ANALYSIS

From the geometry of the isentropic contour shown in Fig. 7a, the following expression for the distance between the throat and the exit section of nozzle can be derived:

$$\frac{L_t}{r_{se}} = \cot\frac{\theta}{2}\left[1 - \frac{1}{\frac{r_{se}}{r^*}}\right] \qquad \text{(B-1)}$$

The ratio r_{se}/r^* can be calculated from the area ratio for the isentropic contour, or:

$$\frac{r_{se}}{r^*} = \sqrt{\frac{A}{A^*}} \qquad \text{(B-2)}$$

The area ratio is known from the specified Mach number and value of ν for a particular case. Equation (B-1) can be rewritten as:

$$\frac{L_t}{r_{se}} = \cot\frac{\theta}{2}\left[\frac{\sqrt{A/A^* - 1}}{\sqrt{A/A^*}}\right] \qquad \text{(B-3)}$$

It is assumed that the boundary layer thickness at the exit of the nozzle can be calculated from the following equation:

$$\frac{\delta}{L_t} = \frac{C}{\sqrt{\frac{\rho_{se} V_{se} L_t}{\mu_{se}}}} \qquad \text{(B-4)}$$

where C is obtained from Fig. 26. Equation (B-4) can be re-written as:

$$\delta = \frac{C \sqrt{L_t} \sqrt{D_{se}}}{\sqrt{Re_{Dse}}} \qquad \text{(B-5)}$$

where the exit diameter Reynolds number for the isentropic contour, Re_{Dse}, is defined as:

$$Re_{Dse} = \frac{\rho_{se} V_{se} D_{se}}{\mu_{se}} \qquad \text{(B-6)}$$

Combining Eqs. (B-3) and (B-5) yields:

$$\frac{\delta}{r_{se}} = \frac{\sqrt{2}\ C \sqrt{\cot\frac{\theta}{2}} \sqrt{1 - \frac{1}{\sqrt{A/A^*}}}}{\sqrt{Re_{Dse}}} \qquad \text{(B-7)}$$

The actual exit radius of the nozzle, r_e, is determined by the equation:

$$r_e = r_{se} + \delta^* \qquad \text{(B-8)}$$

Since the boundary layer thickness and the displacement thickness are related by the following equation:

$$\delta^* = \delta(1 - B) \qquad \text{(B-9)}$$

Equation (B-8) can be written:

$$r_e = r_{se} + (1 - B)\ \delta \qquad \text{(B-10)}$$

Thus an expression for δ/r_e is:

$$\frac{\delta}{r_e} = \frac{\delta}{r_{se} + (1 - B)\delta} = \frac{1}{(r_{se}/\delta) + (1 - B)} \qquad \text{(B-11)}$$

or substituting Eq. (B-7) into Eq. (B-11) yields:

$$\frac{\delta}{r_e} = \frac{1}{\dfrac{\sqrt{Re_{Dse}}}{\sqrt{2}\, C \sqrt{\cot\frac{\theta}{2}} \sqrt{1 - \dfrac{1}{\sqrt{A/A^*}}}} + (1 - B)} \qquad \text{(B-12)}$$

The following expression for Re_{Dse} can be obtained from Eq. (B-12):

$$Re_{Dse} = 2\, B^2 C^2 \cot\frac{\theta}{2} \left[1 - \frac{1}{\sqrt{(A/A^*)}}\right] \left\{ \frac{1}{B}\left[\frac{1}{(\delta/r_e)} - 1\right] + 1 \right\}^2 \qquad \text{(B-13)}$$

Equation (B-5) can be combined with Eq. (B-3) to give:

$$\delta = C \sqrt{r_{se}} \sqrt{\cot\frac{\theta}{2}} \sqrt{1 - \frac{1}{\sqrt{(A/A^*)}}} \sqrt{\frac{D_{se}}{Re_{Dse}}} \qquad \text{(B-14)}$$

Further rearrangement of Eq. (B-14) yields:

$$\delta = \frac{\sqrt{2}\, C}{2} \sqrt{\frac{D_{se}}{Re_{Dse}}} \sqrt{Re_{Dse}} \sqrt{\cot\frac{\theta}{2}} \sqrt{1 - \frac{1}{\sqrt{(A/A^*)}}} \sqrt{\frac{D_{se}}{Re_{Dse}}} \qquad \text{(B-15)}$$

or

$$\delta = \frac{\sqrt{2}\,C}{2} \sqrt{\cot\frac{\theta}{2}} \sqrt{1 - \frac{1}{\sqrt{(A/A^*)}}} \frac{\sqrt{Re_{Dse}}}{(Re_{Dse}/D_{se})} \qquad \text{(B-16)}$$

However, Eq. (B-13) is an expression for Re_{Dse} and:

$$\frac{Re_{Dse}}{D_{se}} = \frac{Re}{L} \qquad \text{(B-17)}$$

Using this information in Eq. (B-16) yields the final expression for δ:

$$\delta = \frac{BC^2 \cdot \cot\frac{\theta}{2} \cdot \left[1 - \frac{1}{\sqrt{(A/A^*)}}\right]\left\{\frac{1}{B}\left[\frac{1}{(\delta/r_e)} - 1\right] + 1\right\}}{Re/L} \qquad \text{(B-18)}$$

REFERENCES

1. Brown, G.A. and Bergles, A.E., "A Literature Survey on Rarefied Gas Dynamics and Low Density Wind Tunnels," Engineering Projects Laboratory, Department of Mechanical Engineering, Massachusetts Institute of Technology, Cambridge, Massachusetts, April, 1962.

2. Maslach, G.J. and Schaaf, S.A., "Cylinder Drag in the Transition from Continuum to Free Molecular Flow," Technical Report HE-150-194, Institute of Engineering Research, University of California, Berkeley, California, March, 1962.

3. Masson, D.J., Morris, D.N. and Bloxsom, D.E., "Measurements of Sphere Drag from Hypersonic Continuum to Free-Molecule Flow," Rand Report RM-2678, Rand Corporation, Santa Monica, California, November, 1960.

4. Harnett, J.P., "A Survey of Thermal Accommodation Coefficients," Published in "Rarefied Gas Dynamics", L. Talbot, Editor, Academic Press, New York.

5. Hansen, C.F., "Approximations for the Thermodynamic and Transport Properties of High-Temperature Air," NASA TR R-50, 1959.

6. Romig, M.F. and Dore, F.J., "Solutions of the Compressible Laminar Boundary Layer Including the Case of a Dissociated Free Stream," Convair Report No. ZA-7-012, August, 1954.

7. Van Driest, E.R., "Investigation of Laminar Boundary Layer in Compressible Fluids Using the Crocco Method," NACA TN 2597, January, 1952.

8. Howarth, L., "Concerning the Effect of Compressibility on Laminar Boundary Layers and Their Separation," Proceedings of the Royal Society of London, Series A, Vol. 194, 1948, pp. 16-42.

9. Guentert, E.C. and Neumann, H.E., "Design of Axisymmetric Exhaust Nozzles by Method of Characteristics Incorporating a Variable Isentropic Exponent," NASA TR-33, 1959.

10. Owen, J.M. and Sherman, F.S., "Design and Testing of a Mach 4 Axially Symmetric Nozzle for Rarefied Gas Flows," Report No. HE-150-104, University of California, Institute of Engineering Research, Berkeley, California, July 23, 1952.

11. Maslach, G.J. and Sherman, F.S., "Design and Testing of an Axisymmetric Hypersonic Nozzle for a Low Density Wind Tunnel," Report HE-150-134, University of California, Institute of Engineering Research, Berkeley, California, February 15, 1956.

12. Sreekanth, A.K., "Performance of a Mach 4 Axially Symmetric Nozzle Designed to Operate at 40 Microns Hg in the UTIA Low Density Wind Tunnel," Technical Report No. 10, Institute of Aerophysics, University of Toronto, September, 1956.

13. Walter, S.A., "Reduction of the Boundary Layer Thickness in a Hypersonic Nozzle," USCEC Report 56-213, Engineering Center, University of Southern California, Los Angeles, California, May 20, 1960. Also AFOSR TN 60-514.

14. Enkenhus, K.R., "The Design, Instrumentation and Operation of the UTIA Low Density Wind Tunnel," UTIA Report No. 44, Institute of Aerophysics, University of Toronto, June, 1957.

15. Emerson, D.E. and Schaaf, S.A., "Performance of a Supersonic Nozzle in the Rarefied Gas Dynamics Regime," Report No. HE-150-72, Institute of Engineering Research, University of California, Berkeley, August 30, 1950.

16. Lynes, L.L., "Design, Fabrication, and Evaluation of Axisymmetric Nozzles," Technical Report HE-150-174, Institute of Engineering Research, University of California, Berkeley, September, 1959.

17. Owen, J.M. and Sherman, F.S., "Design and Testing of a Mach 4 Axially Symmetric Nozzle for Rarefied Gas Flows," Report No. HE-150-104, Institute of Engineering Research, University of California, Berkeley, July, 1952.

18. Sreekanth, A.K., "Performance of a Mach 4 Axially Symmetric Nozzle Designed to Operate at 40 Microns Hg in the UTIA Low Density Wind Tunnel," Technical Note No. 10, Institute of Aerophysics, University of Toronto, September, 1956.

19. Maslach, G.J. and Sherman, F.S., "Design and Testing of an Axisymmetric Hypersonic Nozzle for a Low Density Wind Tunnel," Technical Report HE-150-134, Institute of Engineering Research, University of California, Berkeley, February, 1956.

20. Boyer, D.W., Eschenroeder, A.C. and Russo, A.L., "Approximate Solutions for Nonequilibrium Airflow in Hypersonic Nozzles," Report No. AD-1345-W-3, Cornell Aeronautical Laboratory, Inc., Buffalo, New York, August, 1960. Also AEDC-TN-60-181.

21. Bray, K.N.C., "Atomic Recombination in a Hypersonic Wind Tunnel Nozzle, A.R.C. 20, 562, November 21, 1958.

22. Bray, K.N.C. and Appleton, J.P., "Atomic Recombination in Nozzles: Methods of Analysis for Flows with Complicated Chemistry," University of Southhampton Aero. and Astro. Report No. 166, 1961.

23. Bray, K.N.C., "Departure From Dissociation Equilibrium in a Hypersonic Nozzle," A.R.C. 19, 983, March 17, 1958.

24. Bray, K.N.C. and Makin, B., "Recombination of Oxygen in a Nozzle; Comparison with Experimental Results for Air from General Electric Research Laboratory," U.S.A.A. Report No. 143, 1960.

25. Bray, K.N.C., "Simplified Sudden-Freezing Analysis for Non-Equilibrium Nozzle Flows," J. ARS., Vol. 31, No. 6, June, 1961.

26. Bray, KN.C. and Appleton, J.P., "The Choice of an Optimum Set of Measurements to Study Atomic Recombination in Nozzles," University of Southhampton Aero. and Astro. Report No. 120, November, 1959.

27. Broer, L.J.F., "Characteristics of Equations of Motion of a Reacting Gas," J. Fluid Mech., Vol. 4, Part 3, July, 1958.

28. Erickson, W.D. and Creekmore, H.S., "A Study of Equilibrium Real-Gas Effects in Hypersonic Air Nozzles, Including Charts of Thermodynamic Properties for Equilibrium Air," NASA TN D-231, April, 1960.

29. Freeman, N.C., "Dynamics of a Dissociating Gas III Non-Equilibrium Theory," AGARD Report 133, July, 1957.

30. Freeman, N.C., "Non-Equilibrium Flow of an Ideal Dissociating Gas," J. Fluid Mechanics, Vol. 4, Part 4, August, 1958.

31. Freeman, N.C., "Non-Equilibrium Theory of an Ideal-Dissociating Gas Through a Conical Nozzle," A.R.C., C.P. No. 438, 1959.

32. Glowacki, W.J., "Effect of Finite Oxygen Recombination Rate on the Flow Conditions in Hypersonic Nozzles," NOLTR 61-23, U.S. Naval Ordnance Laboratory, White Oak, Maryland, September 15, 1961.

33. Hall, J.G., "Dissociation Nonequilibrium in Hypersonic Nozzle Flow," American Institute of Chemical Engineers, Preprint 7, 1959.

34. Hall, J.G., Eschenroeder, A.C. and Klein, J.J., "Chemical Non-Equilibrium Effects on Hydrogen Rocket Impulse at Low Pressures," C.A.L. Report No. AD-1118-A-8, AFOSR TN 59-1192, November, 1959.

35. Hall, J.G. and Russo, A.L., "Studies of Chemical Nonequilibrium in Hypersonic Nozzle Flows," Cornell Aeronautical Laboratory, AFOSR TN 59-1090, November, 1959.

36. Heims, S.P., "Effect of Oxygen Recombination on One-Dimensional Flow at High Mach Numbers," NACA TN 4144, January, 1958.

37. Heims, S.P., "Effects of Chemical Dissociation and Molecular Vibrations on Steady One-Dimensional Flow," NASA TN D-87, August, 1959.

38. Li, T.Y., "Non-Equilibrium Flow in Gas Dynamics," ARS Preprint No. 852-59, June, 1959. Also RPI, Troy, New York, AFOSR TN 59-389, AD213 893, RPI TRAE5901, May, 1959.

39. Li, T.Y., "Recent Advances in Non-Equilibrium Flow in Gas Dynamics," Rensselaer Polytechnic Institute, Troy, New York, AFOSR TN 60-597, RPI TR AE6001, May, 1960.

40. Lighthill, M.J., "Dynamics of a Dissociating Gas. I. Equilibrium Flow," A.R.C., F.M. 2481, November 14, 1956.

41. Nagamatsu, H.T., Workman, J.B. and Sheer, R.E., Jr., "Hypersonic Nozzle Expansion with Air Atom Recombination Present," Report No. 60-RL-2332C, General Electric Research Laboratory, Schenectady, New York, January, 1960.

42. Reynolds, T.W. and Baldwin, L.V., "One Dimensional Flow with Chemical Reaction in Nozzle Expansion," AIChE Preprint No. 6, May, 1959.

43. Wegener, P.P., "Experiments on the Departure from Chemical Equilibrium on a Supersonic Flow," ARS Journal, 30(4), 1960.

44. Wegener, P.P., "Measurement of Rate Constants of Fast Reactions in a Supersonic Nozzle," Journal of Chemical Physics, Vol. 28, 1958.

45. Wegener, P.P., "Study of Supersonic Flows with Chemical Reactions: III. Experiments on the Departure from Chemical Equilibrium in a Supersonic Flow," California Institute of Technology, Progress Report No. 20-388, June 1, 1959.

46. Wilde, K.A., "Effect of Radical Recombination Kinetics on Specific Impulse of High Temperature Systems," Jet Propulsion, Vol. 28, No. 2, February, 1958.

47. Williams, J.C., "One-Dimensional Flow of a Decaying Nitrogen Plasma," USCEC Report 68-201, January 31, 1959.

48. Yoshikawa, K.K. and Katzen, E.D., "Charts for Air-Flow Properties in Equilibrium and Frozen Flows in Hypervelocity Nozzles," NASA TN D-693, April, 1961.

49. Hansen, C.F. and Hodge, M.E., "Constant Entropy Properties for an Approximate Model of Equilibrium Air," NASA TN D-352, January, 1961.

50. Beckwith, I.E., Ridyard, H.W. and Cramer, N., "The Aerodynamic Design of High Mach Number Nozzles Utilizing Axisymmetric Flow with Application to a Nozzle of Square Test Section," NACA TN 2711, June, 1952.

51. Sandberg-Serrell Corporation, 2550 East Foothill Boulevard, Pasadena, California.

52. Enkenhaus, K.R. and Rucker, N.B., "Design and Testing of an Axisymmetric Flow Nozzle for Mach Number Seven," UTIA Report, January, 1955.

53. Potter, J.L. and Durand, J.A., "Analysis of Very Thick Laminar Boundary Layers in Axisymmetric High-Speed Fluid Flow," Presented at the Southeastern Conference on Theoretical and Applied Mechanics, Gatlinburg, Tennessee, May, 1962 (Contact AEDC for report).

54. Leninsky, E.S., "Laminar Boundary Layers in Dissociated Air with Finite Rate Chemical Reactions," 1962 (Contact AEDC for report).

55. Michel, R., "Development de la Couche Limite dans Une Tuyere Hypersonique," Presented at the "High Temperature Aspects of Hypersonic Flow" AGARD Specialists' Meeting, Rhode Saint Genese, Belgique, Avril, 1962.

56. Hilsenrath, J., Klein, M. , and Woolley, H.W., "Tables of Thermodynamic Properties of Air Including Dissociation and Ionization from 1500 K to 15000 K," AEDC TR-59-20, Arnold Engineering Development Center, December, 1959.

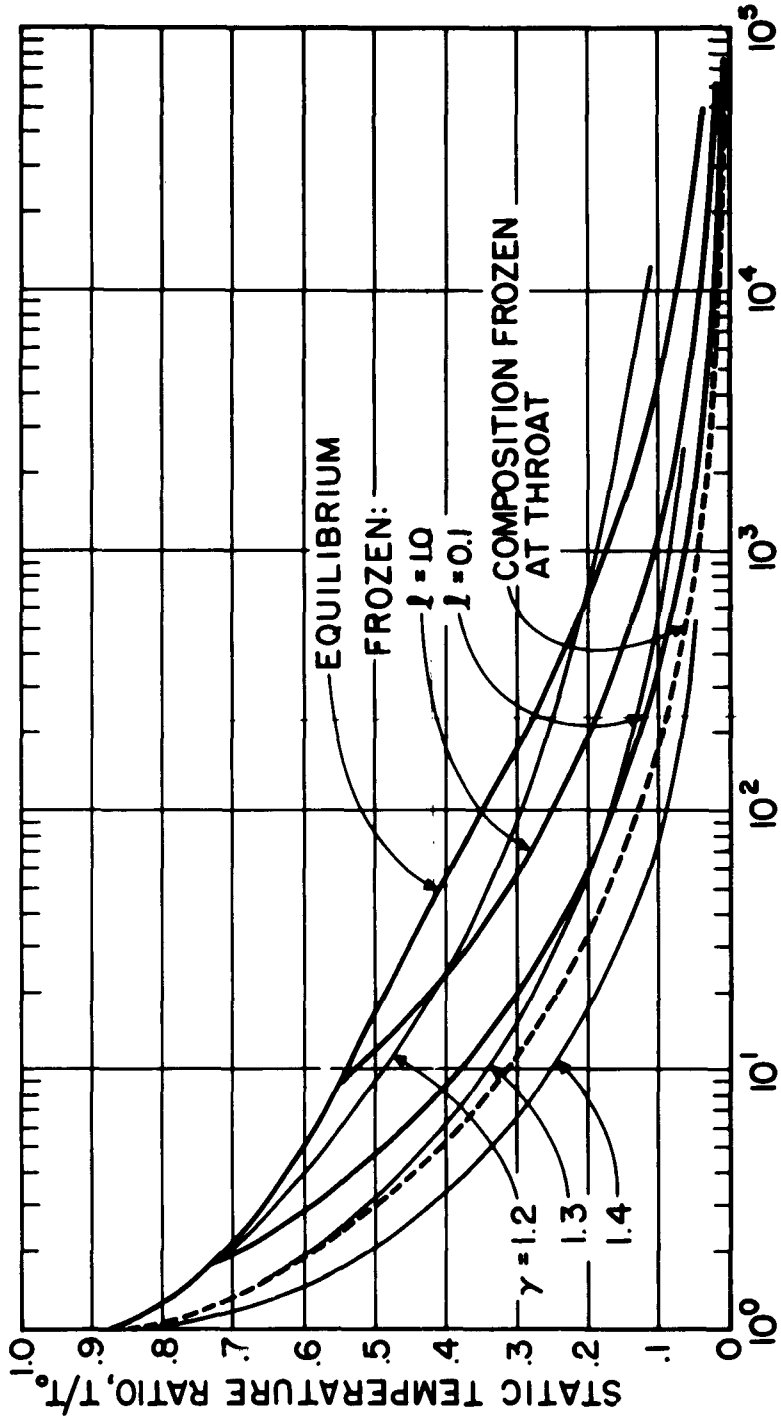

FIGURE 20 VARIATION OF STATIC TEMPERATURE FOR THE EXPANSION OF AIR IN A HYPERSONIC NOZZLE, T_o = 6000K, p_o = 100 ATM. (FIGURE 29e OF REF. 20)

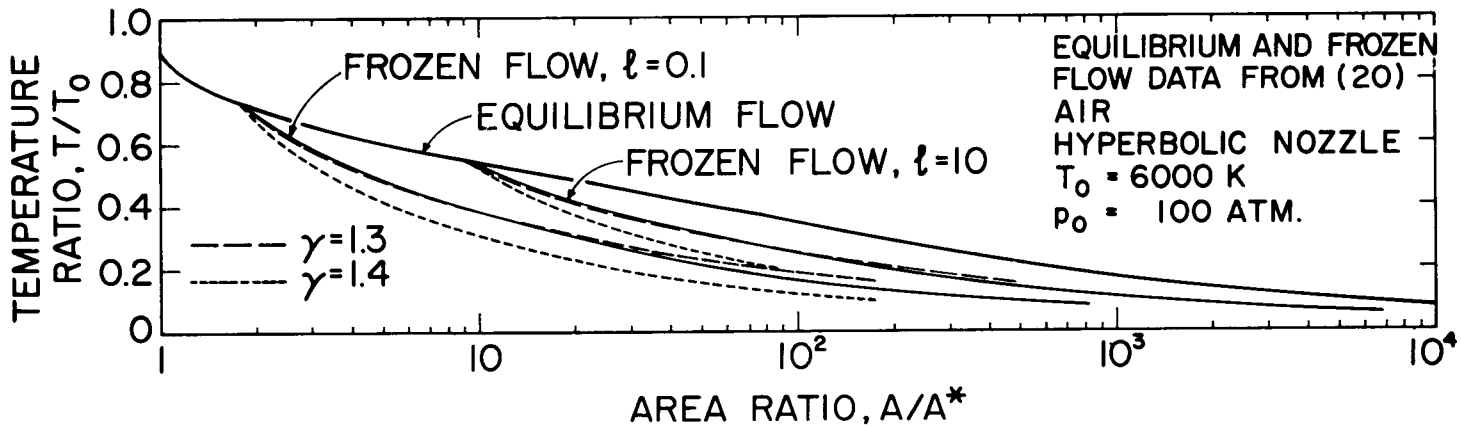

FIG. 21 - CONSTANT γ APPROXIMATIONS FOR FROZEN FLOW REGIONS OF A HYPERSONIC NOZZLE EXPANSION PROCESS

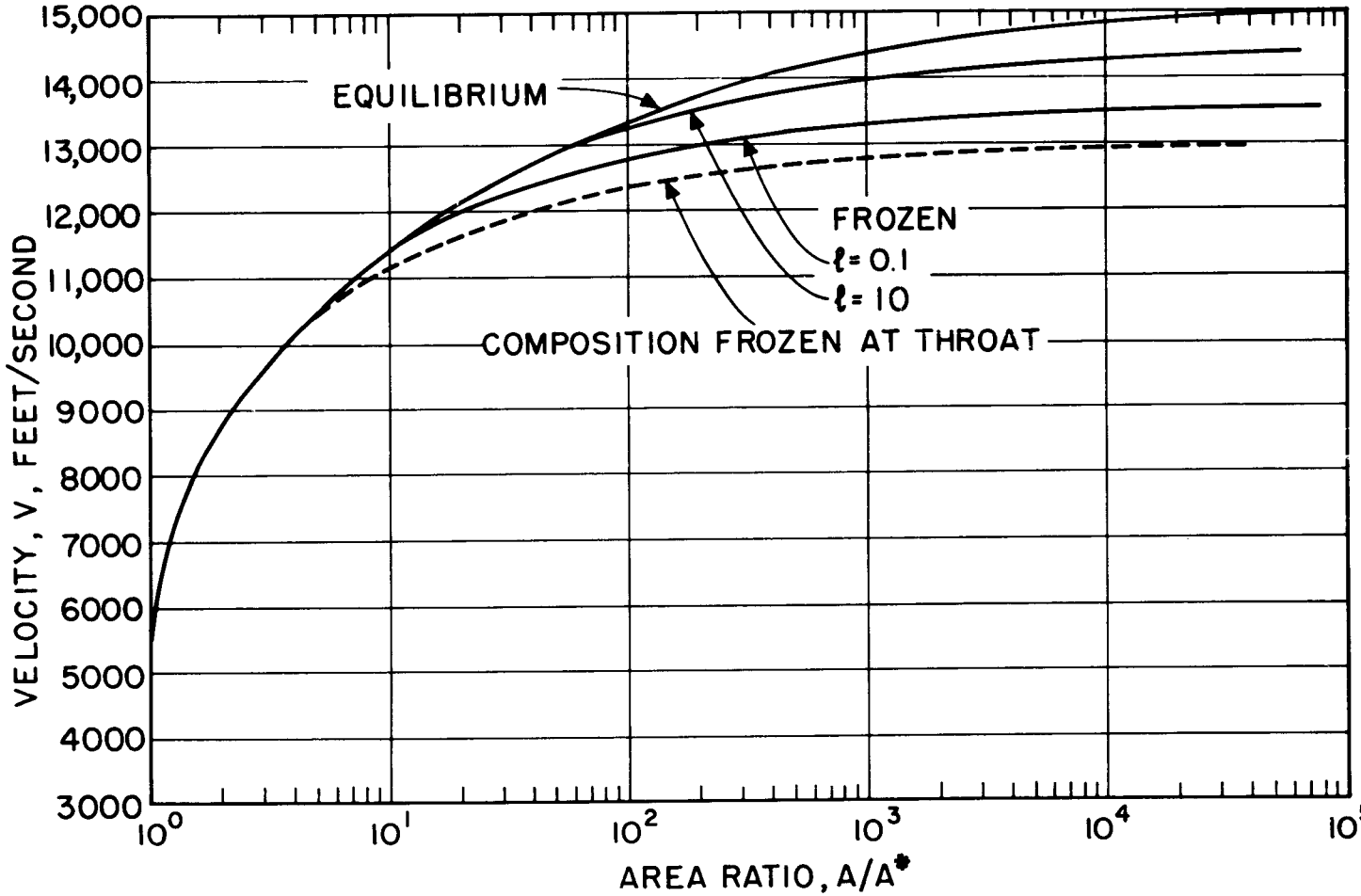

FIGURE 22 VARIATION OF VELOCITY FOR THE EXPANSION OF AIR IN A HYPERSONIC NOZZLE $T_o = 6000K$, $p_o = 100$ ATM. (FIGURE 29 d OF REF. 20)

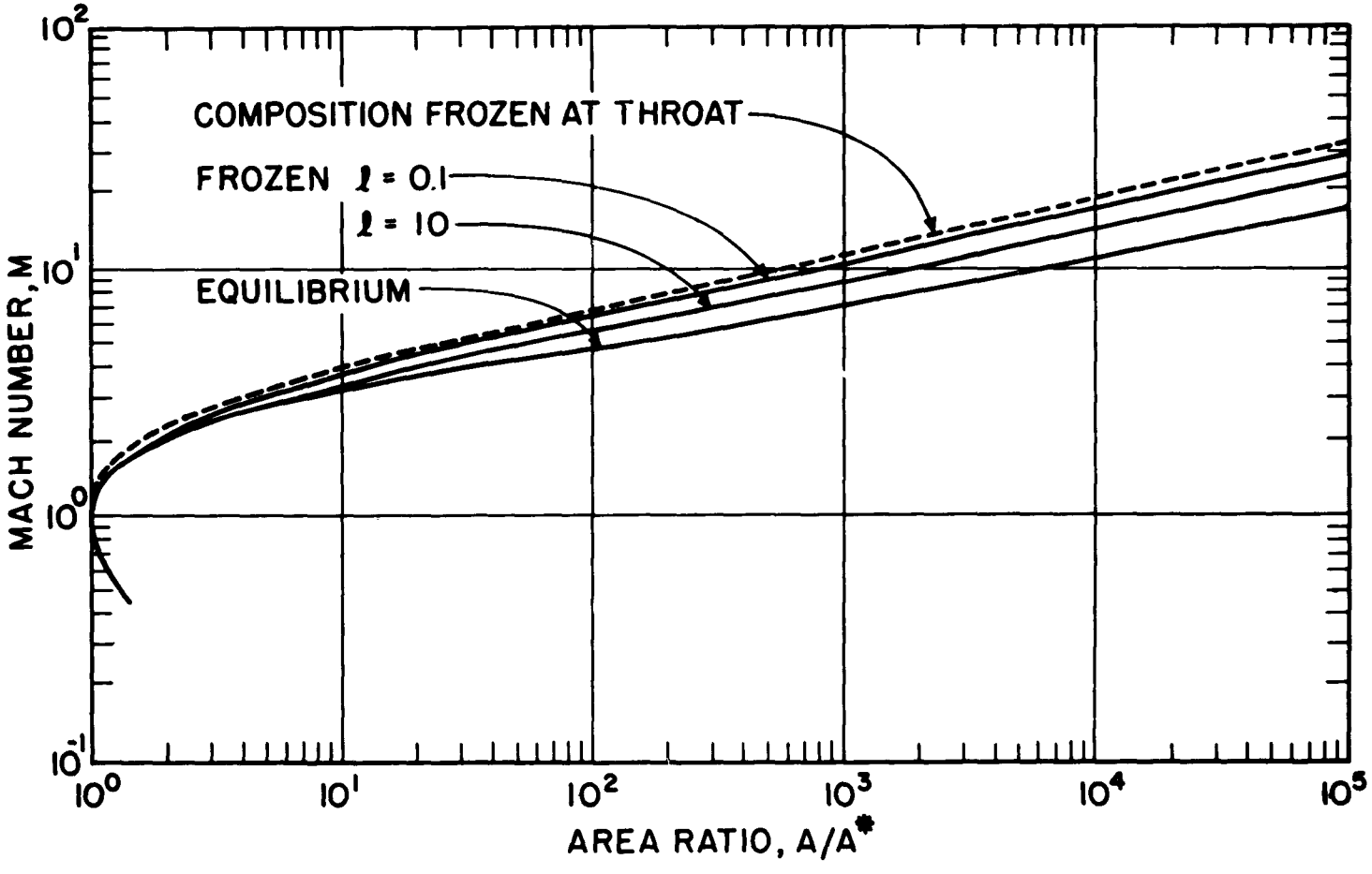

FIGURE 23 VARIATION OF MACH NUMBER FOR THE EXPANSION OF AIR IN A HYPERSONIC NOZZLE, T_o = 6000K, p_o = 100 ATM. (FIGURE 29c OF REF. 20)

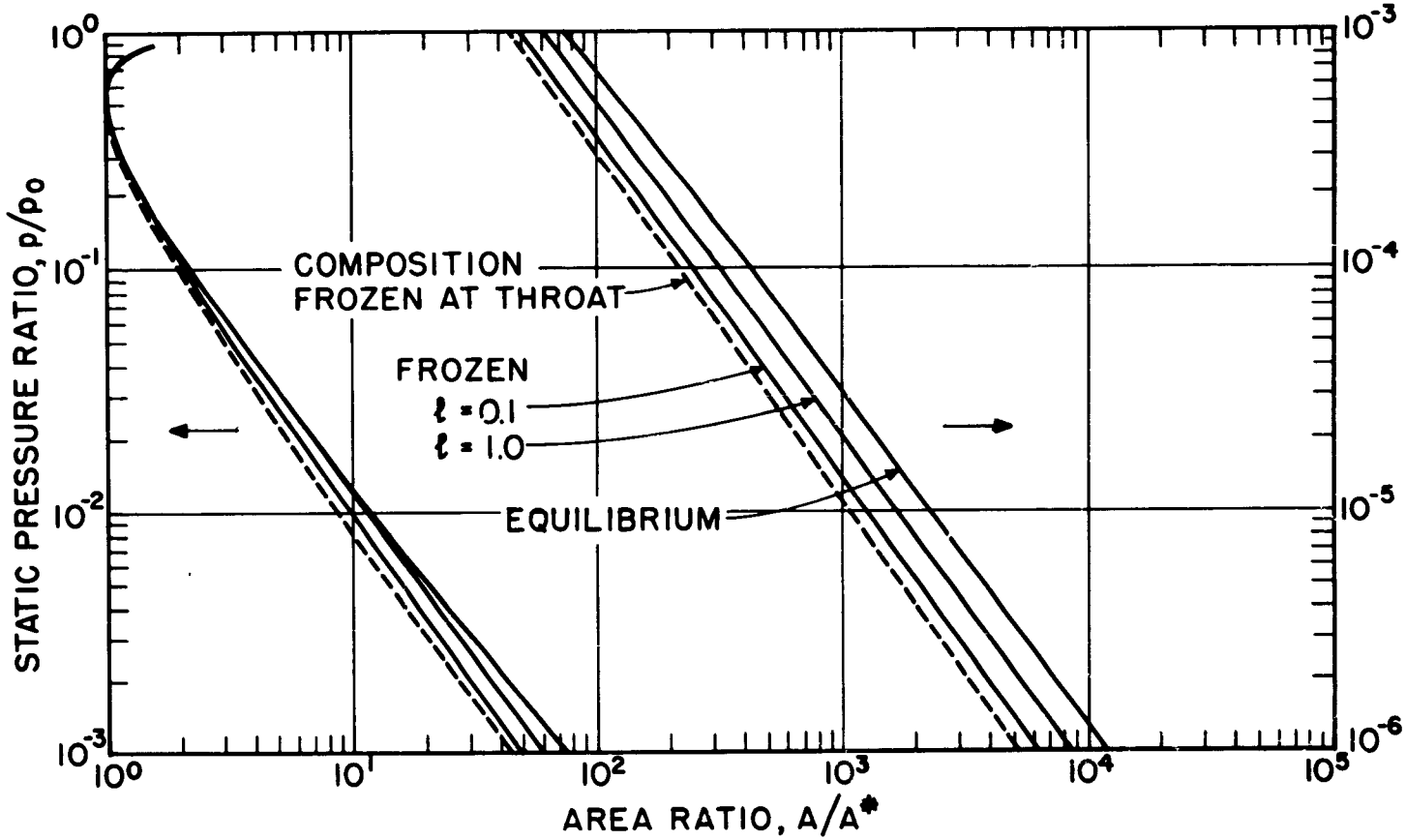

FIGURE 24 VARIATION OF STATIC PRESSURE FOR THE EXPANSION OF AIR IN A HYPERSONIC NOZZLE, $T_0 = 6000K$, $p_0 = 100$ ATM. (FIGURE 29b OF REF. 20)

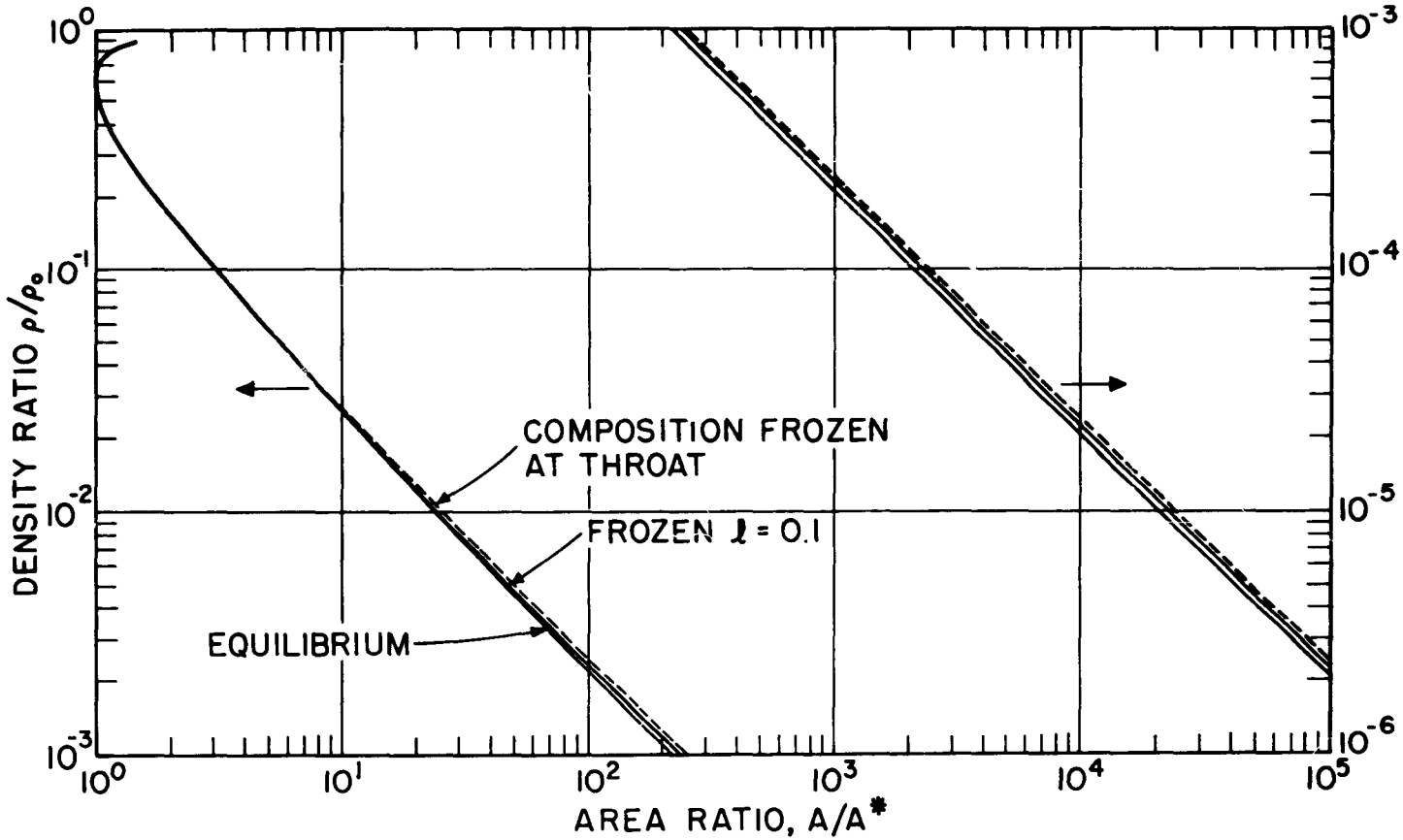

FIGURE 25 VARIATION OF DENSITY FOR THE EXPANSION OF AIR IN A HYPERSONIC NOZZLE, $T_o = 6000K$, $p_o = 100$ ATM.
(FIGURE 29a OF REF. 20)

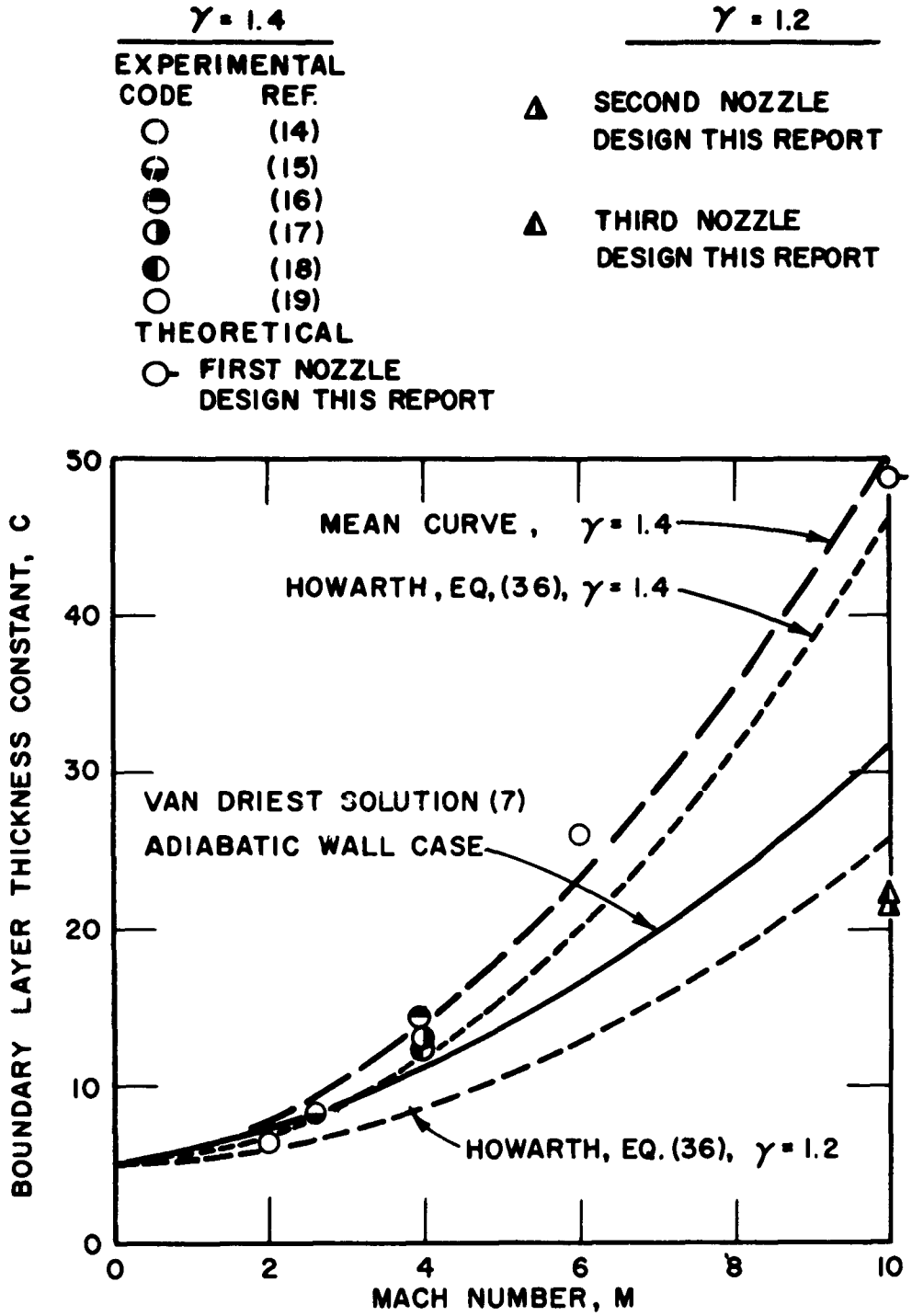

FIGURE 26 RECOMMENDED VALUES FOR THE BOUNDARY LAYER THICKNESS CONSTANT C

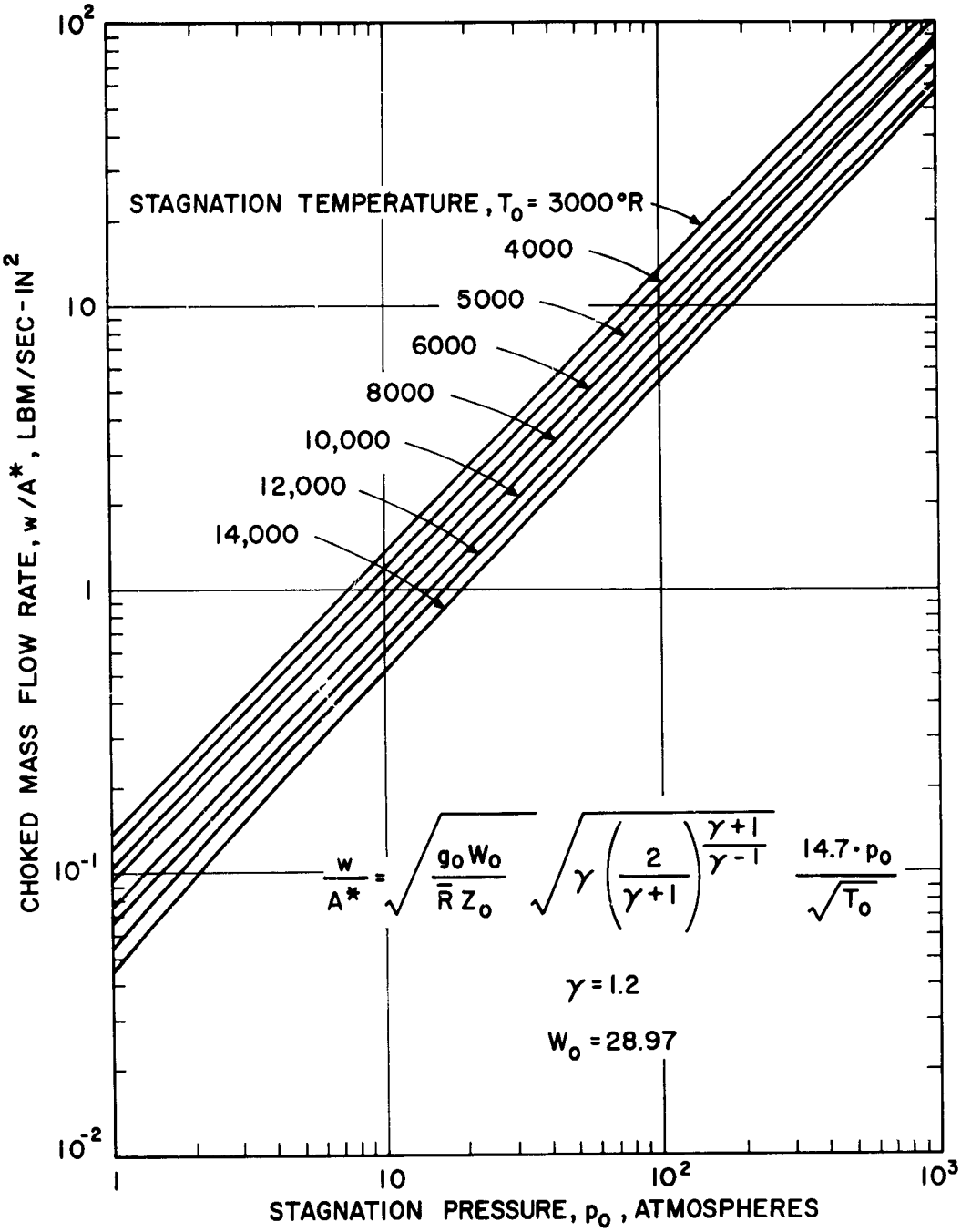

FIG. 27 - MASS FLOW RATE REQUIREMENTS FOR LOW-DENSITY WIND TUNNELS USING AIR

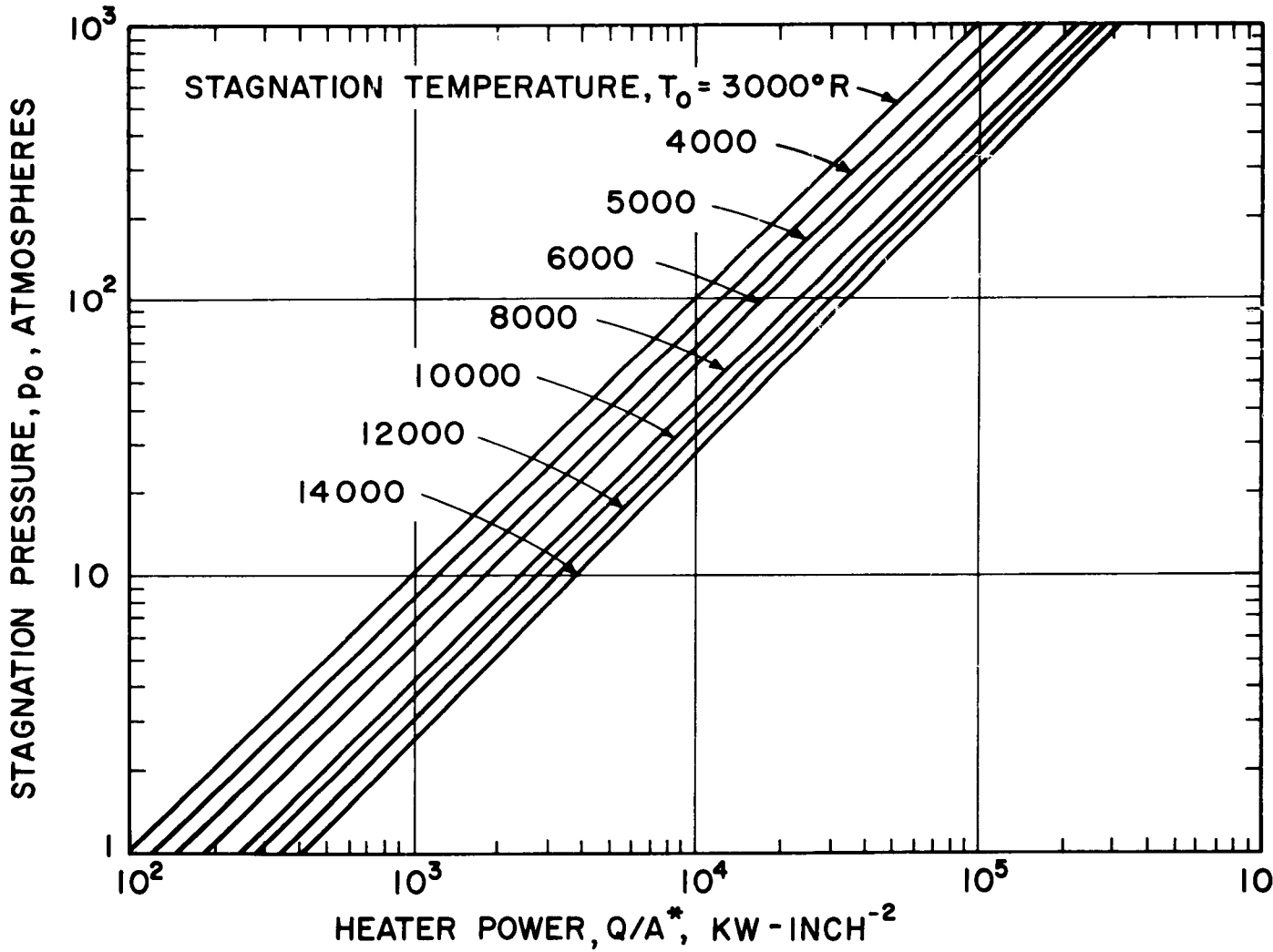

FIG. 28 HEATER REQUIREMENTS FOR LOW-DENSITY WIND TUNNELS USING AIR

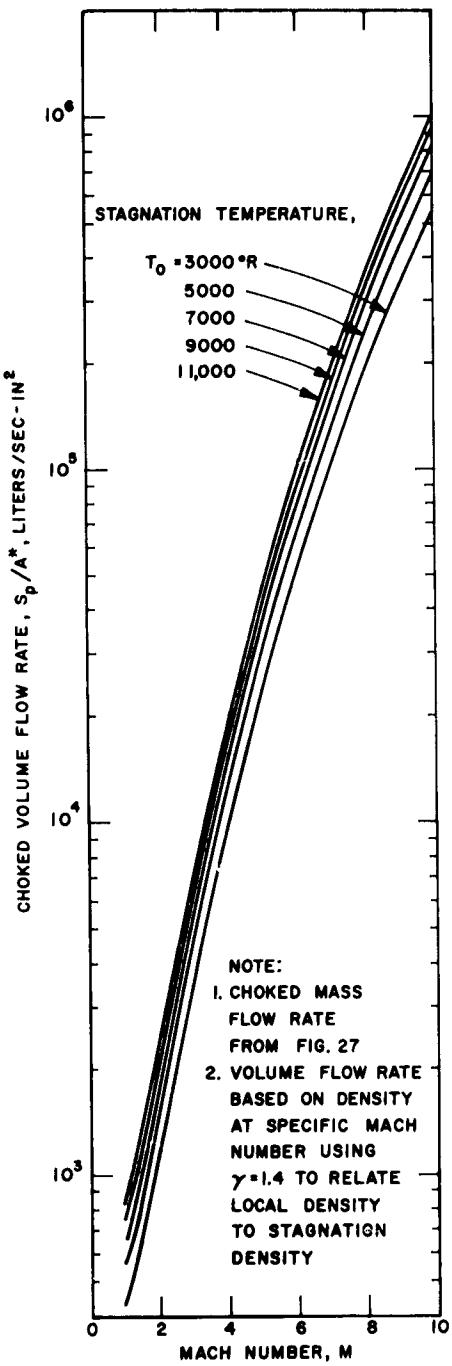

FIG. 29. VOLUME FLOW RATE REQUIREMENTS FOR LOW-DENSITY WIND TUNNELS USING AIR

Aeronautical Systems Division, Dir/Materials and Processes, Aerodynamics Division, Wright-Patterson AFB, Ohio
Rpt No. ASD-TDR-63-154. DESIGN CONSIDERATIONS AND METHODS FOR LOW-DENSITY WIND TUNNELS OPERATING WITH HIGH STAGNATION TEMPERATURES.
Final Report, Apr 63, 136p. incl illus., tables, 56 refs.

Unclassified Report

A study was made of design techniques for low-density wind tunnels operating with high stagnation temperatures and hypersonic flow. An approximate boundary layer analysis was developed to predict feasible ranges of operating conditions for low-density wind tunnels.
Detailed calculations were made for three nozzles including boundary layer corrections for isentropic contours.
It became obvious that the use of a high stagnation temperature wind tunnel for investigations of rarefied gas dynamics could produce situations in which it would not always be clear whether the experimental results were associated with rarefied gas flow phenomena or related to high temperature physical phenomena.
It appears that unless an enormous amount of money is devoted to the construction of an extremely large low-density wind tunnel, it will never be feasible to test large models.

(over)

1. Low-density wind tunnels
2. Gas flow
3. Wind tunnel nozzles
   I. AFSC Project 1426, Task 142603
   II. Contract No. AF 33(616)-6582
   III. Massachusetts Inst of Technology, Cambridge, Mass.
   IV. G. A. Brown
   A. E. Bergles
   V. Aval fr OTS
   VI. In ASTIA collection

Aeronautical Systems Division, Dir/Materials and Processes, Aerodynamics Division, Wright-Patterson AFB, Ohio
Rpt No. ASD-TDR-63-154. DESIGN CONSIDERATIONS AND METHODS FOR LOW-DENSITY WIND TUNNELS OPERATING WITH HIGH STAGNATION TEMPERATURES.
Final Report, Apr 63, 136p. incl illus., tables, 56 refs.

Unclassified Report

A study was made of design techniques for low-density wind tunnels operating with high stagnation temperatures and hypersonic flow. An approximate boundary layer analysis was developed to predict feasible ranges of operating conditions for low-density wind tunnels.
Detailed calculations were made for three nozzles including boundary layer corrections for isentropic contours.
It became obvious that the use of a high stagnation temperature wind tunnel for investigations of rarefied gas dynamics could produce situations in which it would not always be clear whether the experimental results were associated with rarefied gas flow phenomena or related to high temperature physical phenomena.
It appears that unless an enormous amount of money is devoted to the construction of an extremely large low-density wind tunnel, it will never be feasible to test large models.

(over)

1. Low-density wind tunnels
2. Gas flow
3. Wind tunnel nozzles
   I. AFSC Project 1426, Task 142603
   II. Contract No. AF 33(616)-6582
   III. Massachusetts Inst of Technology, Cambridge, Mass.
   IV. G. A. Brown
   A. E. Bergles
   V. Aval fr OTS
   VI. In ASTIA collection